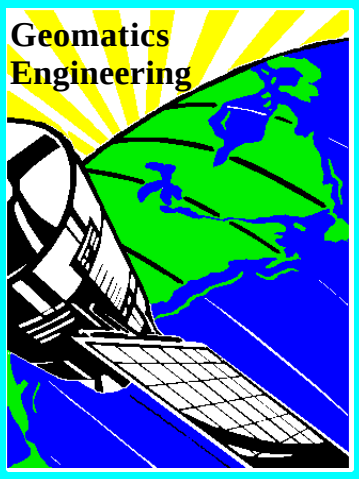

UCGE Reports
Number 20109

Department of Geomatics Engineering

Effect of Constraints and Multiple Receivers for On-The-Fly Ambiguity Resolution

By

Shawn D. Weisenburger

April, 1997

Calgary, Alberta, Canada

THE UNIVERSITY OF CALGARY

EFFECT OF CONSTRAINTS AND MULTIPLE RECEIVERS FOR ON-THE-FLY AMBIGUITY RESOLUTION

by

SHAWN D. WEISENBURGER

A THESIS

SUBMITTED TO THE FACULTY OF GRADUATE STUDIES

IN PARTIAL FULFILLMENT OF THE REQUIREMENTS FOR THE

DEGREE OF MASTER OF SCIENCE

DEPARTMENT OF GEOMATICS ENGINEERING

CALGARY, ALBERTA

APRIL, 1997

ABSTRACT

On-The-Fly (OTF) ambiguity resolution is affected by many factors such as satellite geometry and the distance between the monitor and rover receivers. These effects are investigated and are used to develop a new approach to increase the reliability and decrease the time required to resolve the integer ambiguities. This method makes use of two rover receivers, from which several constraints can be formed including the length of a baseline, heading, pitch, and ambiguities. Along with a height constraint, the usefulness of each constraint is assessed individually as well as collectively by analyzing several sets of field and marine data. Also, by using more than one monitor, the time to ambiguity resolution can be decreased further. A condition adjustment is implemented to make use of the multiple monitor station information. It was found that by using two rovers, three monitors, and all possible constraints in a marine environment, the time to ambiguity resolution could be reduced by approximately 79%. Finally, the performance of the Least squares AMBiguity Adjustment (LAMBDA) is investigated.

ACKNOWLEDGMENTS

I would like to express my appreciation to my supervisor, Professor M. E. Cannon, for her support and guidance throughout my graduate studies. Her advice and continuous encouragement were greatly appreciated.

I would also like to thank my colleagues, especially Thomas Morley, Jamie Henriksen, Robert Harvey, Huangqi Sun, and Chris Varner for their technical advice, field assistance, and most of all their friendship. Susan Skone and John Raquet are also thanked for reviewing and editing this thesis.

The Canadian Coast Guard is also thanked for their partial funding of this thesis as part of a contract.

Finally, I would like to thank my family for putting up with me for all these years. I could not have done it without their support.

TABLE OF CONTENTS

LIST OF TABLES

Table **Page**

LIST OF FIGURES

NOTATION

i) Conventions

a) Matrices are represented by upper case bold letters.

b) Vectors are represented by lower case bold letters.

c) The following operators are defined as:

$\mathbf{x}^-$	the superscript - denotes a Kalman prediction
$\dot{\mathbf{x}}$	derivative with respect to time
$\mathbf{A}^T$	matrix transpose
$\mathbf{N}^{-1}$	matrix inverse
Δ	single difference between receivers
∇	single difference between satellites
$\nabla\Delta$	double difference between receivers and satellites
$f(\ )$	function of
$\hat{\mathbf{x}}$	adjusted value

ii) Symbols

l	vector of observations (nx1),
x	state vector (ux1),
n	number of observations,
u	number of unknowns,
m	number of mathematical models,
A	design matrix (mxu),
B	observation design matrix (mxn),
d	correction vector (ux1),
r	residual vector (nx1),
w	misclosure vector (mx1),
N	normal matrix (uxu),
N	double difference integer ambiguity,
$\mathbf{C}_{\hat{\mathbf{x}}}$	state covariance matrix (uxu),
$\mathbf{C}_\mathbf{l}$	observation covariance matrix (lxl),

F	dynamics matrix (uxu),
Gu	forcing function (ux1),
f	transition matrix (uxu),
ϕ	carrier phase in cycles,
σ	standard deviation,
e	vector containing system white noise (ux1),
Q	system process noise (uxu),
I	identity matrix,
K	Kalman gain matrix (uxn),
df	degrees of freedom,
In	innovation sequence,
p	measured pseudorange in metres,
ρ	geometric range in metres,
$d\rho$	orbital error in metres,
c	speed of light in metres/second,
dt	satellite clock error in seconds,
dT	receiver clock error in seconds,
d_{ion}	ionospheric error in metres,
d_{trop}	tropospheric error in metres,
ε_p	code noise and multipath in metres,
ε_Φ	phase noise and multipath in metres,
Φ	carrier phase observable in metres,
λ	wavelength in metres,
R_N	prime vertical radius in metres,
e^2	first eccentricity,
L	lower triangular matrix,
D	diagonal matrix,
Z	transformation matrix,
z	transformed ambiguity states.

2) **Acronyms**

AFM	Ambiguity Function Method
AS	Anti-Spoofing,
C/A code	Coarse Acquisition code,
DOP	Dilution of Precision,
FASF	Fast Ambiguity Search Filter,
GPS	Global Positioning System,
LAMBDA	Least squares AMBiguity Decorrelation Adjustment,
OTF	On The Fly,
P code	Precise code,
RDOP	Relative Dilution of Precision,
SA	Selective Availability,
WGS	World Geodetic System.

CHAPTER 1
INTRODUCTION

1.1 Background

Over the past several years, the demand for centimetre level positioning and navigation has been growing exponentially and is expected to keep growing at a similar pace (Hatch, 1990). Several applications of such high accuracy positioning requirements in a marine environment include dredging (Frodge et al. 1995), hydrographic surveying (Burgess and Frodge 1992, Kielland and Hagglund 1995), and water leveling and tide monitoring (Lachapelle et al. 1994, Hamada et al. 1996).

One of the systems which can provide such accuracies is the Global Positioning System (GPS) which is a satellite-based, all weather, line-of-sight radio-navigation system. This system was developed by the United States Department of Defense as a replacement of the Transit Navy Navigation Satellite System and became fully operational in 1994 (Parkinson et al., 1995).

The GPS satellite constellation consists of 24 satellites in six nearly circular orbits (Wells et. al., 1987). Each satellite broadcasts on two frequencies, L1 at 1575.45 MHz and L2 at 1227.6 MHz. Both the Coarse Acquisition (C/A) code and the Precise (P) code are modulated onto the L1 carrier, while only the P code is modulated onto the L2 carrier. In order to make range measurements, a receiver replicates these codes and the time delay between the received signal and the replicated signal is multiplied by the speed of light and translated into a pseudorange observation. This pseudorange can be used for positioning, however, in order to achieve higher accuracies, carrier phase observations

must be used. The major drawback of using the carrier phase for positioning is that the receiver can only measure the integrated Doppler, which results in a phase measurement. To convert this phase into a range, the number of integer cycles between the satellite and the receiver must be known. This number of cycles is commonly referred to as the integer ambiguity (Lachapelle et al., 1992).

Because the L1 carrier wavelength is quite small (i.e. 19 cm), the resolution of these integer ambiguities is not a trivial task. In order to resolve the correct integer, the position should be known to an accuracy of slightly better than half a wavelength. Generally, this is not the case and other means of determining this ambiguity must be used (Lachapelle et al., 1992). Traditionally, this ambiguity was determined by remaining stationary at a given point for a long enough period of time such that the errors averaged out and the estimated ambiguities could simply be rounded to the nearest integer (Landau and Euler, 1992). Although this method works, it is quite tedious as it may require several hours of static initialization, which is not acceptable in many applications. For example, if a ship required centimetre accuracy positioning, it could not simply stop and remain static long enough to resolve the ambiguities. Many different methods for kinematic ambiguity resolution have been proposed including the Fast Ambiguity Search Filter (Chen and Lachapelle, 1994), extrawidelaning (Wubbena, 1989), least squares search (Hatch, 1990), and the Ambiguity Function Method (Counselman and Gourevitch, 1981 and Mader, 1990). Of these methods, all except the Ambiguity Function Method (which can be searched in the position domain) search through a set of possible integer ambiguity sets and try to determine the correct set based upon some type of statistical criterion.

This statistical criterion is generally based on the assumption that all errors effecting the measurements are Gaussian. Unfortunately, this is not the case. One method to aid in both the reduction of these non-Gaussian errors as well as act as quality control checks is

to use more than two receivers. That is, instead of only using one monitor and one rover receiver, two rovers could be used, or more than one monitor station could be used. By using more than one rover, several constraints can be formed which can speed up the time to ambiguity resolution as well as act as checks on the chosen integer ambiguities. More than one monitor receiver can be used to help reduce the effects of multipath and receiver noise (Raquet, 1997). These two approaches are closely examined.

The objective of this thesis is to investigate ambiguity resolution on the fly, with particular attention given to the marine environment. Although ambiguity resolution in a marine environment has been successfully implemented, several problems were encountered. In particular, Frodge et al. (1995) had problems resolving the integer ambiguities under conditions in which poor geometry prevailed. The main results of this problem were very long times to ambiguity resolution as well as incorrect integer ambiguity resolution in some cases. Carrier phase multipath has also been shown (Shi and Cannon, 1995) to be a hindrance when attempting to resolve integer ambiguities on the fly.

The main focus of this thesis is to investigate methods to decrease the amount of time required for integer ambiguity resolution as well as increase the reliability of this process. The methods to be implemented are the multiple rover and multiple monitor station approaches. By using multiple monitor stations, several constraints including a baseline, heading, pitch, and ambiguity constraints can be formed. In a marine environment, some height information is often available, which can also be used as a constraint. The effect of each constraint on ambiguity resolution is investigated under both ideal and reduced satellite constellations using field data. By adding more than one monitor station, multipath and receiver noise can also be reduced (Raquet, 1996). This method will also be implemented and the results discussed. The effect of a combined multiple monitor and multiple rover station configuration on integer ambiguity resolution is also

investigated. Before these algorithms are studied, however, the effects of the monitor rover separation is investigated for both the L1 only observable and the widelane observable.

1.2 Thesis Outline

Chapter two of this thesis briefly describes the GPS observables, including differenced observables, linear combinations, and some of the error sources present in GPS observables. The error sources discussed include the ionosphere, the troposphere, multipath, Anti-Spoofing (AS) and Selective Availability (SA).

Chapter three gives some of the basic concepts behind On The Fly (OTF) ambiguity resolution approaches. The basic mathematics involved in least squares and Kalman filtering are described, followed by a brief explanation of different search strategies and distinguishing tests. Several different OTF approaches are also discussed.

Chapter four examines OTF ambiguity resolution as a function of satellite geometry and the separation between monitor and rover stations.

Chapters five and six present the theory, implementation, and results of using several different constraints to aid the ambiguity resolution process. These constraints include heading, pitch , baseline, and ambiguity constraints, which are implemented by using two rover receivers as opposed to only one. The effect of a height constraint is also investigated.

Chapter 7 extends the multiple receiver concept to include several monitor stations as well as the two rover stations. Again, the theory and test results are discussed.

Chapter 8 takes a look at the affect of the Least squares AMbiguity Decorrelation Adjustment (LAMBDA) on the time to integer ambiguity resolution. It is combined with the Fast Ambiguity Search Filter (FASF) and compared against the FASF only method.

Finally, chapter 9 summarizes the general conclusions and recommendations.

CHAPTER 2
GPS OBSERVABLES AND ERROR SOURCES

Ambiguity resolution on the fly is affected by several different error sources including multipath, tropospheric error, ionospheric error, and receiver noise. Multipath and atmospheric errors can cause the estimated ambiguities to be biased. If these biases become too large, the search for the correct integers may fail because of the assumption of Gaussian errors. In this chapter, the GPS observables are described followed by a brief discussion of each of the above error sources.

2.1 GPS Observables

There are three fundamental observables available from GPS: pseudorange, carrier phase, and instantaneous Doppler (Wells et al., 1987). The code pseudorange is a measure of the time required for the signal to travel from the satellite to the receiver. This measurement also includes the error due to the offset of the receiver clock from GPS time, thus it is called a pseudorange as opposed to a range. The integrated carrier phase measurement is made on the beat frequency. The beat frequency is the difference between the receiver generated reference frequency and the actual received frequency. Finally, the instantaneous Doppler observable is a measure of the frequency shift between the actual and receiver replicated signals. Depending on the application, any combination of these data types can be collected. GPS satellites transmit on two frequencies, L1 (1575.42 MHz) and L2 (1227.6 MHz), of which the C/A code is modulated only on L1 while the P code is modulated on both frequencies (Parkinson, 1996). Presently, the P code is being encrypted by the United States Department of Defense (see Chapter 2.3.5).

Mathematically, the pseudorange observable is formulated as follows (Wells et al., 1987)

$$p = \rho + d\rho + c(dt - dT) + d_{ion} + d_{trop} + \varepsilon_p \qquad (2.1)$$

where p is the measured pseudorange in metres,

ρ is the geometric range in metres,

$d\rho$ is the orbital error in metres,

c is the speed of light in metres/second,

dt is the satellite clock error in seconds,

dT is the receiver clock error in seconds,

d_{ion} is the ionospheric error in metres,

d_{trop} is the tropospheric error in metres,

ε_p is the receiver code noise plus multipath in metres.

In the above equation, there are four unknowns, the three components of the user position and the receiver clock error. Thus, assuming that all other errors are either removed by modelling or are zero mean, at least four pseudoranges must be observed in order to obtain a solution.

The carrier phase observable is very similar to the pseudorange observable, i.e.

$$\Phi = \rho + d\rho + c(dt - dT) + \lambda N - d_{ion} + d_{trop} + \varepsilon_\Phi \qquad (2.2)$$

where Φ is the observed integrated carrier phase in metres,

λ is the wavelength in metres,

N is the integer ambiguity,

ε_Φ is the receiver carrier phase noise plus multipath in metres.

The integer ambiguity can be conceptualized as the integer number of wavelengths between the satellite and the receiver.

Finally, the instantaneous Doppler observable can be expressed as

$$\dot{\Phi} = \dot{\rho} + \dot{d}\rho + c(\dot{dt} - \dot{dT}) - \dot{d}_{ion} + \dot{d}_{trop} + \dot{\varepsilon}_\Phi \qquad (2.3)$$

where the dots represent the derivatives with respect to time.

Although the above observables described in equations 2.1, 2.2, and 2.3 are similar in many respects, several differences should be noted. Firstly, the ionospheric correction is negative for the phase and Doppler observables and positive for the pseudorange observable. This is due to the fact that in the ionosphere the code is delayed, while the phase is advanced by the same amount. Also, the pseudorange observable is absolute while the carrier phase is ambiguous due to the existence of the ambiguity term. The code noise is generally less than 1% of the chipping rate (i.e. <3m for C/A and <0.3m for P code) while the phase noise is normally <1% of the wavelength (i.e. <0.002m). Instantaneous Doppler in often used for velocity determination though it can also be used for position information. Finally, unlike the phase observable, the pseudorange and Doppler observables are not affected by cycle slips, thus, the Doppler can also be used for cycle slip detection.

In an attempt to reduce the errors in positioning results using equations 2.1, 2.2, and 2.3, a derived type of differenced observation can be formed which eliminates and significantly reduces several of the errors. By taking the difference between observations from two different receivers but the same satellite, the satellite clock error, dt, is completely eliminated while the atmospheric and orbital errors are significantly reduced. The amount of reduction depends on the spatial distance between the two stations. As the distance increases, so do the residual differential errors.

This method is commonly referred to as differential GPS and is used for relative positioning of one receiver with respect to another. If the coordinates of one receiver are known, the relative coordinates can be determined using this method. The station with known coordinates is often referred to as a monitor, base, or reference station, while the station to be positioned is referred to as the remote or rover station.

The derived observable, known as a single difference between receivers, is represented by the Δ symbol. Differencing equation (2.1), the following equation is formed:

$$\Delta p = \Delta\rho + \Delta d\rho + c\Delta dT + \Delta d_{ion} + \Delta d_{trop} + \Delta\varepsilon_p . \qquad (2.4)$$

In this equation, the satellite clock, ionospheric, tropospheric, and orbital errors are reduced. By further differencing the observables between satellites (see Figure 2.1), the receiver clock error term is also eliminated and the double difference equations (represented by $\Delta\nabla$) become

$$\Delta\nabla p = \Delta\nabla\rho + \Delta\nabla d\rho + \Delta\nabla d_{ion} + \Delta\nabla d_{trop} + \Delta\nabla\varepsilon_p \qquad (2.5)$$

$$\Delta\nabla\Phi = \Delta\nabla\rho + \Delta\nabla d\rho + \lambda\Delta\nabla N - \Delta\nabla d_{ion} + \Delta\nabla d_{trop} + \Delta\nabla\varepsilon_\Phi \qquad (2.6)$$

and $$\Delta\nabla\dot{\Phi} = \Delta\nabla\dot{\rho} + \Delta\nabla\dot{d}\rho - \Delta\nabla\dot{d}_{ion} + \Delta\nabla\dot{d}_{trop} + \Delta\nabla\dot{\varepsilon}_\Phi \qquad (2.7)$$

One major drawback of differencing observations is that the noise term is multiplied by $\sqrt{2}$ every time a difference is performed. Thus, for a double difference observation, the noise is multiplied by a factor of 2.

The main advantage of the double difference observation is that the receiver clock errors are eliminated.

2.2 Phase Combinations

Aside from the derived single and double difference observables, several different derived phase observables can be formed if both L1 and L2 frequencies are available. Of these derived phase combinations, the most common include the widelane, the narrowlane, and the ionosphere free observable (Borge, 1996).

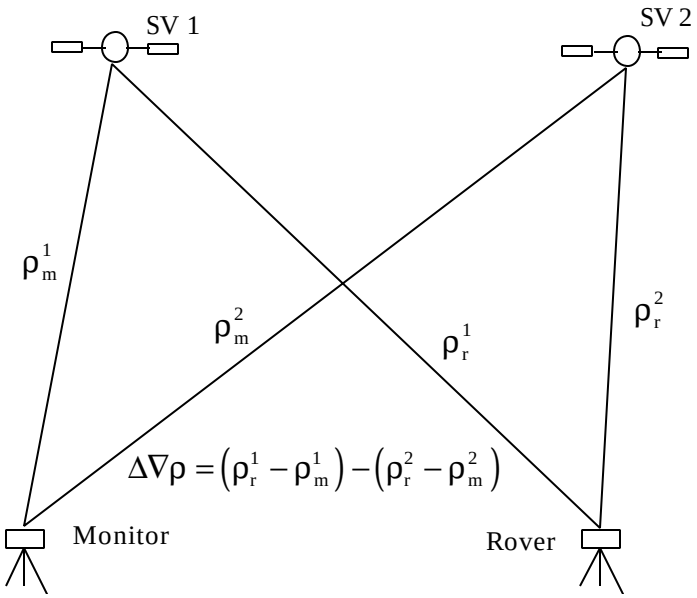

Figure 2.1 Double Difference Observation

In general, a phase combination can be formed using the equation

$$\phi_{ij} = i\phi_1 + j\phi_2 \tag{2.8}$$

where ϕ_1 is the measured carrier phase on L1 in cycles,

and ϕ_2 is the measured carrier phase on L2 in cycles.

Table 2.1 shows the relationship between i and j for several possible observables where f_{L1} and f_{L2} are the L1 and L2 carrier frequencies respectively (Borge, 1996). Note that each combination corresponds to a different wavelength.

Disadvantages of using these combinations are the increased phase noise and the requirement for dual frequency receivers. The noise due to a phase combination can be found using the covariance law, i.e.

$$\sigma_{\phi ij} = \lambda_{ij}\sqrt{i^2\sigma_1^2 + j^2\sigma_2^2} \tag{2.9}$$

where λ_{ij} is the wavelength of the linear combination, σ_1^2 and σ_2^2 are the variances in cycles of the L1 and L2 observables respectively, and $\sigma_{\phi ij}$ is the standard deviation of the

phase combinations in metres. Thus, of the combinations presented in Table 2.1, the narrowlane has the smallest amount of noise.

Table 2.1 Derived Observables

Observable	i	j	Wavelength (m)
Widelane ($\phi_{1,-1}$)	1	-1	0.862
Narrowlane ($\phi_{1,1}$)	1	1	0.107
Ionosphere Free ($\phi_{2.546,-1.984}$)	$\frac{f_{L1}^2}{f_{L1}^2 - f_{L2}^2}$	$\frac{f_{L1}f_{L2}}{f_{L1}^2 - f_{L2}^2}$	0.190
$\phi_{-7,9}$	-7	9	14.663

One of the characteristics of some of the phase combinations is the odd-even ambiguity relationship (Borge, 1996). When the ambiguities have been found for particular phase combinations, in certain cases the ambiguities of a different phase combination can often be known to be either even or odd, whichever the known ambiguities are. This relationship exists between the widelane and narrowlane, as well as the -7/9 lane and the widelane. Thus, if the widelane ambiguities are known, the narrowlane ambiguities can be found if the positional accuracy is known within ± 1 narrowlane cycle as opposed to $\pm 1/2$ a cycle.

The most commonly used combinations are the widelane and ionospheric free observables. The widelane is typically used because it has a much longer wavelength, without adding a large amount of noise (as the -7/9 lane). Thus, the widelane allows for ambiguity resolution quicker than if a single frequency is used. The ionospheric free observable is used when there is a large separation between monitor and rover stations. As the name suggests, the major advantage is that the effects of the ionosphere are removed. The disadvantage, however, is that the ambiguities do not retain their integer properties, thus, ambiguity resolution is not possible (Leick, 1995).

2.3 Error Sources

As shown above, GPS observables are affected by many different errors. The errors which effect OTF ambiguity resolution are discussed below, along with methods of reducing these errors when applicable.

2.3.1 Multipath

Multipath is defined as "the phenomena whereby a signal arrives at a receiver via multiple paths" (Qiu, 1993). It can be caused by almost any reflective surface near the antenna (see Figure 2.2). A complete description of multipath and its properties can be found in Braasch (1996).

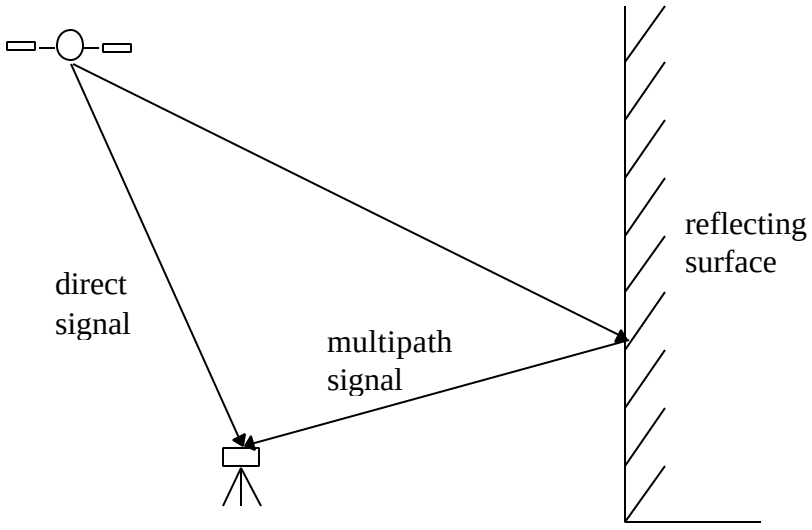

Figure 2.2 Multipath

For short baselines (i.e. <10 km), multipath is usually the largest error source which impedes ambiguity resolution. Under severe multipath conditions, errors can reach 1 wavelength (i.e. 1 chip length) for code observations or 1/4 of a wavelength for phase

observations. Such conditions can have varying effects including loss of phase lock, reduced signal to noise ratio, and increased observation noise (Abidin, 1990).

Recently, improvement has been made in receiver design to reduce the effect of multipath in code measurements. Such improvements include the narrow correlator spacing (Van Deirendonck et al. 1992), Multipath Elimination Technology (MET) (Townsend and Fenton, 1994) and Multipath Estimating Delay Lock Loops (MEDLL) (van Nee et al. 1994, Townsend et al. 1995). A comparison of these technologies has been done by Lachapelle et al. (1996) demonstrating the improvement from conventional receivers in the marine environment. The MEDLL technology, as well as a deconvolution approach (Kumar and Lau, 1996), have been found to reduce code multipath by as much as 75%, depending on the multipath delay (Townsend and Fenton, 1994). By reducing these multipath errors, the GPS position solution can converge to the correct solution quicker than if these errors are larger.

The effects of carrier phase multipath on both position accuracies and double difference measurement residuals is shown in Shi and Cannon (1995). It was found that the phase multipath could result in a bias like position error (up to 10 cm in height) as well as cause the residuals to increase to as much as several centimetres for a very short baseline (<50 m). For the tests conducted, it was concluded that multipath was the main error source for the airborne GPS positioning.

The simplest approach to reducing multipath is to avoid multipath environments. This can be done by choosing receiver sights which are clear of any structures that could cause multipath. Also, choke rings and ground planes have been found to be quite effective for reducing multipath (Lachapelle, 1989). Other external methods of reducing multipath effects include filtering using the carrier phase measurements (Hatch, 1982) and a multiple reference station technique (Raquet, 1996). The method of carrier phase

smoothing reduces the code multipath by making use of the carrier phase, which is affected much less by multipath in comparison to the code. The method of using multiple reference stations (discussed in more detail in Chapter 7) reduces both phase and code multipath as well as atmospheric effects because the errors are smoothed throughout the reference network.

2.3.2 Tropospheric Error

The troposphere is the portion of the atmosphere extending up to 60 km above the earth's surface. Approximately 80-90% of the delay is due to the wet portion of the troposphere which is contained within the first 10 km. Unfortunately, this is the most difficult portion to model as it is effected by weather patterns, temperature, pressure, humidity, and satellite elevation (Qui, 1993). At low satellite elevations, the tropospheric error can reach 30 m.

By differencing observations the tropospheric error can be significantly reduced for short baselines. However, even for short baselines, if the height difference between the two antennas is significantly different, the tropospheric error can become a significant error source (Shi and Cannon, 1995).

Because the troposphere is nondispersive at frequencies less than 30 GHz, dual frequency measurements cannot be used to compute the delay in the troposphere. Fortunately, several models have been developed to compute this delay.

The best known models include the Hopfield model (Hopfield, 1969), the modified Hopfield model (Goad and Goodman, 1974), and the Saastamoinen model (Saastamoinen, 1973). Goad and Goodman (1974) have shown that the modified

Hopfield model gives the best results for low elevation satellites. The previously mentioned models give similar results for satellites above 20 degrees.

The effect of the troposphere on carrier phase positioning and residuals is demonstrated in Shi and Cannon (1995) and Tiemeyer et al. (1994). It was shown that when height differences between the monitor and rover receivers vary up to 6000 m, the height errors due solely to the troposphere can reach 5 m if not modeled. It was also shown that an unmodeled troposphere can contribute up to several centimetres to the carrier phase residuals under the given circumstances. Biases in the order of several metres due to the troposphere can have a detrimental effect on carrier phase ambiguity resolution and it was shown in Tiemeyer et al. (1994) that when no tropospheric modeling was implemented, the incorrect ambiguity of a new satellite entering the solution may be found even though all of the other ambiguities were correct before the new satellite.

2.3.3 Ionospheric Error

The ionosphere is the portion of the atmosphere in which free electrons exist. It extends from approximately 60 km to 400 km above the earth's surface. The effects of the ionosphere on waves with frequencies greater than 100 MHz include group delay, carrier phase advance, polarization rotation, angular refraction, and amplitude and phase scintillation (Lachapelle, 1995). The most significant factors affecting the ionosphere include the time of day, time of year, solar cycle, and geomagnetic latitude. The solar cycle was minimum in 1995, while the solar maxim is expected to occur in 2001, which may have a significant impact on GPS.

The group delay, which is equal in magnitude to the phase advance, is directly proportional to the total electron content and inversely proportional to the frequency

squared. The total electron content varies with the local time, season, solar cycle, geomagnetic latitude, and sunspot activity (Lachapelle, 1995).

The ionospheric error can be handled in one of three ways. Firstly, if differenced observations are used, the error is significantly reduced, depending on the baseline length. Secondly, an ionospheric correction is broadcast with the almanac data which can be used by single frequency users. Finally, if a dual frequency receiver is available, the ionospheric free pseudorange can be computed as follows (Leick, 1995):

$$p_{L1,L2} = \frac{f_{L1}^2}{f_{L1}^2 - f_{L2}^2} p_{L1} - \frac{f_{L2}^2}{f_{L1}^2 - f_{L2}^2} p_{L2} \tag{2.10}$$

while the ionospheric free phase can be computed as

$$\Phi_{L1,L2} = \frac{f_{L1}^2}{f_{L1}^2 - f_{L2}^2} \Phi_{L1} - \frac{f_{L1} f_{L2}}{f_{L1}^2 - f_{L2}^2} \Phi_{L2}. \tag{2.11}$$

Generally, a differencing technique is used to reduce the ionospheric error. If the separation between the monitor and rover is relatively large (>30 km is used in Neumann et al. (1996)), the ionospheric free observable is often used in combination with a differencing technique. Aside from the increased noise of the ionospheric free phase, one major drawback is that the ambiguities no longer retain their integer properties. Thus, the ambiguities can only be estimated as floating numbers (Neumann et al., 1996).

The effect of the ionosphere can be quite significant for large separations between the monitor and rover receiver. Shi and Cannon (1995) showed that the ionospheric effects are highly correlated with the receiver separation. The L1 RMS double difference phase residuals were shown to increase up to 3.3 cm for distances up to 175 km while the height errors due to the ionosphere for the same distances were shown to reach 50 cm.

2.3.4 Receiver Noise

A general rule for receiver noise is that it is normally less than 0.1% of the observable wavelength. For example, C/A code noise should be less than 3 m, P-code noise should be less than 0.3 m, and L1 phase noise should be less than 0.0019 m. It was shown in Cannon et al. (1993) that the RMS single difference carrier phase noise for a low cost receiver ranged from 0.9 to 2.0 mm. Weisenburger (1995) confirmed these results for a similar receiver and also showed that the RMS code noise ranged from 0.6 to 2.3 m. Note that when Anti-Spoofing (AS) is on, receiver noise on the P-code and L2 phase may be significantly increased (see following section).

Several techniques are available to reduce the code noise (and multipath). This can be done internally to the receiver by reducing the correlator spacing (Van Dierendonck, 1992) or externally to the receiver by using a carrier phase smoothing algorithm (Hatch, 1982). For the example above by Weisenburger (1995), the RMS code noise was reduced to 0.09 m to 0.19 m.

2.3.5 Selective Availability and Anti-Spoofing

Selective availability (SA) is the intentional degradation of the navigational accuracy by the United States Department of Defense. This is achieved through satellite clock dithering and degradation of the reported orbit parameters. At this point, SA is realized through the clock dithering, although this could change at any time. SA causes the single receiver positioning accuracy of GPS to be 100 m 2DRMS in the horizontal and 120 m 2DRMS in the vertical (Spilker, 1996).

There are several ways to reduce the effects of SA. Firstly, by differencing between receivers, the satellite clock error is completely removed while the orbital error is

significantly reduced. Secondly, if postprocessing is acceptable, precise orbits and clocks are available and can be used to significantly reduce these errors.

Anti-Spoofing (AS) is the denial of the P-code through encryption. This is done by the United States Department of Defense to prevent hostile forces from jamming the GPS signals. When the P-code is encrypted, it becomes the Y-code. In order to utilize the Y-code, a codeless or semi- codeless receiver is needed (Van Dierendonck, 1994).

There are two methods commonly used to get information from the L2 signal in the existence of AS (Van Dierendonck, 1994). These are a squaring technique and a cross-correlation technique. The squaring method is implemented by multiplying the received signal by itself. This results in a signal which is stripped of any modulated data (including the encrypted P-code) and is at twice the original frequency. This higher frequency signal presents a major drawback if ambiguity resolution is one of the user goals. Also, the signal strength suffers a 30 dB loss. This results in the signal becoming more susceptible to jamming as well as increased phase noise. The cross-correlation method is implemented by mixing the received L2 signal with slightly delayed L1 signal (the delay is required because the L2 signal is slowed more in the ionosphere). The mixing process results in a signal which is again stripped of the codes and data, however, the frequency is the difference between the L1 and L2 frequencies (i.e. the widelane). This is an advantage for carrier phase users. Also, because the P-code on L1 is 3 dB stronger than the P-code on L2, there is approximately a 1.25 dB increase over the squaring technique (Van Dierendonck, 1994).

Both of the above mentioned techniques are codeless techniques, since the data is completely stripped from the carrier and pseudoranging is not possible. The knowledge of the approximate chipping rate of the encryption code can be used to our advantage. This is realized by reducing the predetection bandwidth from 10 MHz to 500 kHz

(Ashjaee and Lorenz, 1992). By introducing a P-coder aided by the known C/A code, the encrypted P-code can actually be tracked, resulting in Y-code pseudoranges (Van Dierendonck, 1994). This method can be combined with either the squaring or cross-correlation method to obtain phase measurements on L1 along with the Y-code pseudoranges. Because of the reduced predetection bandwidth, the signal to noise ratio is improved by another 13 dB compared to the signal to noise ratio for the 10 MHz bandwidth. Note that if AS was not implemented, a 50 Hz bandwidth could be used.

These methods of obtaining L2 phase information (especially through cross-correlation which results in the widelane frequency) are very important for carrier phase ambiguity resolution (see later Chapters for comparison between dual frequency results and single frequency results). There are several drawbacks including the reduced signal strength, the increased phase noise, the increased susceptibility to jamming, and the increased receiver costs.

CHAPTER 3
AMBIGUITY RESOLUTION

In order to achieve centimetre level positioning, it is necessary to make use of the carrier phase observables and solve for the unknown carrier phase integer ambiguities. For many applications, this task must be done both quickly and reliably. Unfortunately, these two requirements are of conflicting nature, thus many different algorithms have been developed in hopes of balancing both requirements.

All ambiguity resolution strategies consist of three basic steps (see Figure 3.1). The first step is the determination of an initial approximate solution, which is generally computed using either a carrier phase smoothed code solution (Lachapelle, 1992), or a Kalman filtered float solution (Ford and Neumann, 1994). The second step consists of the search strategy, which can be performed in either the position or ambiguity domain (Hein and Werner, 1995). The final step of ambiguity resolution, which may be necessary if more than one possible ambiguity combinations exist, is the distinguishing test. This test is to determine which of the possible sets is the correct one. It should be noted that several different algorithms are given for each of these steps and many of the three steps can be used in different combinations, depending upon the application at hand.

Before describing several different methods of ambiguity resolution, a general description of the two most commonly used estimation techniques (least squares and Kalman filtering) is given.

3.1 Least Squares Estimation

As mentioned above, a starting point for the ambiguity search is needed. This is shown in Figure 3.1 as the top box. In order to achieve the best possible solution of an overdetermined problem, least squares estimation can be used.

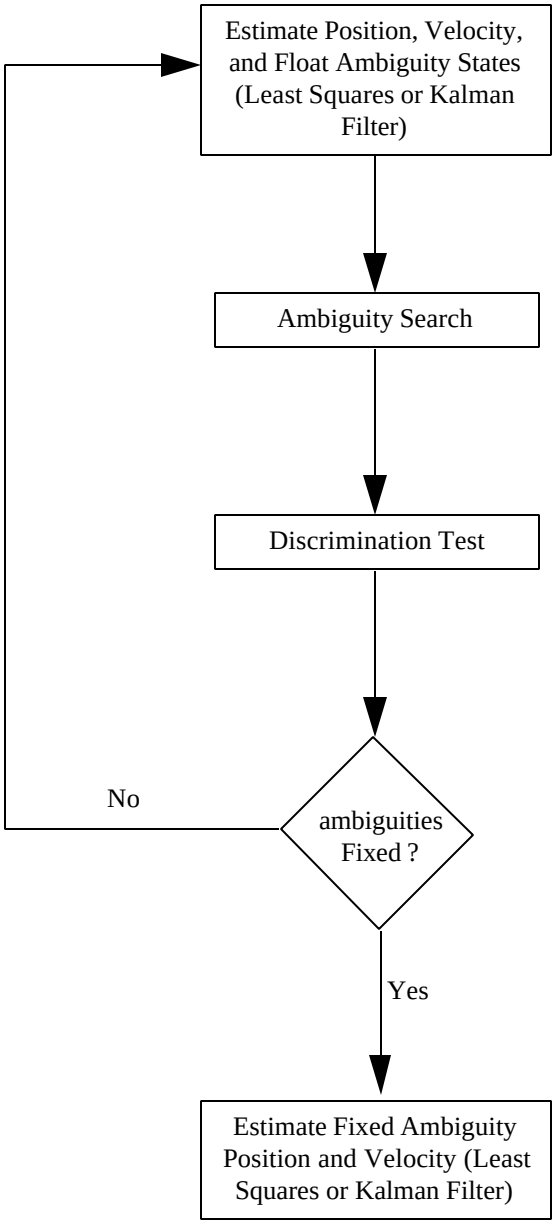

Figure 3.1 Ambiguity Estimation

The least squares parametric equations are reviewed below, however a more detailed derivation can be found in Krakiwsky (1989).

Assuming the unknown parameters are related to the observables using a parametric model:

$$\mathbf{l} = \mathrm{f}(\mathbf{x}). \tag{3.1}$$

The state vector $\mathbf{x}$ is related to the observation vector $\mathbf{l}$ using the equations

$$\hat{\mathbf{x}} = \mathbf{x^o} + \hat{\mathrm{d}} \tag{3.2}$$

$$\hat{\mathrm{d}} = -\mathbf{N^{-1}u} = -(\mathbf{A^T C_l^{-1} A})^{-1}\mathbf{A^T C_l^{-1} w} \tag{3.3}$$

$$\mathbf{w} = \mathbf{f}(\mathbf{x^o}) - \mathbf{l} \tag{3.4}$$

$$\mathbf{A} = \left.\frac{\partial \mathrm{f}}{\partial \mathrm{x}}\right|_{(\mathrm{x}^o,\mathrm{l})} \tag{3.5}$$

while the corrections to the observations, called the residuals, are given by

$$\hat{\mathbf{r}} = \mathbf{A}\hat{\mathrm{d}} + \mathbf{w} \tag{3.6}$$

and using the covariance law, the state covariance matrix becomes

$$\mathbf{C}_{\hat{\mathbf{x}}} = \mathbf{N^{-1}} = \left(\mathbf{A^T C_l^{-1} A}\right)^{-1}. \tag{3.7}$$

Setting n to the number of observations and u to the number of unknowns, the parameters are defined as:

- $\hat{\mathbf{x}}$ is the estimated state vector (ux1),
- $\mathbf{x^o}$ is the initial approximate state vector,
- $\hat{\mathbf{l}}$ is the observation vector (nx1),
- $\mathbf{A}$ is the design matrix (nxu),
- $\hat{\mathrm{d}}$ is the correction vector (ux1),
- $\mathbf{N}$ is the normal matrix (uxu),
- $\mathbf{w}$ is the misclosure vector (nx1),
- $\hat{\mathbf{r}}$ is the residual vector (nx1),
- $\mathbf{C}_{\hat{\mathbf{x}}}$ is the state covariance matrix (uxu),
- $\mathbf{C_l}$ is the covariance matrix of the observations (nxn).

If the mathematical model is non-linear (as is the case for GPS observations), it is necessary to linearize about a nominal state value $\mathbf{x}_o$ and iterate the solution until the correction vector $\hat{\delta}$ converges towards a zero threshold.

The main assumptions of least squares are that the state vector is static (i.e. not changing over time) and that all errors are Gaussian in nature.

Figure 3.1 shows how least squares (or Kalman filtering) is applied to ambiguity resolution. It is used in both the top and bottom boxes in the figure. If the ambiguity states have not been fixed, these states, along with the position and velocity states must be estimated. This is referred to as the floating ambiguity solution. Once the integer ambiguities have been determined (bottom box in Figure 3.1), least squares (or Kalman filtering) must again be implemented to obtain an optimal position and velocity solution. This is often referred to as the fixed ambiguity solution.

3.2 Kalman Filtering

Kalman filtering can be thought of as an extension of least squares from a static problem to a kinematic one. Thus, the state vector is no longer assumed to be a constant as in the case of least squares, but is allowed to change over time. Again, only the basic equations will be presented. More complete derivations can be found in Krakiwsky (1989) and Brown and Hwang (1992). Figure 3.1 shows where a Kalman filter would be implemented for ambiguity resolution.

A Kalman filter consists of two phases, update and prediction. The update equations are

$$\hat{\mathbf{x}}_{\mathbf{k}} = \hat{\mathbf{x}}_{\mathrm{k}}^{-} + \mathbf{K}_{\mathbf{k}}\left(\mathbf{l}_{\mathrm{k}} - \mathbf{A}\hat{\mathbf{x}}_{\mathbf{k}}^{-}\right) \tag{3.8}$$

$$\mathbf{C}_{\hat{\mathbf{x}}\mathbf{k}} = \left(\mathbf{I} - \mathbf{K}_{\mathbf{k}}\mathbf{A}_{\mathbf{k}}\right)\mathbf{C}_{\hat{\mathbf{x}}_{\mathbf{k}}}^{-} \tag{3.9}$$

$$\mathbf{K}_{\mathbf{k}} = \mathbf{C}_{\hat{\mathbf{x}}\mathbf{k}}^{-}\mathbf{A}_{\mathbf{k}}^{\mathbf{T}}\left(\mathbf{A}_{\mathrm{k}}\mathbf{C}_{\hat{\mathrm{x}}_{\mathrm{k}}}^{-}\mathbf{A}_{\mathbf{k}}^{\mathbf{T}} + \mathbf{C}_{\mathbf{l}_{\mathbf{k}}}\right)^{-1} \tag{3.10}$$

where $\mathbf{K_k}$ is the Kalman gain matrix at time t_k (uxn),

$\mathbf{I}$ is an identity matrix (uxu),

$^-$ denotes a matrix or vector before measurement update.

The prediction equations are

$$\hat{\mathbf{x}}_{\mathbf{k}+1}^{-} = \mathrm{f}_{\mathbf{k}}\hat{\mathbf{x}}_{\mathbf{k}} \tag{3.11}$$

$$\mathbf{C}_{\hat{\mathbf{x}}_{\mathbf{k}+1}}^{-} = \phi\mathbf{C}_{\hat{\mathbf{x}}}\phi^{\mathrm{T}} + \mathbf{Q}_{\mathbf{k}} \tag{3.12}$$

where f_{k} is the transition matrix (uxu) and

$\mathbf{Q_k}$ is the process noise matrix (uxu).

The implementation of these equations is shown in Figure 3.2.

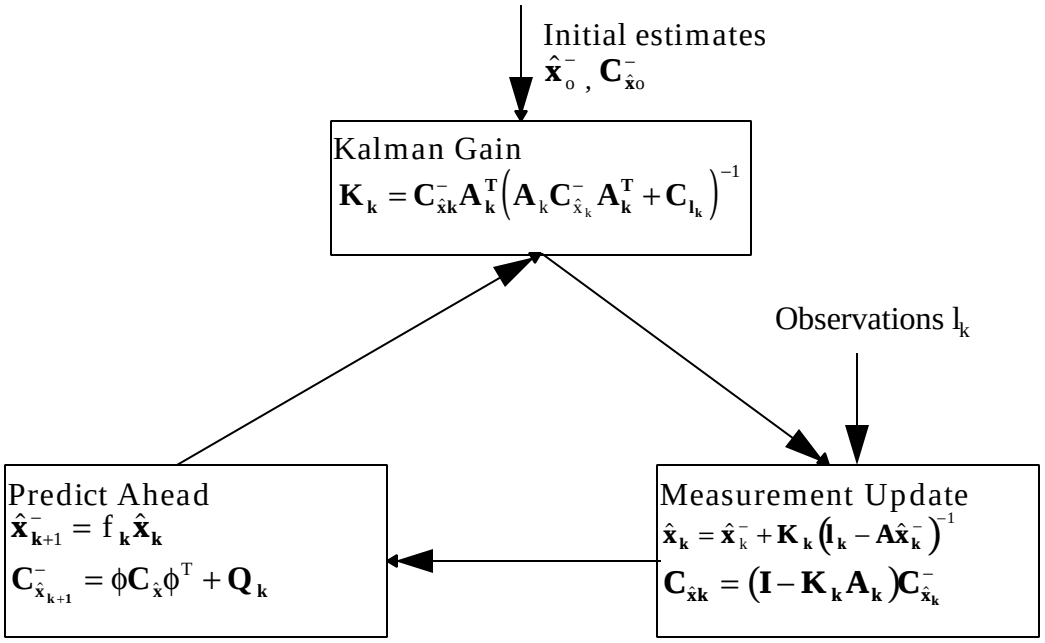

Figure 3.2 Kalman Filter

For most navigation problems, the dynamics of the system are modeled using a random walk model or a Gauss-Markov model, thus, the transition matrix is easily obtained. Unfortunately, the process noise is not so easy to model and must frequently be determined by empirical means (Brown and Hwang, 1992).

3.3 Float Solution

An important part of any algorithm that relies on the output covariance matrix is the floating ambiguity solution. In this section, the float solution (shown as the top box in Figure 3.1) is presented using a Kalman filter.

In order for the search algorithm to include the correct ambiguity set, it is critical for the filter state covariance matrix to accurately reflect the errors present in the estimated states. Naturally, this can be somewhat problematic as many of the errors such as multipath, residual atmospheric error, and residual orbital errors are non-Gaussian, which may cause the covariance to become overly optimistic or overly pessimistic. Before describing such details, the float solution is developed mathematically.

Beginning with a constant velocity model (Lan and Cannon, 1996), the state vector is

$$\mathbf{x} = \begin{bmatrix} \delta\phi & \delta\lambda & \delta h & \delta\dot{\phi} & \delta\dot{\lambda} & \delta\dot{h} & \delta N_1 & \delta N_2 & \cdots & \delta N_n \end{bmatrix}^T \tag{3.13}$$

where $\delta\phi$, $\delta\lambda$, and δh are the corrections to the latitude, longitude, and height states respectively. The dot above the parameters represents the time derivative (i.e. velocities in this case), and δN is a correction to a double difference ambiguity state. Because the dynamics of the system were modeled as a random walk, the transition matrix is easily derived as

$$\phi = \begin{bmatrix} 1 & 0 & 0 & \Delta t & 0 & 0 & 0 & 0 & \cdots & 0 \\ 0 & 1 & 0 & 0 & \Delta t & 0 & 0 & 0 & \cdots & 0 \\ 0 & 0 & 1 & 0 & 0 & \Delta t & 0 & 0 & \cdots & 0 \\ 0 & 0 & 0 & 1 & 0 & 0 & 0 & 0 & \cdots & 0 \\ 0 & 0 & 0 & 0 & 1 & 0 & 0 & 0 & \cdots & 0 \\ 0 & 0 & 0 & 0 & 0 & 1 & 0 & 0 & \cdots & 0 \\ 0 & 0 & 0 & 0 & 0 & 0 & 1 & 0 & \cdots & 0 \\ 0 & 0 & 0 & 0 & 0 & 0 & 0 & \ddots & \cdots & 0 \\ \vdots & \vdots & \vdots & \vdots & \vdots & \vdots & \vdots & \vdots & \ddots & 0 \\ 0 & 0 & 0 & 0 & 0 & 0 & 0 & 0 & 0 & 1 \end{bmatrix} \tag{3.14}$$

where Δt is the difference between the current time and a future time. The development of the design matrix **A** for both the pseudoranges and carrier phase observations is developed in the Appendix as well as in Cannon (1991).

As mentioned above, most errors encountered in GPS observations are not Gaussian in nature. One way to keep the filter from becoming overly optimistic is to add process noise to the ambiguity states and make the process noise on the position and velocity states slightly larger than their theoretical values. This may result in a conservative covariance matrix which is non-optimal, but it is less likely to cause errors in resolving the integer ambiguities.

Also, adapting the process noises throughout the data set can be useful. The adaptive filtering can be approached in either a completely theoretical way (Haykin, 1996), or by using a set of heuristically derived algorithms. In the case of the GPS float solution the latter of the two can be implemented by processing many data sets and determining the best noise values as a function of baselines, varying receiver noises, and multipath conditions. Also, the noise values to be added to the velocity states can be derived by inspecting the changes in the velocity states from the previous epochs. If the velocities change significantly, acceleration can be implied, thus, a significant amount of process

noise should be added. On the other hand, if velocity states do not change from epoch to epoch, very little process noise needs to be added. Typical values for the process noise added to the position and velocity states for a one second update are 0.2 m^2 and 0.25 m^2/s^2 respectively.

Blunders are another important factor when dealing with GPS observations. One way to detect blunders is to look at the innovation sequence and the covariance of the innovations (Maybeck, 1994), namely:

$$\mathbf{In} = \mathbf{l_k} - \mathbf{A_k}\hat{\mathbf{x}}_{\mathbf{k}}^{-} \tag{3.15}$$

$$\mathbf{C_{In}} = \mathbf{A_k}\mathbf{C}_{\hat{\mathbf{x}}\mathbf{k}}^{-}\mathbf{A_k^T} + \mathbf{C}_{\mathrm{lk}} \tag{3.16}$$

where **In** is the innovation sequence (predicted residuals) and

$\mathbf{C_{In}}$ is the covariance of the innovation sequence.

Thus, if the size of the innovation sequence is larger than a given threshold (3σ as derived from $\mathbf{C_{In}}$ matrix is often used), the corresponding observation can either be deweighted or completely rejected.

3.4 Existing OTF Algorithms

As previously mentioned, many different OTF ambiguity resolution algorithms have been developed. Most of these consist of three main steps. These steps include the initial solution, the search procedure, and the distinguishing test. Different approaches to each of these will be briefly described in the following subsections.

3.4.1 Initial Solution

The initial solution is the first step in ambiguity resolution and is shown in Figure 3.1. It provides two pieces of important information. The first piece is an approximate state vector, which can be used as a starting point for the ambiguity search. The second piece

of information comes from the output covariance matrix, which is used in some manner to define an ambiguity search area.

The initial solution is generally derived from one of two different ways, either a carrier phase smoothed code solution or a Kalman filtered solution. For situations in which an instantaneous ambiguity solution is not possible, a Kalman filtered solution may be preferable to the least squares smoothed code solution as it makes use of all previous information. Examples of using smoothed code for an initial solution can be found in Hatch, (1990) and Lachapelle et. al. (1992), while examples of a Kalman filter can be found in Chen and Lachapelle (1994), Ford and Neumann (1994), and Lan and Cannon (1996).

3.3.2 Search Procedures

The second step shown in Figure 3.1 is the procedure of searching through all of the possible ambiguity combinations and determining which ones are feasible. The ambiguity search can be performed in either the position or ambiguity domain. Recent algorithms have concentrated on searching in the ambiguity domain. This is because when searching in the position domain, a very fine grid of points must be searched, thus the number of points to be searched within a given volume can be very large.

Several different search procedures are presented in the following pages. Each of these search procedures can be combined with any combination of the discrimination tests presented in the next section.

Ambiguity Function Method (AFM)

A well known search procedure in the position domain is the Ambiguity Function Method (AFM). The AFM was originally proposed by Counselman and Gourevitch (1981) and later implemented by Remondi (1984) and Mader (1990). The mathematical formulation can be written as follows:

$$AFM(x,y,z) = \frac{\sum_{p=1}^{K} \sum_{j=1}^{M-1} e^{i\theta}}{K(M-1)} \tag{3.17}$$

$$q = 2p\left(\Delta\nabla f^{j}_{obs} - \Delta\nabla f^{j}_{calc}\right) \tag{3.18}$$

where

$e^{i\theta}$ is the real + imaginary = $\cos\theta + i\sin\theta$

K is the number of epochs,

M is the number of satellites observed,

j denotes the given satellite.

The calculated phase double difference is evaluated at coordinates contained inside a given search volume. The search volume used by Remondi (1991) is $\pm 4\sigma_x$, $\pm 4\sigma_y$, and $\pm 4\sigma_z$, where the standard deviations are obtained from the covariance matrix of the initial code solution.

Since it is only the real component of $e^{i\theta}$ which is of interest, equation 3.17 reduces to

$$AFM(x,y,z) = \frac{\sum_{p=1}^{K} \sum_{j=1}^{M-1} \cos\theta}{K(M-1)} \tag{3.19}$$

When the AFM becomes greater than a predefined threshold, the correct ambiguities can be computed using the position corresponding to the largest AFM.

An important advantage of the AFM is that it is not affected by cycle slips. This is because the search is in the position domain as opposed to the ambiguity domain. The disadvantage of the AFM is that the grid within the search volume (which can be derived from the covariance matrix) must be very fine. This causes the number of points which must be searched to be very large and time consuming (Hein and Werner, 1995).

The number of search algorithms in the ambiguity domain far outnumber the procedures in the position domain. This is because the ambiguities must be integers, thus, there are exact integers which can be searched, while if the position domain is to be searched, the grid which must be searched is not explicitly defined.

The simplest search algorithm in the ambiguity domain is to compute the float ambiguities using either least squares or Kalman filter estimation (see Figure 3.1), arbitrarily define a search area, and search all possible combinations within that area. This, however, results in a very large number of possible combinations. For example, if there are seven satellites, and the search area is defined as ± 5 cycles, the result would be 10^6 possible double difference combinations. Even with a very fast computer, checking this many possibilities would not be practical for real-time applications.

Fast Ambiguity Resolution Approach (FARA)

An alternative to this method is the Fast Ambiguity Resolution Approach (FARA) as described by Frei and Beutler (1990) and Erickson (1992). This method involves computing the float solution and only analyzing the ambiguity combinations which pass two tests, namely,

$$P\left(N^j_{float} - x_{t,df,1-a/2}\, s_{N^j_{float}} \le N^j_{int} \le N^j_{float} + x_{t,df,1-a/2}\, s_{N^j_{float}}\right) = 1 - a \qquad (3.20)$$

and

$$P\left(N^{ij}_{float} - x_{t,df,1-a/2}\, s_{N^{ij}_{float}} \le N^{ij}_{int} \le N^{ij}_{float} + x_{t,df,1-a/2}\, s_{N^{ij}_{float}}\right) = 1 - a \qquad (3.21)$$

where

$$N^{ij} = N^{j} - N^{i}, \qquad (3.22)$$

$$s_{N_{ij}} = \sqrt{s^{2}_{N_i} - s_{N_i} s_{N_j} + s^{2}_{Nj}}, \qquad (3.23)$$

$1 - a$ is the significance level,

s_N is the standard deviation derived from the float solution,

df is the degrees of freedom,

x_t is student t distribution,

P() is the probability operator.

All ambiguity combinations passing both of the above tests are then again tested using a discrimination test (to be described in the next section).

The disadvantage of the FARA method compared to the AFM method is that it is effected by cycle slips. On the other hand, because the FARA search is in the ambiguity domain, the grid of possibilities is not as dense as that of the AFM, thus the number of points to be searched is smaller.

Least Squares Search

Another important search technique in the ambiguity domain is the least squares search (Hatch, 1991). In this procedure, a float solution is computed and a search is carried out using only four of the satellites, called the primary satellites. For each of the possible primary combinations, the integer ambiguities are solved for the remaining (secondary) satellites by using the position computed from the fixed primary satellites. The residuals for each of the combinations can then be computed and a discrimination test can be performed. This method is more efficient than the method that searches all possible ambiguities for all satellites because only the primary satellites combinations are

checked. It should be noted (Lachapelle et. al, 1992) that the least squares method and AFM method are equivalent in that they both select the integer ambiguity combination that minimizes the sum of the squared residuals. The main disadvantage of this method is that it is extremely sensitive to blunders. If a blunder occurs on one of the primary satellites, the computed positions will all be incorrect. If the blunder is large enough, it could cause the estimated position to be so far from the true position that the correct ambiguities will not be searched.

FASF

The Fast Ambiguity Search Filter, originally developed by Chen and Lachapelle (1994), has been selected for implementation in this thesis. The float solution was described in Section 3.3 and the Recursive Computation of Search Range strategy is described in the following.

Unlike the methods presented above, the Recursive Computation of Search Range (RSCR), which is the heart of the FASF algorithm, is recursive in nature. The ambiguities are assumed to be arranged in some order, i.e. N_1, N_2, ..., N_n, where n is the number of ambiguity states. If N_1 is considered known, all remaining states and covariances change, with the covariances getting smaller. To demonstrate the recursive nature, consider Figure 3.3. The unbroken arrows represent the floating ambiguities. The dashed arrow on the top graph represents a possible search point which lies within the 4 sigma search area. If the test ambiguity is assumed to be correct at this point, all other ambiguities and their corresponding variances change. That is, if this ambiguity is assumed to be correct, the variance of the other ambiguity states will decrease.

Figure 3.3 shows this reduction. Also, the value of the following ambiguity is changed. If the test integer ambiguities ambiguities are all correct, the following new ambiguities

(denoted by ~) will get closer to their correct integers. Even if one or more of the test ambiguities are set at the incorrect integer, the variances of the following new float ambiguities will keep getting smaller. If at any point in the test the new variance of the new float ambiguities does not include an integer, it can be assumed that an incorrect integer was chosen for one or more of the previous ambiguities. In this case, the search can be aborted before a full set is found. This method results in a minimal number of ambiguity sets which have to be tested with a discrimination test and is very efficient because many of the possible sets do not need to be fully searched.

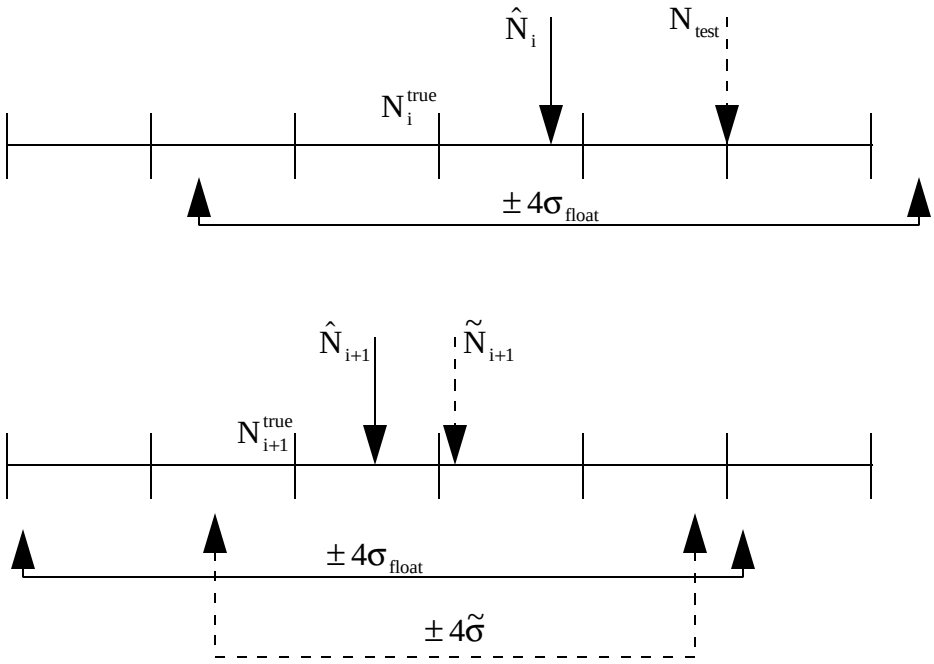

Figure 3.3 Effect of RSCR on Ambiguities

Mathematically, the n^{th} parameter can be removed from the covariance matrix $\mathbf{C}_{\hat{\mathbf{x}}}$ using the equations (Lu, 1995)

$$\mathbf{C}_{\tilde{\mathbf{x}}} = \mathbf{C}_{\hat{\mathbf{x}}} - \mathbf{c_n}\mathbf{c_n}^T / \left(\mathbf{C}_{\hat{\mathbf{x}}}\right)_{n,n} \tag{3.24}$$

$$\tilde{\mathbf{x}} = \hat{\mathbf{x}} - \mathbf{c_n}\left(N_{float} - N_{int}\right) / \left(\mathbf{C}_{\hat{\mathbf{x}}}\right)_{n,n} \tag{3.25}$$

$$\tilde{\Omega} = \Omega + \left(N_{float} - N_{int}\right) / \left(\mathbf{C}_{\hat{\mathbf{x}}}\right)_{n,n} \tag{3.26}$$

where $\tilde{\mathbf{x}}$ is the estimated parameters after the n^{th} parameter has been removed,

$\mathbf{c_n}$ is the n^{th} column of the covariance matrix,

$\left(\mathbf{C}_{\hat{\mathbf{x}}}\right)_{n,n}$ is the variance of the n^{th} parameter which is to be removed,

$\tilde{\Omega}$ is the recursively computed sum of squared residuals.

The recursive computation of the sum of squared residuals is another computational advantage of this method since the residuals are already computed once a complete set of integer ambiguities is found.

The number of points to be searched is the largest for the AFM search technique, followed by the FARA method, the least squares method, and the FASF method. Note that this should not be the only characteristic used to select a search method. For example, if the user experienced a great deal of cycle slips, the AFM method may be the best choice since it is not effected by cycle slips. Also, if the same distinguishing test is used for each of these methods, the number of epochs required to resolve the integer ambiguities will be similar.

Many other search procedures such as Cholesky decomposition (Landau and Euler, 1992) and integer programming methods (Wei and Schwarz, 1995) have been developed. In the following section the LAMBDA method is described.

3.3.3 LAMBDA Method

The Least squares AMBiguity Decorrelation Adjustment (LAMBDA) developed by Teunissen (1993) is neither a distinguishing test or a search algorithm, but a method to reparameterize the ambiguity states and their corresponding covariance matrix. It can be used in conjunction with any search technique which searches in the ambiguity domain. The reparameterization is done in such a way that the number of potential ambiguity sets is reduced.

In general, the confidence ellipsoid of an ambiguity state is extremely elongated due to the high correlation between the ambiguity states (see Figure 3.4). Unfortunately, when solving for ambiguities on the fly, only a very short period of observation is allowed, so the multi-dimensional confidence ellipsoid remains extremely elongated due to the high correlations between ambiguity states. The result of an extremely elongated ellipsoid is a larger search area. The main goal of the LAMBDA method is to transform the ambiguity states in such a way that the correlation between them is minimized. In Figure 3.4, the confidence ellipses for a two dimensional case is shown. Although the actual area of the two ellipses remains the same before and after the LAMBDA transformation, the corresponding area in the box around the second ellipse, which represent the search area, becomes smaller as the ellipse approaches a sphere.

If the ambiguity covariance matrix $\mathbf{C}_{\hat{\mathbf{n}}}$, which is a subset of $\mathbf{C}_{\hat{\mathbf{x}}}$, is decomposed in such a way that (de Jong and Tiberius, 1996)

$$\mathbf{C}_{\hat{\mathbf{n}}} = \mathbf{L}^{\mathrm{T}}\mathbf{D}\mathbf{L} \tag{3.27}$$

where $\mathbf{L}$ is a lower triangular matrix,

$\mathbf{D}$ is a diagonal matrix,

and a matrix $\mathbf{Z}$ could be found such that

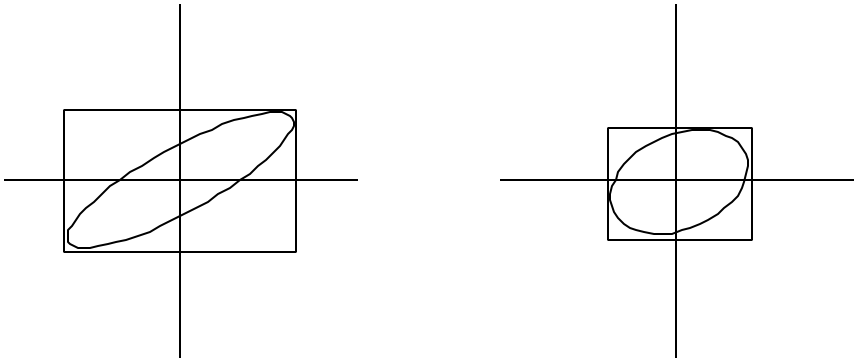

Before LAMBDA After LAMBDA

Figure 3.4 Confidence Ellipses and Search Regions

$$\hat{\mathbf{z}} = \mathbf{Z}^{\mathrm{T}}\hat{\mathbf{n}} \tag{3.28}$$

$$\mathbf{C}_{\hat{\mathbf{z}}} = \mathbf{Z}^{\mathbf{T}}\mathbf{C}_{\hat{\mathbf{n}}}\mathbf{Z} = \mathbf{Z}^{\mathbf{T}}\mathbf{L}^{\mathrm{T}}\mathbf{D}\mathbf{L}\mathbf{Z} \tag{3.29}$$

where $\hat{\mathbf{z}}$ is the transformed ambiguities,

$\mathbf{Z}$ is the transformation matrix,

$\hat{\mathbf{n}}$ is the adjusted ambiguities,

$\mathbf{C}_{\hat{\mathbf{z}}}$ is the covariance matrix of the transformed ambiguities,

the matrix $\mathbf{Z}$ could be selected such that it was equal to $\mathbf{L}^{-1}$ which would result in equation 3.29 reducing to $\mathbf{C}_{\hat{\mathbf{z}}} = \mathbf{D}$ which has no correlation between ambiguities and thus a completely spherical confidence ellipsoid.

Unfortunately, there are three conditions which the Z-transformation must conform to (Teunissen, 1994). The first is that the transformation must retain the integer values of the ambiguities. By selecting $\mathbf{Z} = \mathbf{L}^{-1}$, this condition is not met. The second condition is that the transformation must preserve the volume of the multi-dimensional confidence ellipsoid. Finally, the product of all ambiguity variances must be reduced, otherwise there will not be a reduction in the number of possible ambiguity combinations. This condition comes from the fact that if the magnitude of the diagonal terms of a covariance matrix are reduced, the result is a reduction of the non-diagonal terms.

One of the transformations that satisfies all of the requirements is the Gauss transformation. For a two dimensional case, this transformation can be represented as

$$\mathbf{Z} = \begin{bmatrix} 1 & 0 \\ \alpha & 1 \end{bmatrix} \tag{3.30}$$

By setting α to $-\left[\frac{\sigma_{n_1 n_2}}{\sigma_{n_1}}\right]$ full decorrelation is achieved and the last two conditions are satisfied. The first condition, however, requires that α be an integer. Thus, an approximation must be made by rounding α to the nearest integer value. Finally, for maximum decorrelation, it may be necessary to rearrange the order of the ambiguities. For a complete multi-dimensional description of the formation of the $\mathbf{Z}$ matrix, see de Jong and Tiberius (1996).

As previously mentioned, the LAMBDA method is a transformation of the ambiguity states and a search algorithm is still required. The main advantage of the LAMBDA method is a reduction in the number of possible ambiguity combinations, resulting from the reduction in the product of the ambiguity variances. It should be noted that because of this reduction in the number of possible combinations (see Figure 8.3), the LAMBDA method is highly efficient for real-time applications. In terms of reliability, this method is still limited by the effectiveness of the test used to select the single correct set of integer ambiguities. A comparison between the FASF algorithm and the LAMBDA augmented FASF algorithm is given in Chapter 8.

3.3.4 Distinguishing Tests

Determining the correct integer ambiguity set (out of many candidate sets) is perhaps the greatest challenge for OTF positioning. All methods use a test (or combination of tests) to try to isolate the correct ambiguity set. If the tests are too conservative, the ambiguity

resolution may take too long, while if the tests are too optimistic, the reliability of the results may be significantly decreased.

One common test is the ratio test which is a comparison of the smallest sum of squared residuals to the second smallest, i.e.

$$\frac{\Omega_2}{\Omega_1} > \text{threshold}_1 \tag{3.31}$$

where

Ω_1 is the smallest sum of squares of the residuals residuals in metres,

Ω_1 is the second smallest sum of squares of the residuals in metres.

Landau and Euler (1992) suggest a threshold of 2, though this may be somewhat optimistic for many operational environments.

Another test used by Chen and Lachapelle (1994), Wei and Schwarz (1995), and Han and Rizos (1996) is

$$\frac{\Omega'_2}{\Omega'_1} > \text{threshold}_2 \tag{3.32}$$

where $$\Omega' = \left(\mathbf{N_{float}} - \mathbf{N_{int}}\right)^{\mathrm{T}} \mathbf{C}_{\hat{\mathbf{N}}}^{-1} \left(\mathbf{N_{float}} - \mathbf{N_{int}}\right) \tag{3.33}$$

$\mathbf{N_{float}}$ is a vector of the floating ambiguity states,

$\mathbf{N_{int}}$ is a vector of the potential fixed ambiguity states,

$\mathbf{C}_{\hat{\mathbf{N}}}$ is the covariance matrix for the float ambiguity states.

This test is actually very similar to the ratio test in equation 3.31. It was shown in Chen and Lachapelle (1994) that:

$$\Omega_{\text{fixed}} = \Omega_{\text{float}} + \Omega' \tag{3.34}$$

where Ω_{fixed} and Ω_{float} are the sum of squared residuals for the fixed and float ambiguity solutions. Thus, the only difference between equation 3.31 and 3.32 is a constant factor (the floating sum of squared residuals) which is added to both the numerator and

denominator of equation 3.31. This means that if identical thresholds were used for both tests, equation 3.31 would be slightly more conservative than equation 3.32. One of the advantages of using equation 3.32 is that the sum of squared residuals can be computed recursively (Chen and Lachapelle, 1994).

Wei and Schwarz (1995) also recommend using the following criteria to identify the correct ambiguity set:

$$\Omega'_1 < \text{threshold}_3 \,,\ \Omega'_2 > \text{threshold}_4 \tag{3.35}$$

which is similar to equation 3.32 in that this can also be interpreted as a ratio. There is, however a distinct difference between the ratio test in that the minimum sum of squared residuals must be below a given threshold. In situations where the correct ambiguity set is accidentally discarded, this test may offer more protection against choosing an incorrect set because an incorrect set may be larger than the given threshold.

All of the above tests are based on the assumption that the observations are free of blunders and biases. Unfortunately, this is rarely true in the case of GPS observations. The existence of multipath, atmospheric, and other errors cause effectiveness of these tests to be reduced. If all errors were truly Gaussian in nature, any of the above tests would be sufficient and each test would perform similar to one another if appropriate thresholds were chosen. Two more sophisticated discrimination tests were developed by Han (1995) which make use of internal and external reliability theory (Krakiwsky and Abousalem, 1993). By assuming that the true ambiguity set is the one with either the smallest or second smallest sum of squared residuals, the two sets undergo blunder detection to try and determine which set has the blunder (incorrect ambiguity). Again, this method is based upon the assumption that only one blunder exists and that all other errors are Gaussian in nature.

CHAPTER 4
AMBIGUITY RESOLUTION OVER VARYING BASELINES

In this chapter, the effects of different errors on OTF ambiguity resolution are investigated. This is achieved by analyzing data over various baseline lengths and examining the residuals. The data sets are processed in two modes, the first with all satellites available and the second with a reduced satellite constellation. The reason for the analysis under a reduced geometry is to asses effect of the reduced geometry on both the number of epochs required for ambiguity resolution and the reliability of the solution. The maximum baselines over which L1 ambiguity resolution can be achieved is presented, along with widelane results and the behavior of the time to resolution under varying conditions.

4.1 Data Description

Data were collected during the last two weeks of September 1996 along a straight portion of Highway #1 west of the Calgary city limits. A monitor station was first positioned relative to the known pillars on the roof of the engineering building at The University of Calgary. From this monitor station, sites were positioned at intervals of approximately 2 km for the first 16 km, followed by stations at distances of 20 km, 25 km, 30 km, 35 km, 40 km, and 50 km. Each data set was collected under the same satellite constellation to ensure that geometry effects were consistent from one data set to the next. This was achieved by collecting data on sequential days (adjusted for the 236s difference between the solar and sidereal day).

The data sets were collected using NovAtel MiLLennium^{TM} dual frequency receivers and chokering antennas mounted on tripods. Dual frequency receivers were chosen so that widelaning could be performed. The chokering antennas were selected in order to minimize the multipath effects. All data sets were collected at a rate of 1 Hz for a period of 1 to 1.5 hours.

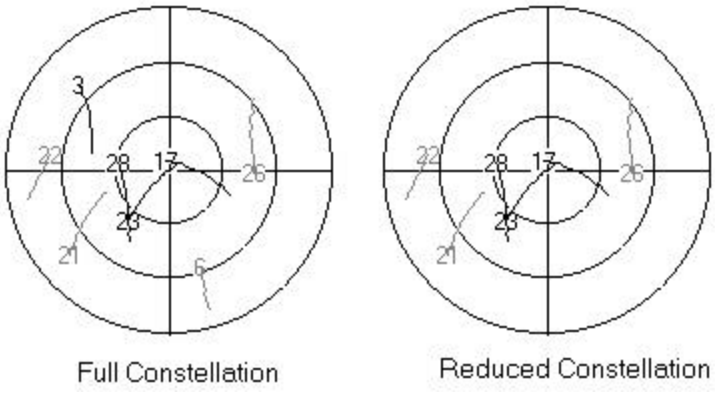

Figure 4.1 Visible Satellites

To allow for a complete analysis, the observation window was chosen such that a large number of satellites (Figure 4.1) was visible with low Dilution Of Precision (DOP) (Figure 4.2).

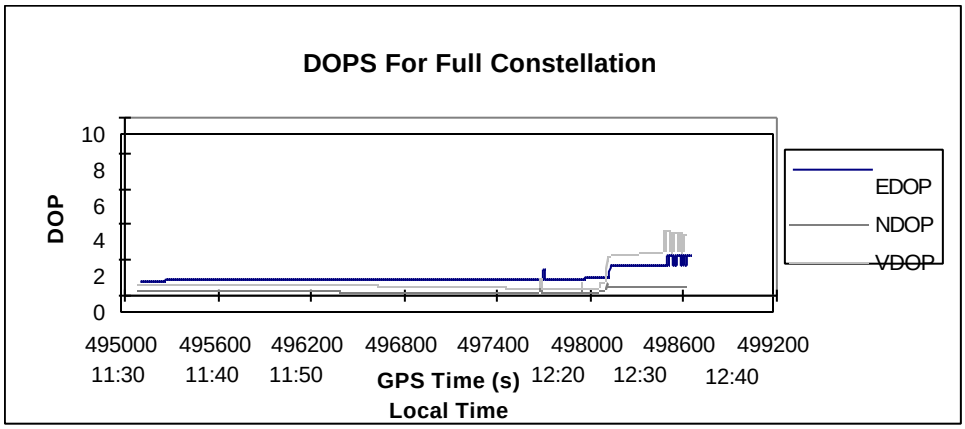

Figure 4.2 Dilution of Precision for Full Constellation

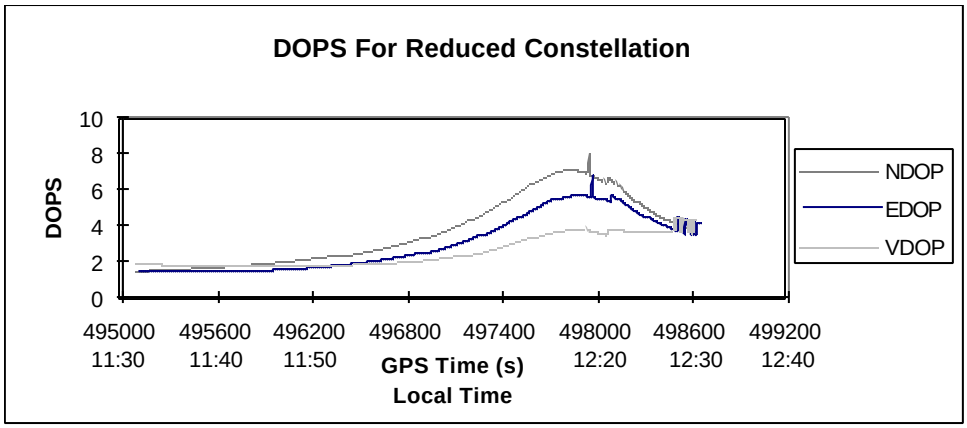

Figure 4.3 Dilution Of Precision for Reduced Constellation

To allow for analysis under a poorer geometry, satellites 6 and 3 were rejected from the solution. These satellites were chosen because the resulting DOPs (Figure 4.3) became considerably worse.

4.2 Processing Software

The software SFLY, which was developed by the author, is based on FLYKIN^{TM}, which is an OTF ambiguity resolution program written at The University of Calgary (Chen and Lachapelle, 1994). SFLY makes use of a Kalman filter for a float solution, the FASF search strategy, and the ratio test for the distinguishing test. It makes use of both pseudorange and carrier phase observations.

The FASF search strategy used a 3σ search range for each ambiguity state. The distinguishing test was the ratio test given in equation (3.21). This test was chosen because it was easily computed in a recursive manner. The threshold used was 4.0. This is a fairly high threshold, compatible with the main goal of the software which was reliability.

It should be noted that a threshold was implemented for the maximum number of possible ambiguity combinations to be searched. If there were more than 2000 possible ambiguity combinations, the search was aborted and the float solution was used. The reasoning behind this is that if there are too many possible combinations, the probability of choosing the correct solution is less likely. Also, this limits the computational burden. The drawback of using this threshold is that it can increase the number of epochs required to resolve the integer ambiguities.

In an attempt to minimize the number of blunders entering the filter, a method of checking innovation sequences was implemented. Two measures of quality control were also implemented to ensure that the chosen integer ambiguities were indeed the correct ones. The first was a comparison of the float solution with the fixed solution. If the fixed ambiguity solution was not within the three sigma threshold of the float solution, the integers were assumed to be incorrect, and a new search was initiated. The second test was a residual test. If any residual exceeded a certain threshold, which was chosen depending upon the approximate baseline length and observable, it was again assumed that the incorrect ambiguities had been chosen and the search was reinitialized. The thresholds used are shown in Table 4.1. These values were decided upon after processing many data sets at various baselines.

Table 4.1 Residual Tolerances

	Observable	
Baseline (km)	L1-only	Widelane
<1 km	2.5 cm	3.5 cm
>1 km	3.0 cm	4.0 cm

4.3 Baseline Effects on Ambiguity Resolution

Figures 4.4 and 4.5 show the number of epochs required to resolve the ambiguities as a function of baseline length using L1 code and carrier phase observables. Each line in the figure represents a different baseline length. In general, the longer baselines result in longer times required to resolve the integer ambiguities.

Several irregularities are apparent in the figures. First, the 14 km data in Figure 4.5 seems to have a rather linear trend throughout the graph. This indicates that the ambiguities are being solved for at approximately the same epoch regardless of the starting point.

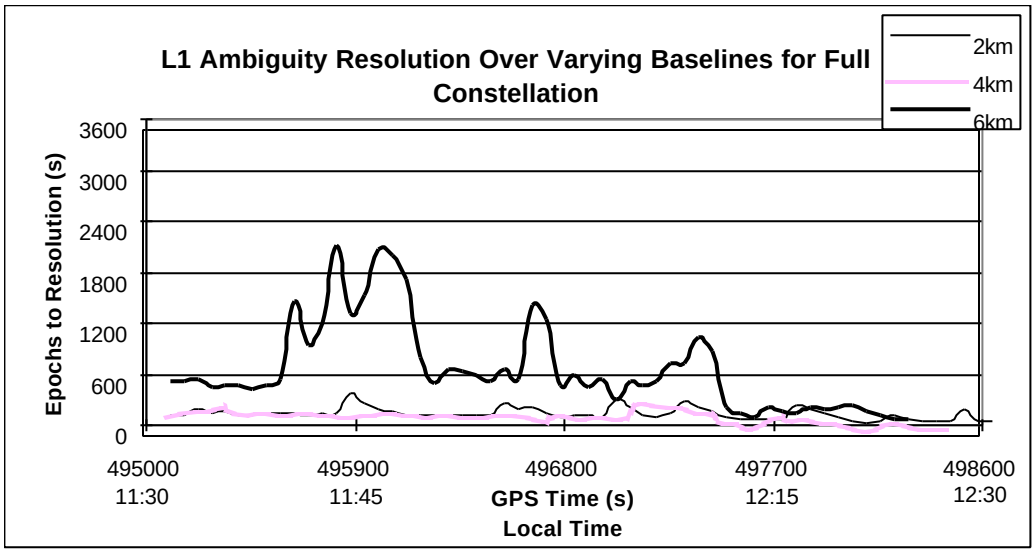

Figure 4.4 L1 Ambiguity Resolution Over Varying Baselines (Full Constellation)

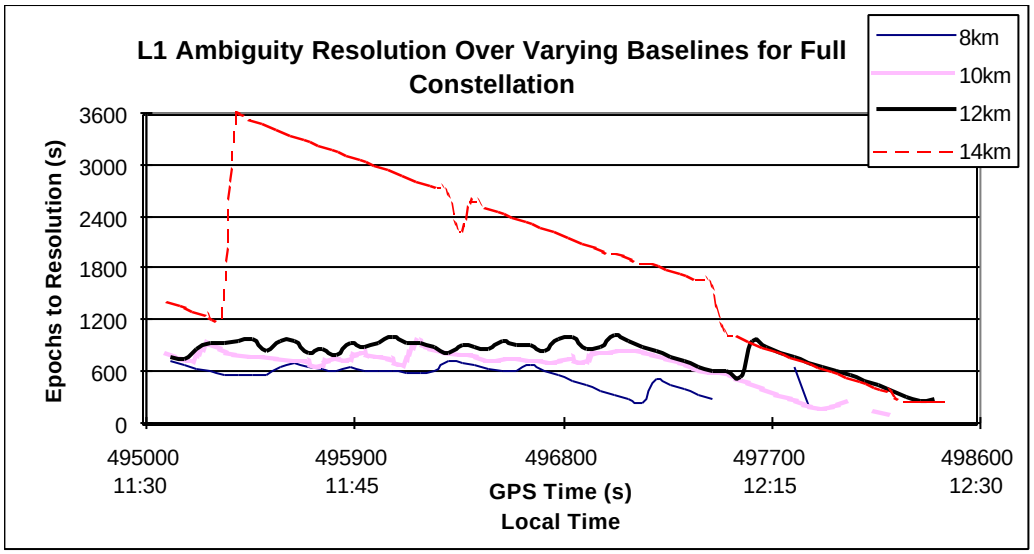

Figure 4.5 L1 Ambiguity Resolution Over Varying Baselines (Full Constellation)

After closely examining the data, it was found that the remote receiver lost lock on all satellites at approximately 12:27. This caused the filter to reset the float solution and search procedure. Thus, although the start time may have been before this time, the filter was always the same after 12:27. The second irregularity appeared in the 6 km data. As shown in Figure 4.4, it does not follow the same general trend as the other baselines. Because this data was collected the same day as other data sets, it is not likely due to the monitor station data. The line does, however, have somewhat of a sinusoidal trend which could be due to multipath. Unfortunately, carrier phase multipath is very difficult to isolate. Some indication can be found by analyzing the fixed ambiguity phase residuals. Figure 4.6 shows these residuals for satellite number 3, which is a low elevation satellite. There are noticeable dips in the residual plot at approximately the same times as the poor times to ambiguity resolution in Figure 4.4. This point was also near a large metallic road sign, which points to multipath.

It should be noted that there is somewhat of a large residual at approximately 12:20 which suddenly drops to expected values. This is due to satellites 22 and 6, which both

drop below the ten degree cutoff at nearly the same time. Because of the two low satellites, the residuals are somewhat larger than after these two satellites leave the solution.

After 14 km for the full constellation, ambiguity resolution becomes extremely difficult. The correct integer ambiguities either could not be solved for at all, or were solved incorrectly. In all cases, incorrect ambiguities are excluded from the figures.

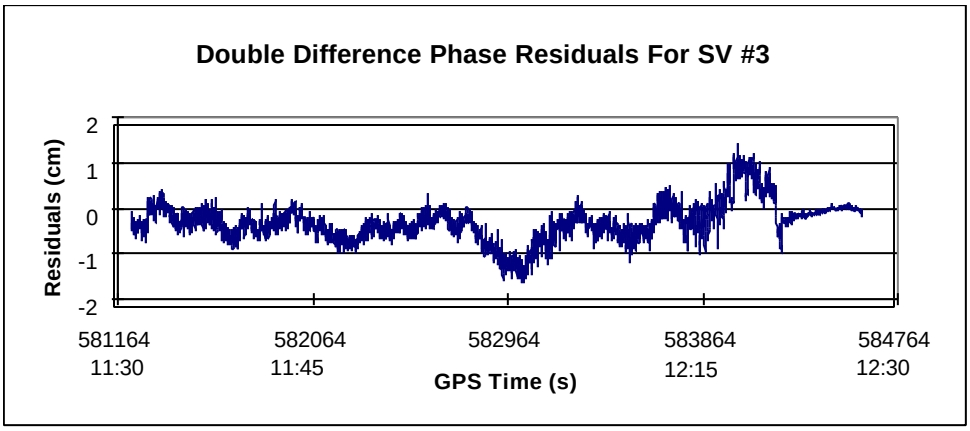

Figure 4.6 Double Difference Phase Residuals For SV #3

Figures 4.7 to 4.11 show the time to ambiguity resolution as a function of baseline using L1 pseudorange and widelane carrier phase observables. Each figure shows several different baselines varying from 2 km to 50 km. Note the scale change in Figure 4.11. In these figures it can be seen that under the given conditions, the results seem to indicate that widelane data is less sensitive to the monitor rover separation. This is expected as the wavelength of the widelane is approximately 4.5 times greater than that of L1, thus, atmospheric errors which are large enough to cause problems for the much smaller L1 wavelength will not have as great an effect on the widelane observable. Also, there is a peak at approximately 12:00 local time for the 40 km and 50 km baselines. This is the effect of several cycle slips at the monitor station. It is also noticeable that the plots

become increasingly more volatile as the baselines increase. Again, this is due to the differential errors which gradually dominate the error budget at larger distances.

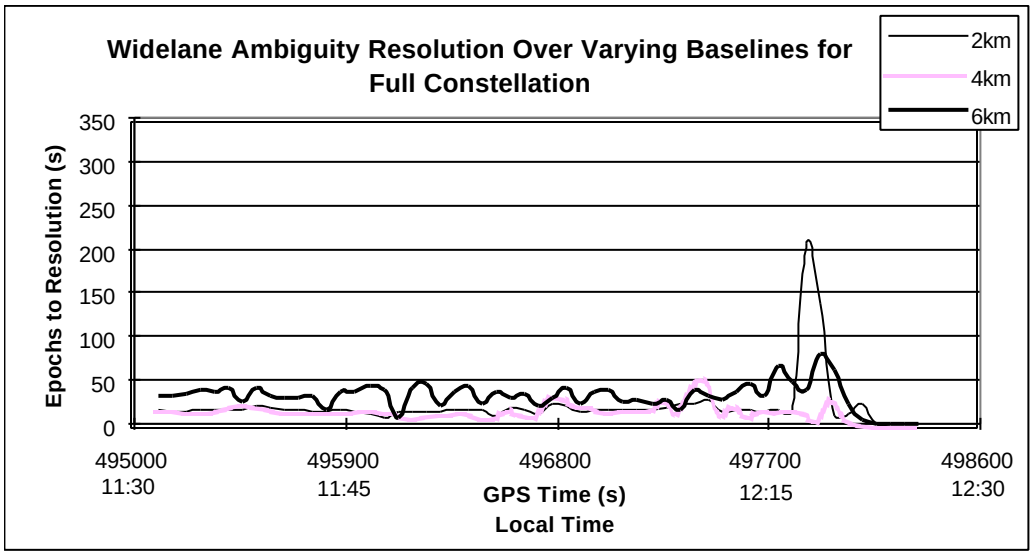

Figure 4.7 Widelane Ambiguity Resolution Over Varying Baselines (Full Constellation)

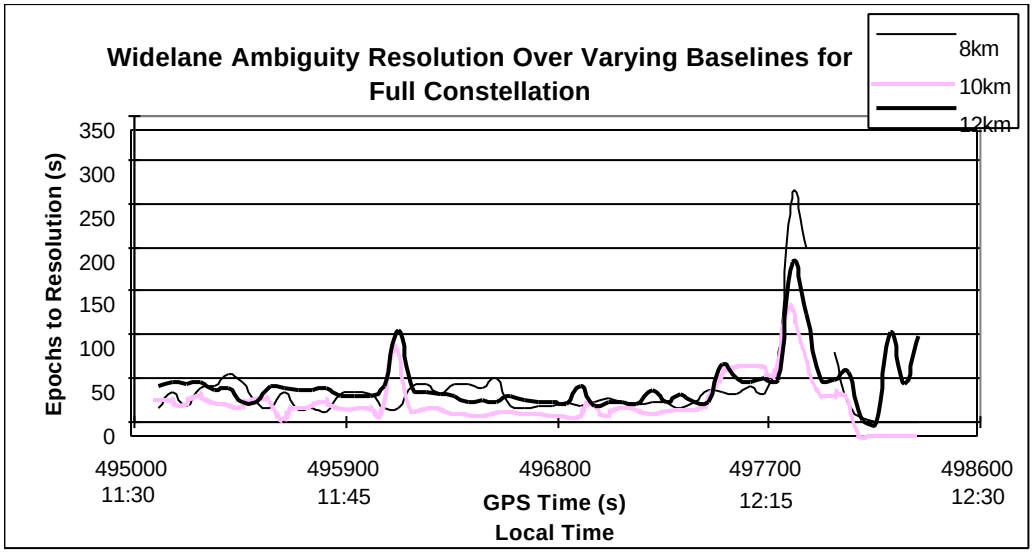

Figure 4.8 Widelane Ambiguity Resolution Over Varying Baselines (Full Constellation)

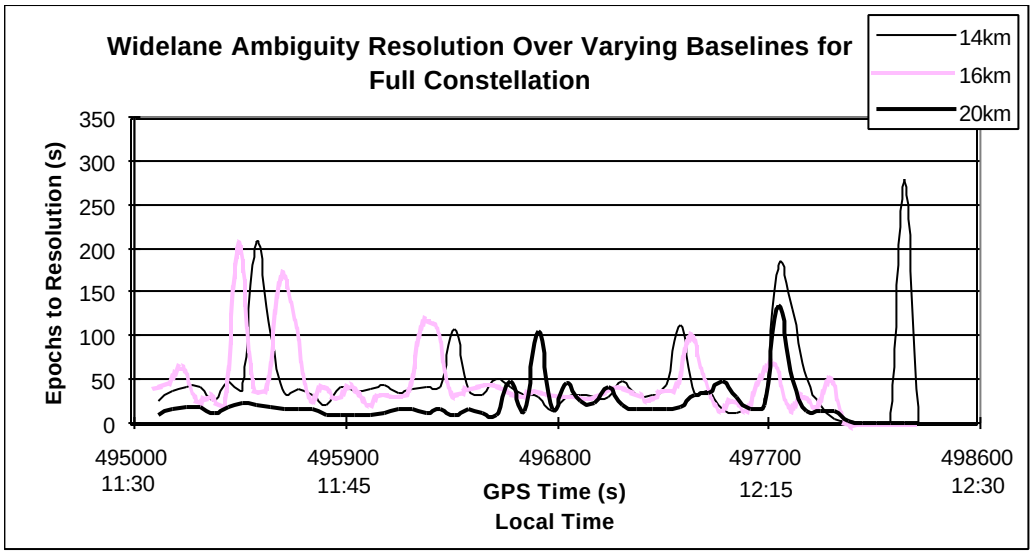

Figure 4.9 Widelane Ambiguity Resolution Over Varying Baselines (Full Constellation)

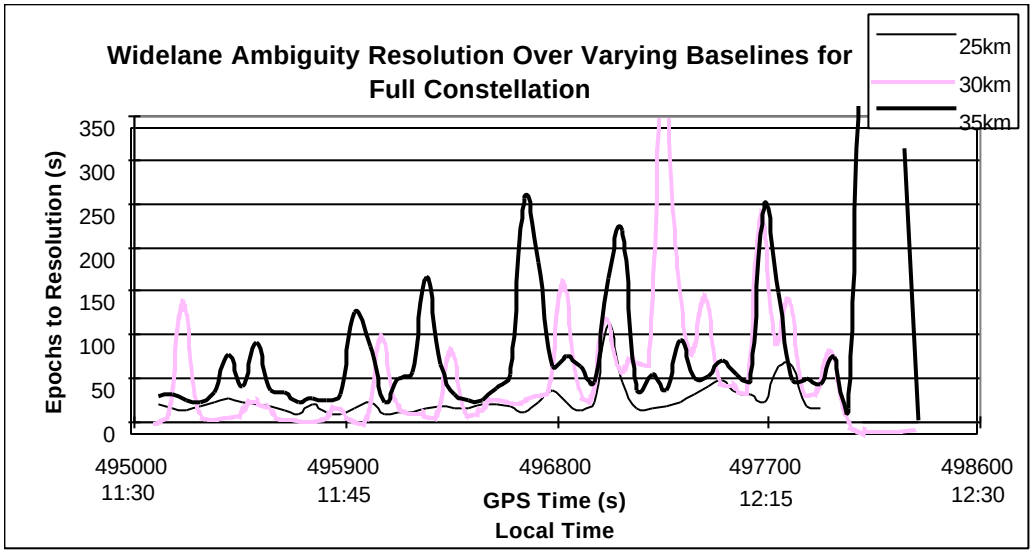

Figure 4.10 Widelane Ambiguity Resolution Over Varying Baselines (Full Constellation)

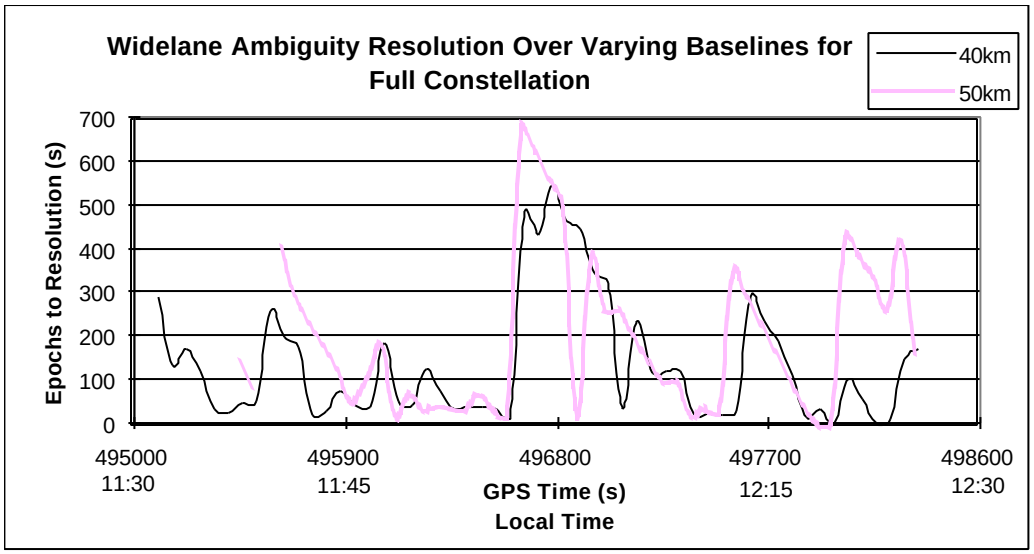

Figure 4.11 Widelane Ambiguity Resolution Over Varying Baselines (Full Constellation)

In several instances, SFLY solved the incorrect integer ambiguities and detected these incorrect parameters before any output. This resulted in a filter reset which again can account for some of the larger times to resolution.

Figures 4.12 and 4.13 show the time to ambiguity resolution as a function of baseline length for the reduced geometry when using the L1 pseudorange and carrier phase observables. These figures are quite similar to Figures 4.4 and 4.5. The 14 km baseline is not included in the figure as the correct ambiguities were rarely found. Again, the baseline effect is obvious as the larger baselines result in longer times to resolution.

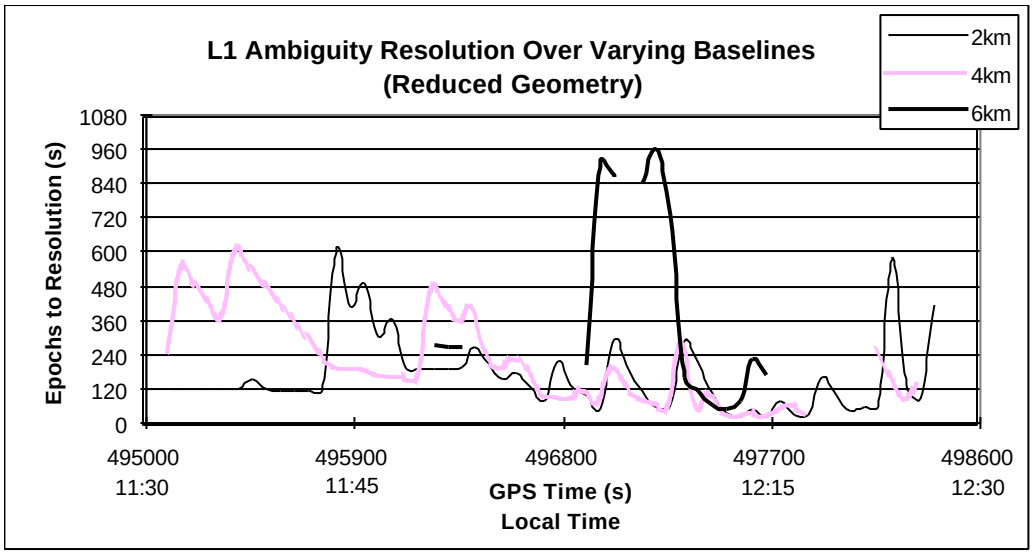

Figure 4.12 L1 Ambiguity Resolution Over Varying Baselines (Reduced Constellation)

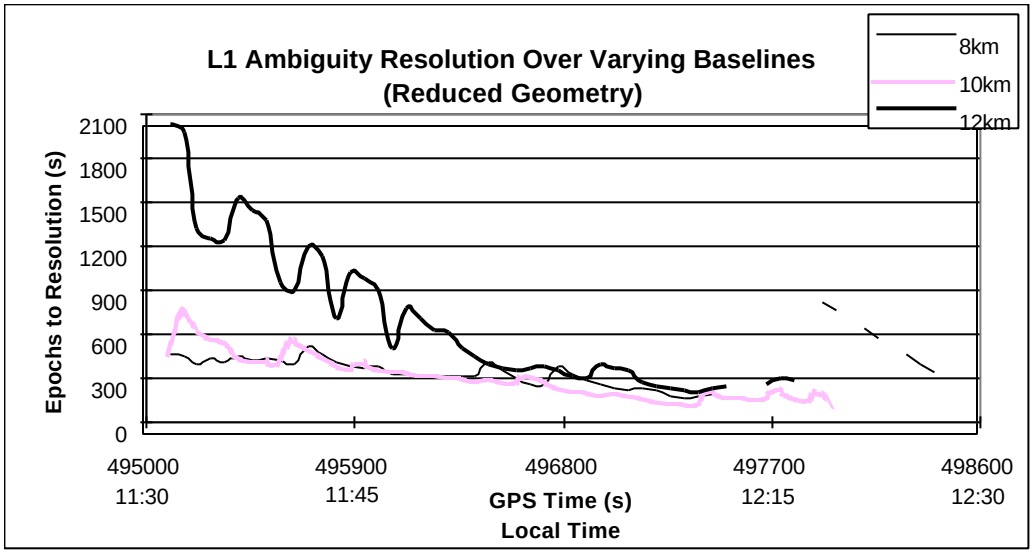

Figure 4.13 L1 Ambiguity Resolution Over Varying Baselines (Reduced Constellation)

Figures 4.14 to 4.18 show the times to ambiguity resolution for the various baselines for the L1 pseudorange and widelane carrier phase observables. All figures are for the reduced geometry case. Under the reduced geometry, the baseline effects become more

obvious. This is likely because there are less observations for the errors to be spread amongst.

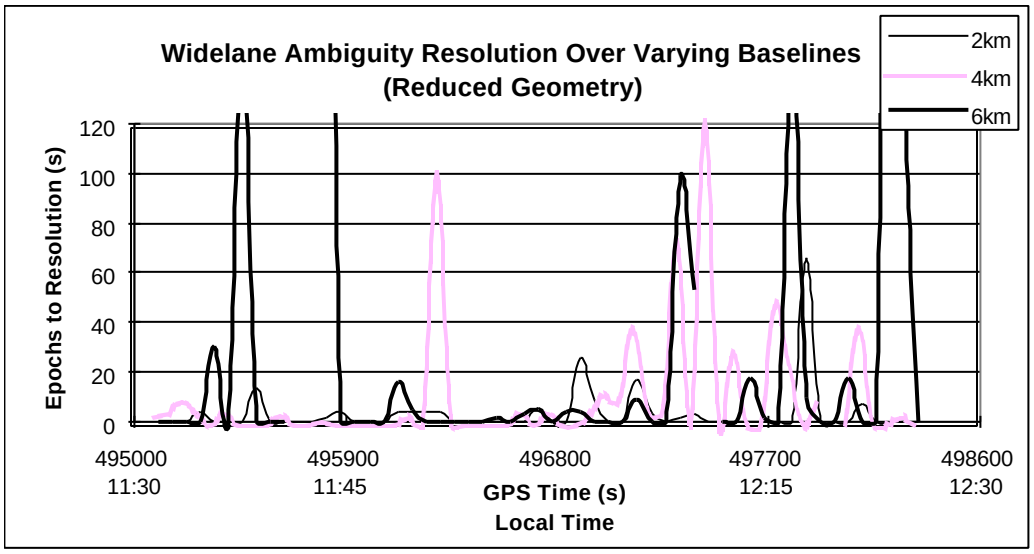

Figure 4.14 Widelane Ambiguity Resolution Over Varying Baselines (Reduced Constellation)

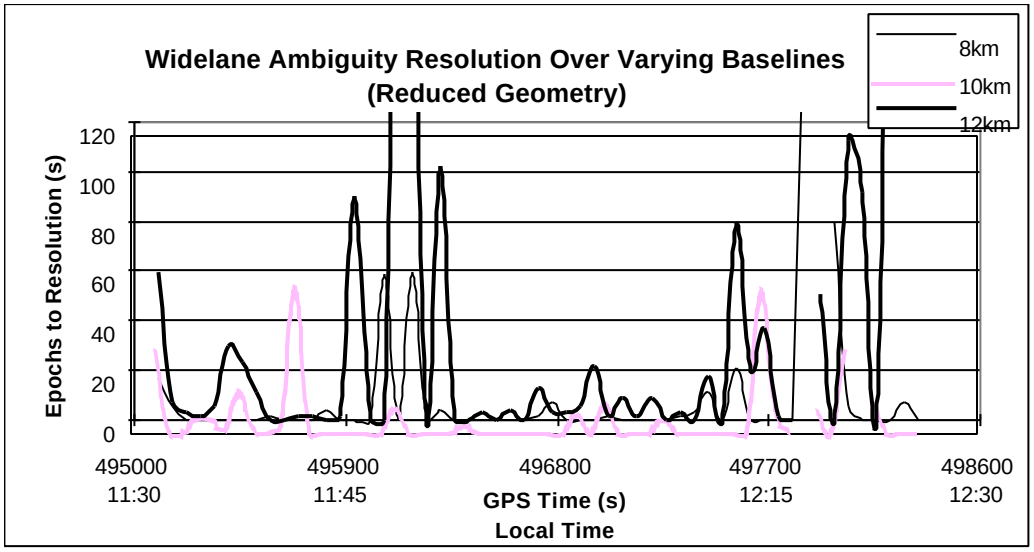

Figure 4.15 Widelane Ambiguity Resolution Over Varying Baselines (Reduced Constellation)

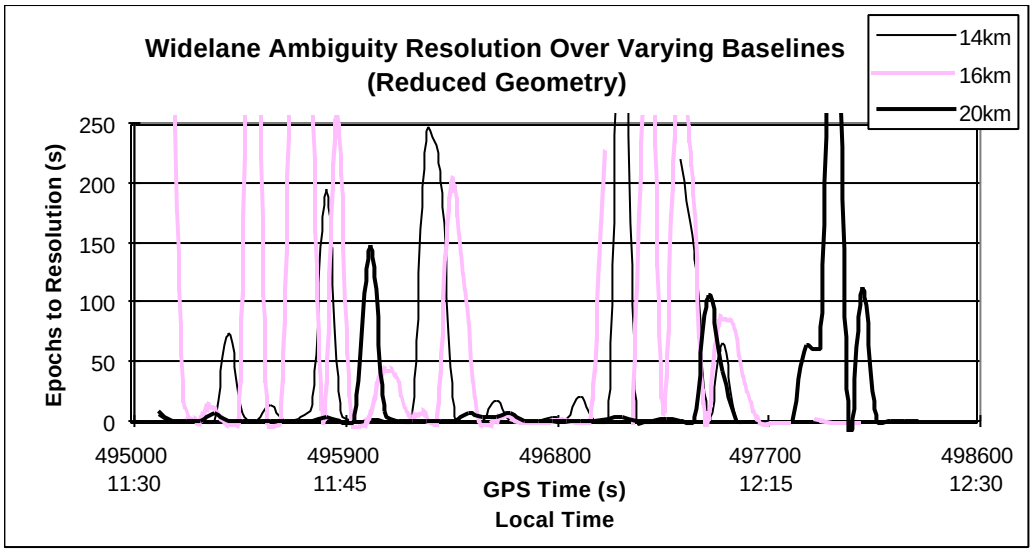

Figure 4.16 Widelane Ambiguity Resolution Over Varying Baselines (Reduced Constellation)

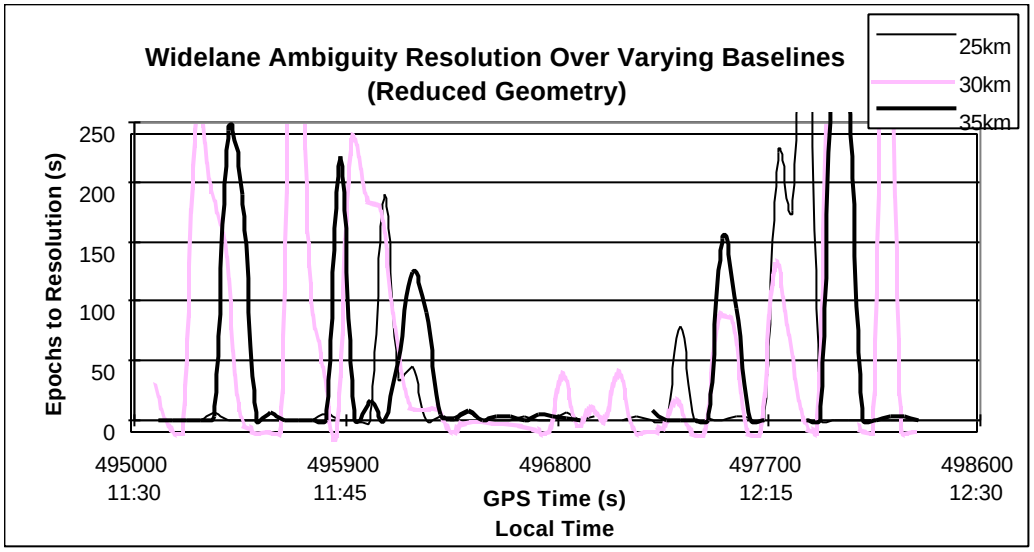

Figure 4.17 Widelane Ambiguity Resolution Over Varying Baselines (Reduced Constellation)

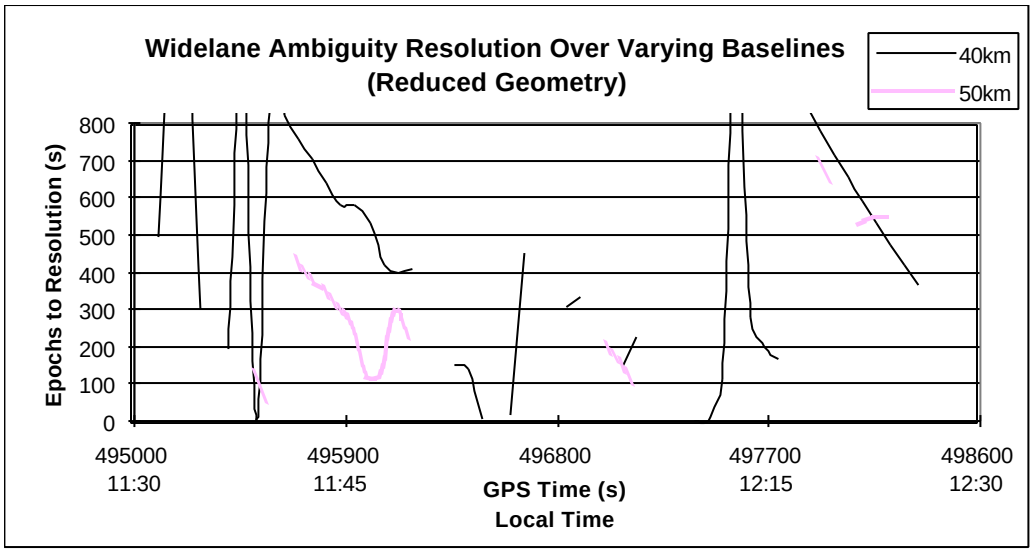

Figure 4.18 Widelane Ambiguity Resolution Over Varying Baselines (Reduced Constellation)

Figures 4.19 and 4.20 show how the percentage of incorrectly resolved ambiguities varies as a function of baseline length. It can be seen that for the L1 case, the baseline length affects the time to resolution more than it effects the reliability of the solution.

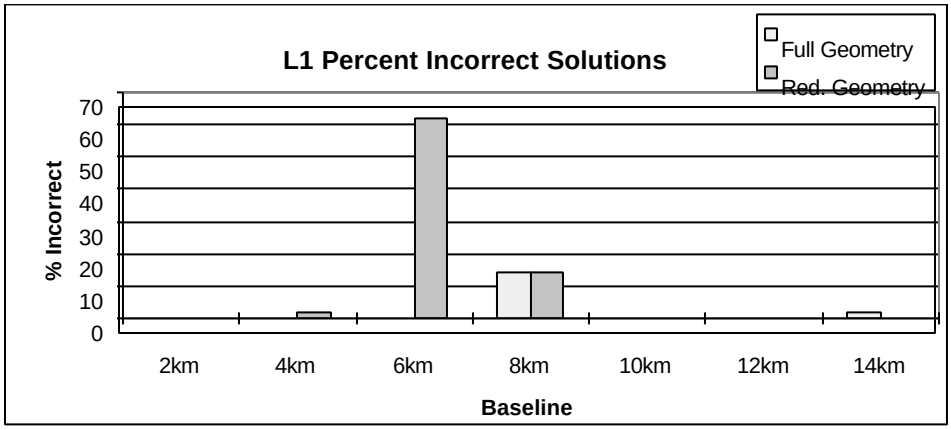

Figure 4.19 L1 Percent Incorrectly Resolved Ambiguities

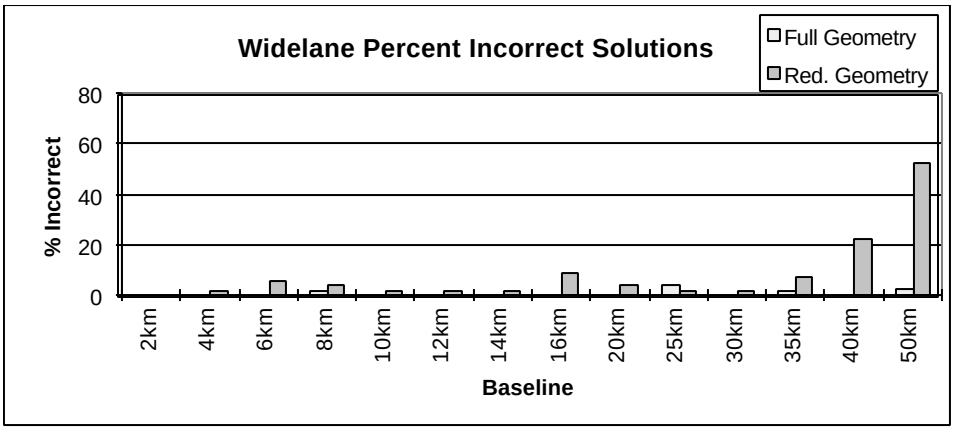

Figure 4.20 Widelane Percent Incorrectly Resolved Ambiguities

Under the given conditions using the SFLY software, the widelane solutions appear to become more susceptible to incorrect ambiguities at longer baselines, especially under the reduced geometry. This is most likely due to the differential atmospheric errors which begin to enter the observations.

4.4 Geometry Effects on Ambiguity Resolution

The influence of geometry on ambiguity resolution comes in several different forms. First, the maximum distance in which the ambiguities can be correctly resolved is decreased. When using the L1-only carrier phase observable under the given conditions, the ambiguities could only be confidently resolved up to approximately 12 km for the reduced constellation while 14 km could be achieved for the full constellation. Second, the time to resolution becomes more unpredictable and irregular. This can be seen in Figures 4.14 to 4.18.

Finally, Figures 4.19 and 4.20 show that the reliability of the resolution decreases. When poor geometric conditions are combined with non-Gaussian errors such as multipath, as is the case for the 6 km baseline, reliable ambiguity resolution becomes difficult.

Figures 4.21 and 4.22 show the RMS epochs to integer ambiguity resolution under both the full and reduced constellations for the L1-only and the widelane cases respectively. It should be noted that the reduced geometry results for the 6 km and 14 km baselines are not shown in Figure 4.21. This is because so few correct ambiguities were found throughout the tests. The figures show that the time to ambiguity resolution is not always shorter in better geometry. There are several reasons for this. The first reason is discussed by Hatch (1991) and that is with poorer geometry (i.e. less satellites), the number of integer combinations decreases. Thus, with less possibilities, the correct ambiguities may be easier to isolate in some cases. However, in other cases, because of the weaker geometry and/or multipath, the residuals from the incorrect ambiguity set may at times be smaller than the residuals from the correct set, thus making resolution take longer. Figure 4.23 shows how the sum of squared residuals varies as a function of time for the situation shown in Figure 4.2 in which the DOPs are ideal. The correct ambiguity set is obvious and can be chosen quite quickly.

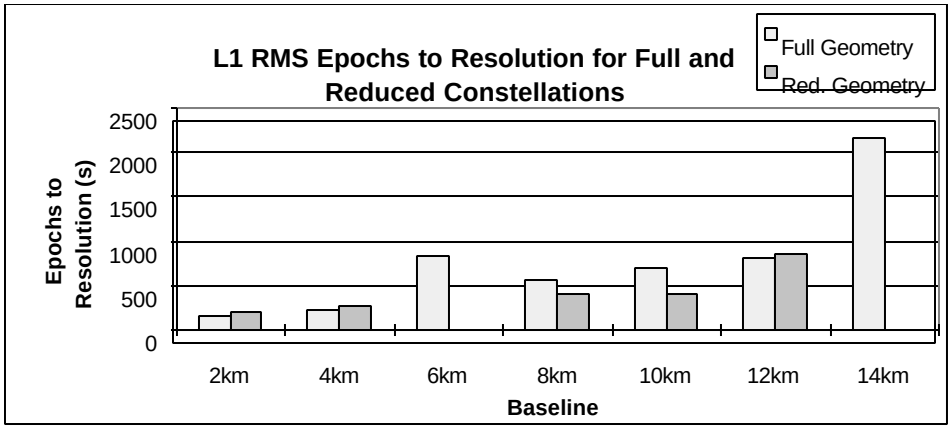

Figure 4.21 L1 RMS Epochs to Resolution for Full and Reduced Constellations

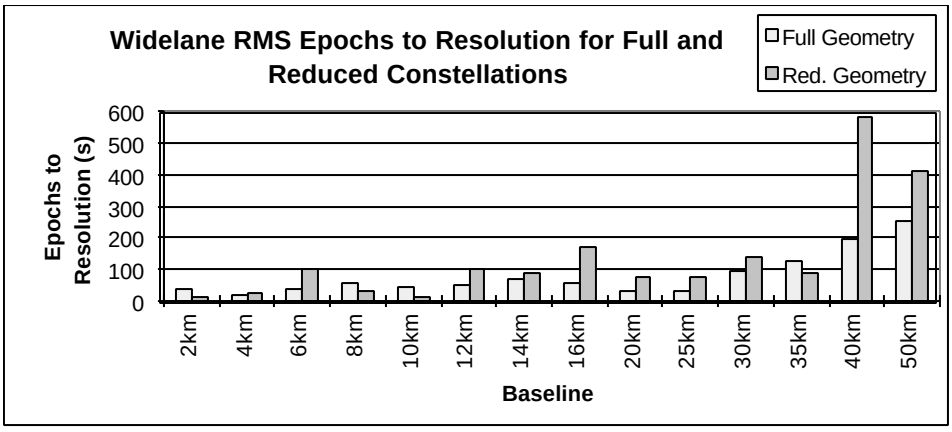

Figure 4.22 Widelane RMS Epochs to Resolution for Full and Reduced Constellations

On the other hand, in cases of poor geometry, as shown in Figure 4.3, the smallest sum of squared residuals may not always be the correct one. Figure 4.24 shows how the sum of squared residuals for both the correct ambiguity set and the second best ambiguity set vary. At approximately 11:37, the incorrect ambiguities would have been chosen if the ratio test was less than 2.0 as the incorrect sum of squared residuals is significantly smaller than the correct sum of squared residuals. Unfortunately, in cases such as this, the ratio test may accept the incorrect integer set.

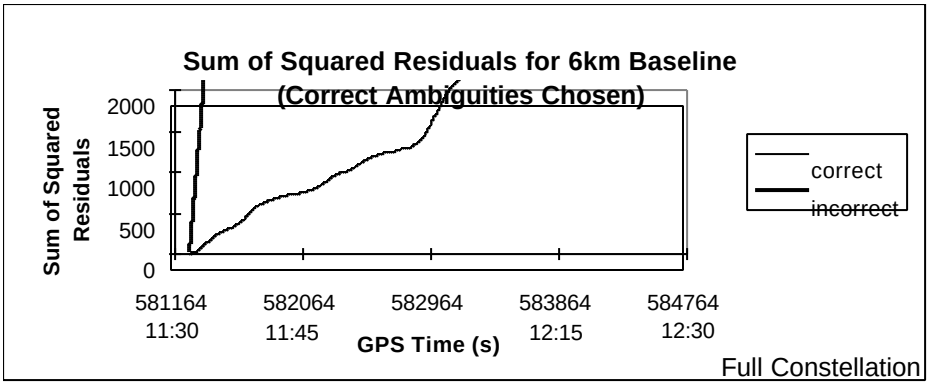

Figure 4.23 Sum of Squared Residuals When Correct Ambiguities Chosen

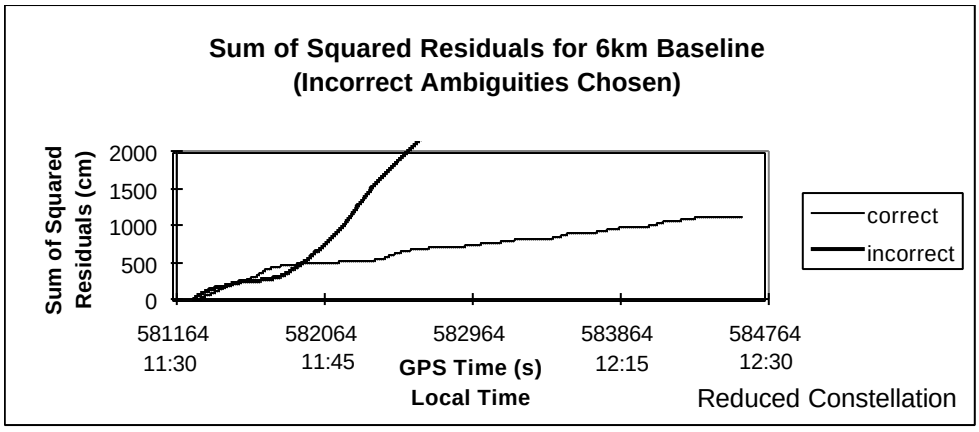

Figure 4.24 Sum of Squared Residuals When Incorrect Ambiguities Could Be Chosen

The effects of geometry on the reliability of choosing the correct ambiguities are shown in Figures 4.19, 4.20, 4.25, and 4.26. Figures 4.19 and 4.20 show that the reliability of correct ambiguity fixing is more a function of geometry than a function of baseline length. Figures 4.25 and 4.26 were formed by breaking all baseline data sets into five minute time intervals and taking the percent of the incorrect ambiguities found for each interval. Both figures are for the reduced constellation shown in Figure 4.1. Because very few incorrect ambiguities were chosen for the full constellation, similar plots are not shown. Comparing Figure 4.26 to 4.3, it is obvious that the majority of incorrect solutions occurred during the period of poorest geometry in the widelane case. The L1 case does not show the same results. The errors seem to be more evenly spread throughout the data set. The larger number of incorrect ambiguities found when the satellite constellation was reduced must be due to a combination of fewer satellites and the effects of multipath. The reason the L1 phase observable is affected more by the number of satellites than the actual geometry is because of the much shorter wavelength. With fewer observations for the non-Gaussian errors to be smoothed throughout, the errors (such as multipath) have a more significant effect than when more satellites are available.

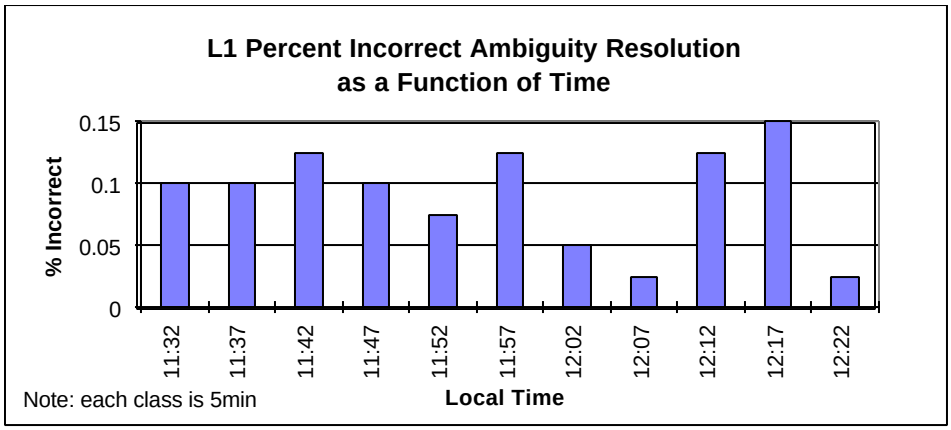

Figure 4.25 L1 Percent Incorrect Ambiguity Resolution as a Function of Time - Reduced Constellation

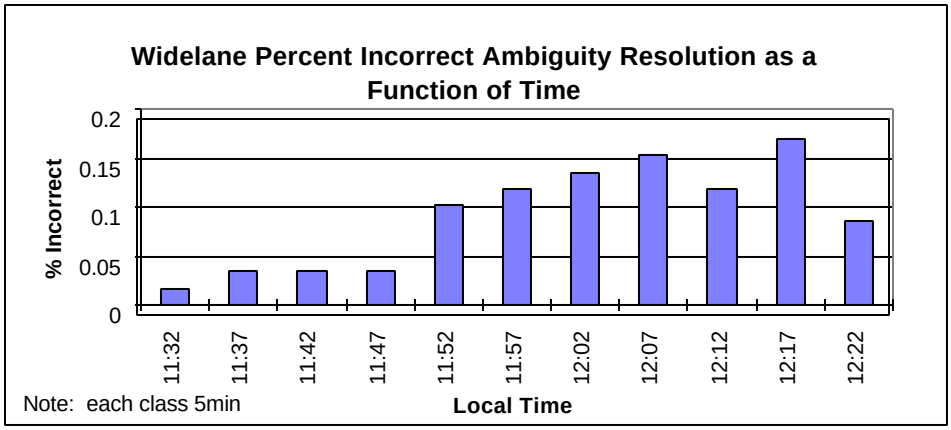

Figure 4.26 Widelane Percent Incorrect Ambiguity Resolution as a Function of Time - Reduced Constellation

CHAPTER 5
CONSTRAINTS

As previously mentioned, both speed and reliability are two concerns for OTF ambiguity resolution. In order to maximize both of these objectives, a two rover station configuration is proposed. By making use of two rovers, several constraints can be utilized, including a fixed baseline between the two rovers, a heading constraint, a pitch constraint, and an ambiguity constraint. Also, for the marine case a height constraint can be implemented. Each of the mentioned constraints shall be described and the elements of the design matrix are derived.

5.1 Dual Rover Constraints

By using two roving receivers (Figure 5.1), more geometric information becomes available and this information can be used to speed up ambiguity resolution and for quality control. Firstly, when two roving antennas are set up on a moving vehicle, the baseline between these two is often precisely measured using a tape measure. Also, by fixing the ambiguities between the moving pair of rover stations, accurate heading and pitch information becomes available. Finally, the sum of a triangle of double difference ambiguities must sum to zero. The baseline constraint has been used in the past to aid the ambiguity resolution for attitude determination systems using GPS (Lu, 1995) while the ambiguity constraint has been used by Lachapelle et al. (1993) to aid the determination of the relative positions of airplanes.

In order to use two rover stations, the state vector for the Kalman filter must be expanded to include the position, velocity, and ambiguity states for both receivers, i.e.

$$\mathbf{x} = \left[\phi_1 \quad \lambda_1 \quad h_1 \quad \dot{\phi}_1 \quad \dot{\lambda}_1 \quad \dot{h}_1 \quad \phi_2 \quad \lambda_2 \quad h_2 \quad \dot{\phi}_2 \quad \dot{\lambda}_2 \quad \dot{h}_2 \quad N_1^1 \quad \cdots \quad N_1^n \quad N_2^1 \quad \cdots \quad N_2^n\right] \tag{5.1}$$

where the subscripts refer to the rover number and the superscripts refer to the satellite number.

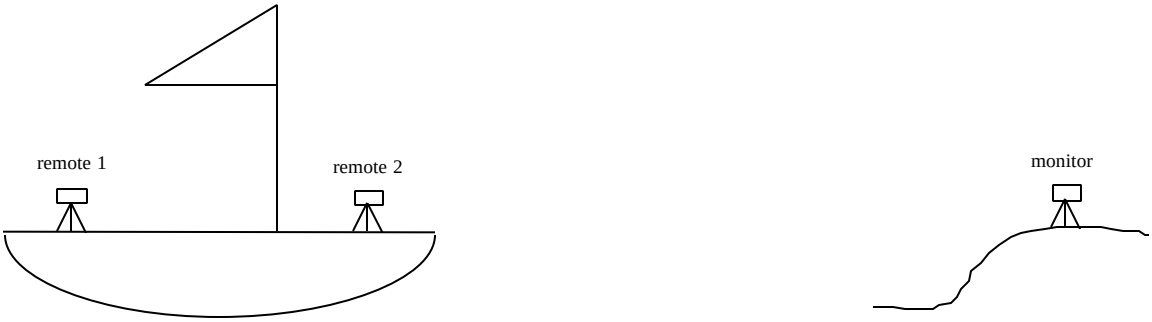

Figure 5.1 Dual Rover Stations

5.1.1 Fixing Ambiguities Between Moving Rover Pair

In order to apply several of the constraints, the ambiguities must first be solved between the roving pair. It is assumed that the roving pair is rigidly fixed with respect to one another, thus, a baseline constraint, and possibly a height constraint (described in following sections) can be applied, making the ambiguity resolution quicker and more reliable. If the roving pair is not fixed with respect to one another, the ambiguities can still be resolved between the two, however, the baseline constraint cannot be used.

To account for the moving "monitor", which is simply one of the rover pairs, a small modification to the Kalman filtering algorithm was implemented. When the state vector is projected ahead in time, the movement of the "monitor" must be accounted for. For example, if a ship is moving due east, and the predicted easting of the moving rover is 10m, but the moving monitor easting has changed by +4m, the predicted easting must be 14m.

5.1.2 Fixed Baseline Constraint

The fixed baseline constraint can be used in several ways including quality control by insuring the final fixed ambiguities result in the given baseline, aiding in fixing ambiguities between the moving rover pair, and aiding in fixing ambiguities between the monitor and two rovers. It is assumed that the fixed baseline length comes from an external source, and not from fixing ambiguities and computing the baseline using GPS data.

The model for the fixed baseline constraint is

$$f_{BL} = \sqrt{(x_2 - x_1)^2 + (y_2 - y_1)^2 + (z_2 - z_1)^2} \tag{5.2}$$

where x, y, z, are the WGS84 rover station coordinates and the subscripts 1 and 2 represent receivers 1 and 2 respectively.

The design matrix for this constraint, which is of dimension 1xu, becomes:

$$\mathbf{A} = \left[\frac{\partial f}{\partial \phi_1} \quad \frac{\partial f}{\partial \lambda_1} \quad \frac{\partial f}{\partial h_1} \quad 0 \quad 0 \quad 0 \quad \frac{\partial f}{\partial \phi_2} \quad \frac{\partial f}{\partial \lambda_2} \quad \frac{\partial f}{\partial h_2} \quad 0 \quad 0 \quad 0 \quad 0 \quad \cdots \quad 0 \right] \tag{5.3}$$

where $$\frac{\partial f}{\partial \phi} = \frac{\partial f}{\partial x}\frac{\partial x}{\partial \phi} + \frac{\partial f}{\partial y}\frac{\partial y}{\partial \phi} + \frac{\partial f}{\partial z}\frac{\partial z}{\partial \phi} \tag{5.4}$$

$$\frac{\partial f}{\partial \lambda} = \frac{\partial f}{\partial x}\frac{\partial x}{\partial \lambda} + \frac{\partial f}{\partial y}\frac{\partial y}{\partial \lambda} + \frac{\partial f}{\partial z}\frac{\partial z}{\partial \lambda} \tag{5.5}$$

$$\frac{\partial f}{\partial h} = \frac{\partial f}{\partial x}\frac{\partial x}{\partial h} + \frac{\partial f}{\partial y}\frac{\partial y}{\partial h} + \frac{\partial f}{\partial z}\frac{\partial z}{\partial h}. \tag{5.6}$$

Assuming that the approximate coordinates are close to the true coordinates, the following can be derived (Cannon, 1991):

$$\frac{\partial f}{\partial \phi_1} = \frac{-(R_N + h_1)\sin\phi_1\cos\lambda_1(x_1 - x_2)}{d_{12}} + \frac{-(R_N + h_1)\sin\phi_1\sin\lambda_1(y_1 - y_2)}{d_{12}} + \frac{\left[R_N(1-e^2) + h_1\right]\cos\phi_1(z_1 - z_2)}{d_{12}} \quad (5.7)$$

$$\frac{\partial f}{\partial \phi_2} = \frac{(R_N + h_2)\sin\phi_2\cos\lambda_2(x_1 - x_2)}{d_{12}} + \frac{(R_N + h_2)\sin\phi_2\sin\lambda_2(y_1 - y_2)}{d_{12}} + \frac{-\left[R_N(1-e^2) + h_2\right]\cos\phi_2(z_1 - z_2)}{d_{12}} \quad (5.8)$$

$$\frac{\partial f}{\partial \lambda_1} = \frac{-(R_N + h_1)\cos\phi_1\sin\lambda_1(x_1 - x_2)}{d_{12}} + \frac{(R_N + h_1)\cos\phi_1\cos\lambda_1(x_1 - x_2)}{d_{12}} \quad (5.9)$$

$$\frac{\partial f}{\partial \lambda_2} = \frac{(R_N + h_2)\cos\phi_2\sin\lambda_2(x_1 - x_2)}{d_{12}} + \frac{(R_N + h_2)\cos\phi_2\cos\lambda_2(x_1 - x_2)}{d_{12}} \quad (5.10)$$

$$\frac{\partial f}{\partial h_1} = \frac{\cos\phi_1\cos\lambda_1(x_1 - x_2)}{d_{12}} + \frac{\cos\phi_1\sin\lambda_1(y_1 - y_2)}{d_{12}} + \frac{\sin\phi_1(z_1 - z_2)}{d_{12}} \quad (5.11)$$

$$\frac{\partial f}{\partial h_2} = \frac{-\cos\phi_2\cos\lambda_2(x_1 - x_2)}{d_{12}} + \frac{-\cos\phi_2\sin\lambda_2(y_1 - y_2)}{d_{12}} + \frac{-\sin\phi_2(z_1 - z_2)}{d_{12}} \quad (5.12)$$

where $$R_N = \frac{a}{\sqrt{1 - e^2\sin^2\phi}} \quad (5.13)$$

$$d_{12} = \sqrt{(x_2 - x_1)^2 + (y_2 - y_1)^2 + (z_2 - z_1)^2} \quad (5.14)$$

a is the WGS 84 semi-major axis

e^2 is the first eccentricity.

Naturally, the standard deviation depends on the external method of measuring the baseline. Typically, if a tape or chain is used, the baseline length should have a small standard deviation of about 1 cm.

5.1.3 Heading Constraint

Before a heading constraint (Figure 5.2) can be applied, integer ambiguities must be fixed between the two rover stations. Once this is done, the heading between them can be considered known with the derived standard deviation. Assuming a spherical earth (which is valid if the baseline between the rover pair is small), the mathematical model for heading becomes:

$$f_{Hd} = \tan^{-1}\left(\frac{\Delta E}{\Delta N}\right) \tag{5.15}$$

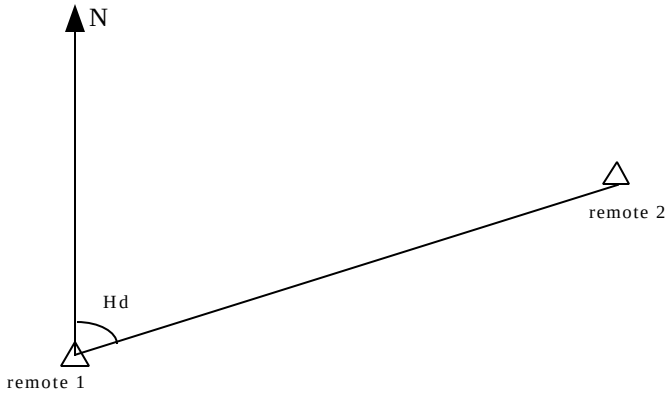

Figure 5.2 Heading

where $\Delta E = (\lambda_2 - \lambda_1) R \cos\phi_1$ (5.16)

$$\Delta N = R(\phi_2 - \phi_1) \tag{5.17}$$

R is a mean radius of the earth in metres

and the design matrix is

$$\mathbf{A} = \left[\frac{\partial f}{\partial \phi_1} \quad \frac{\partial f}{\partial \lambda_1} \quad 0 \quad 0 \quad 0 \quad 0 \quad \frac{\partial f}{\partial \phi_2} \quad \frac{\partial f}{\partial \lambda_2} \quad 0 \quad 0 \quad 0 \quad 0 \quad 0 \quad \cdots \quad 0\right] \tag{5.18}$$

where the elements are

$$\frac{\partial f}{\partial \phi_1} = \frac{R\Delta E}{\Delta N^2 + \Delta E^2} + \frac{-R(\lambda_2 - \lambda_1)\sin\phi_1}{\Delta N + \frac{\Delta E^2}{\Delta N}} \tag{5.19}$$

$$\frac{\partial f}{\partial \phi_2} = \frac{-R\Delta E}{\Delta N^2 + \Delta E^2} \tag{5.20}$$

$$\frac{\partial f}{\partial \lambda_1} = \frac{-R\cos\phi_1}{\Delta N + \frac{\Delta E^2}{\Delta N}} \tag{5.21}$$

$$\frac{\partial f}{\partial \lambda_2} = \frac{R\cos\phi_1}{\Delta N + \frac{\Delta E^2}{\Delta N}} \tag{5.22}$$

Instead of deriving the standard deviation directly from the covariance law, an intuitive approach was taken. Given that the baseline between the rover pair is known, the heading standard deviation can be computed using

$$\sigma_{Hd} = \tan^{-1}\left(\frac{\sigma_{horiz}}{BL}\right) \tag{5.23}$$

where the σ_{horiz} is the standard deviation of the horizontal position of one rover with respect to the other. It can be seen that a longer baseline will result in smaller standard deviations.

5.1.4 Pitch Constraint

The pitch constraint is quite similar to the heading constraint and the two are generally applied together. Again, the ambiguities must be fixed between the roving pair before this constraint can be applied. The mathematical model for the pitch constraint can be written as:

$$f_P = \tan^{-1}\left(\frac{h_2 - h_1}{\sqrt{\Delta N^2 + \Delta E^2}}\right) \tag{5.24}$$

while the design matrix is

$$\mathbf{A} = \left[\frac{\partial f}{\partial \phi_1} \quad \frac{\partial f}{\partial \lambda_1} \quad \frac{\partial f}{\partial h_1} \quad 0 \quad 0 \quad 0 \quad \frac{\partial f}{\partial \phi_2} \quad \frac{\partial f}{\partial \lambda_2} \quad \frac{\partial f}{\partial h_2} \quad 0 \quad 0 \quad 0 \quad 0 \quad \cdots \quad 0 \right] \tag{5.25}$$

Setting $\Delta h = h_2 - h_1$ (5.26)

the elements become

$$\frac{\partial f}{\partial \phi_1} = \frac{R \Delta h \Delta N}{\left(\Delta N^2 + \Delta E^2\right)^{\frac{3}{2}} + \Delta h^2 \left(\Delta N^2 + \Delta E^2\right)^{\frac{1}{2}}} + \frac{R\left(\lambda_2 - \lambda_1\right) \sin \phi_1 \Delta h \Delta E}{\left(\Delta N^2 + \Delta E^2\right)^{\frac{3}{2}} + \Delta h^2 \left(\Delta N^2 + \Delta E^2\right)^{\frac{1}{2}}} \tag{5.27}$$

$$\frac{\partial f}{\partial \phi_2} = \frac{-R \Delta h \Delta N}{\left(\Delta N^2 + \Delta E^2\right)^{\frac{3}{2}} + \Delta h^2 \left(\Delta N^2 + \Delta E^2\right)^{\frac{1}{2}}} \tag{5.28}$$

$$\frac{\partial f}{\partial \lambda_1} = \frac{-R \Delta h \Delta E \cos \phi_1}{\left(\Delta N^2 + \Delta E^2\right)^{\frac{3}{2}} + \Delta h^2 \left(\Delta N^2 + \Delta E^2\right)^{\frac{1}{2}}} \tag{5.29}$$

$$\frac{\partial f}{\partial \lambda_2} = -\frac{\partial f}{\partial \lambda_1} \tag{2.30}$$

$$\frac{\partial f}{\partial h_1} = \frac{-1}{\left(\Delta N^2 + \Delta E^2\right)^{\frac{1}{2}} + \dfrac{\Delta h^2}{\left(\Delta N^2 + \Delta E^2\right)^{\frac{1}{2}}}} \tag{5.31}$$

$$\frac{\partial f}{\partial h_2} = -\frac{\partial f}{\partial h_1}. \tag{5.32}$$

Similar to the standard deviation for heading, the standard deviation for pitch can be found using the equation

$$\sigma_P = \tan^{-1}\left(\frac{\sigma_{vert}}{BL}\right) \tag{5.33}$$

where σ_{vert} is the standard deviation in the vertical position of one rover with respect to the other. Again, a longer baseline will result in a smaller standard deviation.

5.1.5 Ambiguity Constraint

The final dual rover constraint to be presented is the ambiguity constraint. The idea behind this constraint is that the sum of a triangle of double difference ambiguities (Figure 5.3) is zero (Lachapelle, 1993, Lachapelle, 1994). The mathematical model is

$$f_A = \Delta\nabla N_{12} - \Delta\nabla N_{m2} + \Delta\nabla N_{m1} = 0 . \tag{5.34}$$

Assuming the ambiguities are fixed between the roving pair, the nxu design matrix becomes

$$\mathbf{A} = \begin{bmatrix} 0 & 0 & 0 & 0 & 0 & 0 & 0 & 0 & 0 & 0 & 0 & 0 & 1 & 0 & 0 & 0 & -1 & 0 & 0 & 0 \\ \vdots & \vdots & \vdots & \vdots & \vdots & \vdots & \vdots & \vdots & \vdots & \vdots & \vdots & \vdots & 0 & 1 & 0 & 0 & 0 & -1 & 0 & 0 \\ 0 & 0 & 0 & 0 & 0 & 0 & 0 & 0 & 0 & 0 & 0 & 0 & 0 & 0 & \ddots & 0 & 0 & 0 & \ddots & 0 \\ 0 & 0 & 0 & 0 & 0 & 0 & 0 & 0 & 0 & 0 & 0 & 0 & 0 & 0 & 0 & 1 & 0 & 0 & 0 & -1 \end{bmatrix} . \tag{5.35}$$

The input standard deviation of this constraint is theoretically 0, however, a small number such as 0.001 cycles was used to avoid numerical problems.

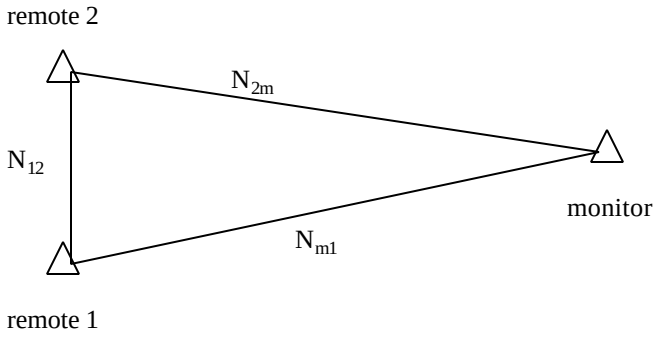

Figure 5.3 Ambiguity Constraint

5.2 Height Constraint

The final constraint is a height constraint. This constraint is extremely useful in a marine environment where the height is generally well known. Because the height is the weakest component of GPS, this constraint is the most useful, however, it is only applicable to a

few specific environments. Remondi (1992) discusses the use of height constraints to directly aid in rejecting possible ambiguity sets. As will be shown, the proposed constraints are used to aid ambiguity resolution in a different manner.

The mathematical model for height constraints is

$$f_h = h \tag{5.36}$$

while the 2xu design matrix is (referring to equation 3.29)

$$\mathbf{A} = \begin{bmatrix} 0 & 0 & 1 & 0 & 0 & 0 & 0 & \cdots & 0 \\ 0 & 0 & 0 & 0 & 0 & 1 & 0 & \cdots & 0 \end{bmatrix} \tag{5.37}$$

and the standard deviation of the constraint must be determined from the knowledge of the height and dynamics of the vehicle. For example, if a ship was sailing in an area where the maximum expected wave height from trough to crest is 3 m, the appropriate standard deviation would be ± 0.5 m which is 1/3 of the maximum displacement from zero. In the case of reacquisition of the ambiguities, the standard deviation of the height constraint could be taken from the previous several minutes of data.

5.3 Approximate Coordinates

One problem that arises with the baseline, heading, and pitch is the approximate values used in the design matrices. If the approximate values are poor, as is generally the case during the filter warm-up, the output covariance matrix after the constraints are applied may be skewed due to the nonlinear mathematical models for these constraints. As an example, consider the baseline constraint. If the true and estimated coordinates are as shown in Figure 5.4, after the baseline constraint is applied, the newly estimated coordinates of both rovers are actually worse than before the constraint. The covariance matrix, however, will show that the accuracy should have improved.

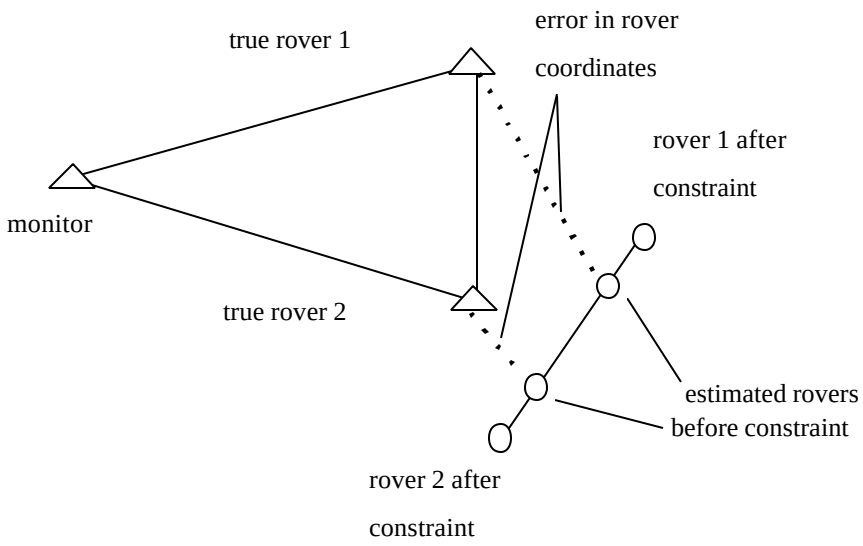

Figure 5.4 Effect of Poor Approximate Coordinates

There are three ways of overcoming this problem. The first and most rigorous method is to include the second order terms as done by Widnall (1972). The second method is to simply increase the input standard deviation of the constraint. This method works, but it does not really solve the problem. The final method is to simply wait several epochs while the filter warms up before applying the constraints. This is the method chosen since the heading and pitch constraints cannot be applied immediately because of the fact that the ambiguities must first be resolved between the two rovers. Thus, after the ambiguities between the rovers were fixed, all constraints were applied.

If this problem is ignored, the resulting covariance matrix output by the filter will be overly optimistic. This could result in the incorrect ambiguities being chosen.

5.4 Constraint Implementation

As mentioned in previous chapters, the OTF software makes use of a Kalman filter and the FASF ambiguity resolution technique. With these algorithms in place, the simplest

form of implementing the described constraints is to treat them as observations. Thus, at each epoch, if a height constraint is to be applied, an extra observation of the height is added with the appropriate standard deviation.

Unfortunately, the heading, pitch, and ambiguity constraint cannot be applied until the ambiguities are solved between the two rovers. This is generally very quick because of the fixed baseline approach described above. Also, in the case of a shipborne application or an application in which the pitch of the vehicle is expected to be minimal, the height of rover2 with respect to rover1 will on the average be the same. Thus, the height of rover2 can be constrained to the height of rover1 with the standard deviation depending on the expected pitch of the ship. This will speed up the resolution between the rover pair even more. In general, if a widelane observation is used, this ambiguity resolution is instantaneous, thus there is no waiting to apply all available constraints.

5.5 Correlation Between Constraints

At first glance, it may seem that several of the above described constraints may have a relatively high correlation among one another. This, however, is not the case. Firstly, the covariance between two measurements, x and y, is defined as

$$\sigma_{xy} = E[\delta x \delta y] \tag{5.38}$$

where $E[\bullet]$ is the expectation operator and δx and δy are the measurement errors which are considered to be zero mean white sequences.

In the case of the ambiguity constraint, the expected variance of the "observation" is zero, as explained in Section 5.1.5. Thus, the covariance between the ambiguity constraint and any other constraint must also be zero. Also, the correlation between the heading and pitch constraints must also be zero since they are orthogonal to one another. That is, if there is an error in pitch, it will have no effect on the error in the heading and vice versa.

Because it is assumed that the baseline between the two rovers is measured before the mission, this observation should also have no correlation with any other constraints. Again, an error in the baseline constraint would not have an effect on the errors in any of the other constraints. Finally, the same logic applies for the height constraint.

It should be noted, however, that there may be some correlation due to the nonlinear effects presented by these constraints. Because the constraints are not applied immediately (see Section 5.3), the nonlinearities should be minimal. For the work done in this thesis, it is assumed, however, that the correlations are zero.

CHAPTER 6
CONSTRAINT TESTS, RESULTS, AND DATA ANALYSIS

In order to determine the effectiveness of the previously described constraints, several marine tests were carried out. In this chapter, the tests are described in detail followed by an analysis of the results for both L1-only and widelane data sets. To test the performance of the constraints under a reduced geometry, one of the tests was purposely degraded by rejecting several satellites.

6.1 Field Trial Description

In order to test the validity of the constraints described in the previous chapters, two data sets were collected. The first data set was recorded at a water reservoir in Calgary. Two NovAtel MiLLennium dual frequency receivers were mounted 5.86 m apart on a small vessel and another receiver was placed on the shore. The second data set was collected on the Okanagan Lake near Kelowna, British Columbia. In this case, two NovAtel MiLLennium receivers were used on the vessel with Trimble 4000SSi receivers set up in Kelowna and Peachland. The antennas mounted on the vessel were separated by 11.3 m. Chokering antennas were used with the MiLLennium receivers for both tests while a groundplane was used with the Trimble antennas in an attempt to keep multipath to a minimum. All data was collected at a rate of 1 Hz.

The observed satellite geometry plots for the Calgary, Kelowna, and Peachland stations are shown in Figures 6.1, 6.2, and 6.3 respectively. Figures 6.4 and 6.6 show the vessel trajectories, while Figures 6.5 and 6.7 show the vessel heights versus time.

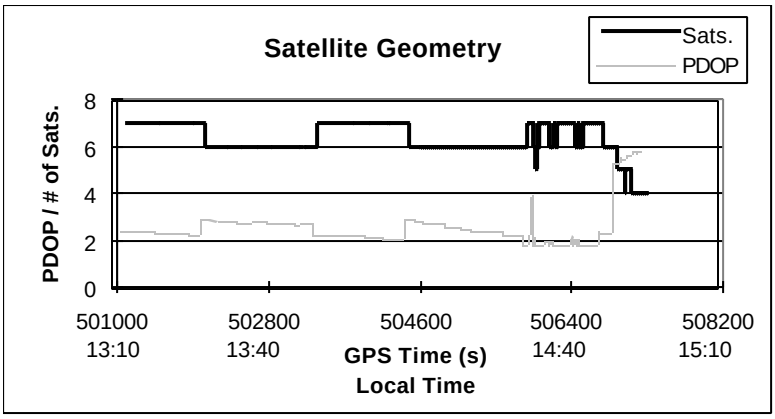

Figure 6.1 Satellite Geometry in Calgary

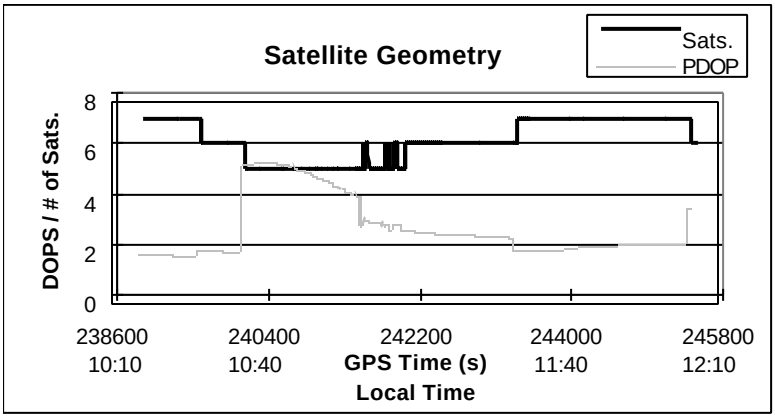

Figure 6.2 Satellite Geometry in Kelowna

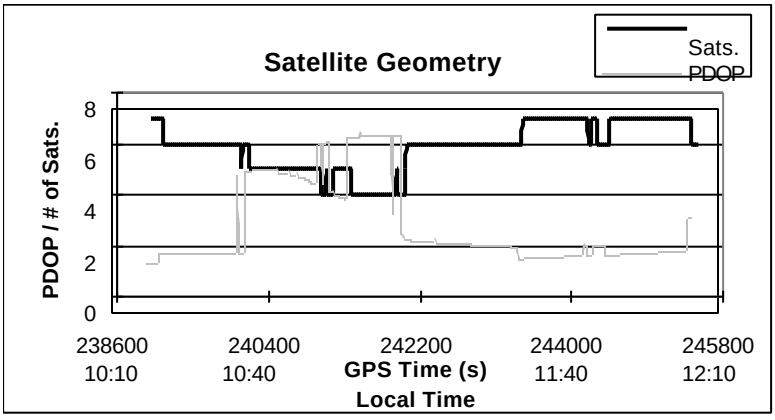

Figure 6.3 Satellite Geometry in Peachland

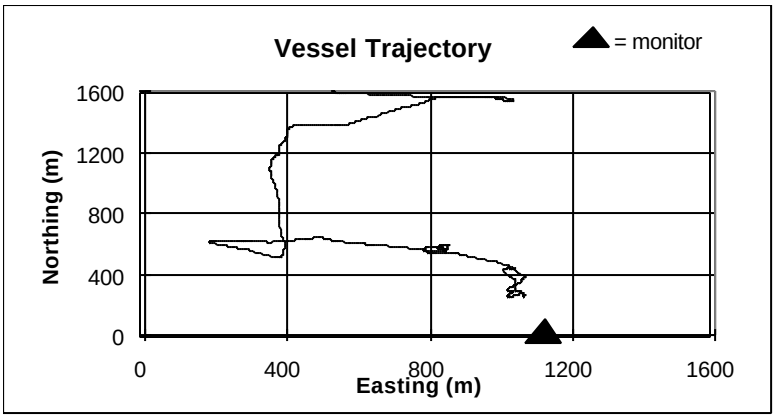

Figure 6.4 Vessel Trajectory - Calgary Trial

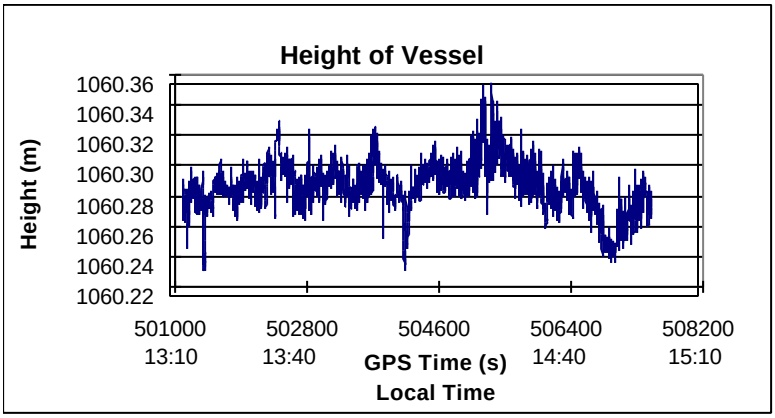

Figure 6.5 Vessel Height - Calgary Trial

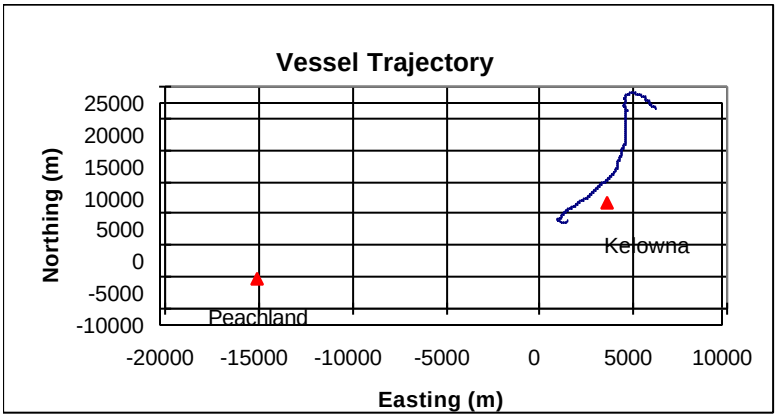

Figure 6.6 Vessel Trajectory - Okanagan Trial

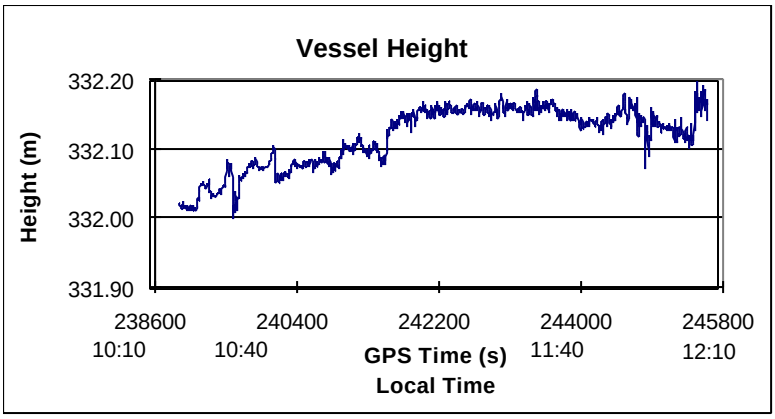

Figure 6.7 Vessel Height - Okanagan Trial

As shown in Figure 6.4, the trajectory taken in Calgary did not exceeded 2 km between the monitor and vessel, while the separation between the Kelowna monitor and vessel ranged between 2 km and 18 km and the separation between the Peachland monitor and vessel ranged between 20 km and 40 km.

All data was collected at a rate of 1 Hz while all processing was done with a 10 degree elevation cutoff.

6.2 Data Processing Approach

The processing software SEAFLY, which is an extension of the SFLY software discussed in Chapter 4.2, was developed to allow for two rover receivers to be mounted on a moving platform and for the previously described constraints to be applied. The main ambiguity resolution algorithm consists of a Kalman filter, which allows for optimal estimation of the floating ambiguities, and the FASF method, previously described. The general flow of the program is shown in Figure 6.8. It can be seen that there are actually two filters running at the same time. The primary filter runs between the monitor and the two rover stations while the secondary filter runs between the two rover stations. Also, before any of the constraints are applied, it is necessary for the ambiguities to be fixed

between the two rover stations. This is done to allow the filter to warm up to avoid problems with poor approximate coordinates (see section 5.3). Once the ambiguities have been fixed between the two rover stations, the heading and pitch are computed even if no monitor is available. It should be noted that in order to fix the ambiguities between the monitor and rovers quickly and reliably, a fixed baseline constraint is also applied (not shown in figure).

Along with the residual test and the comparison of the fixed ambiguity solution to the float solution, two other quality checks were implemented. The resulting baseline between the two rovers as computed with respect to the monitor had to agree with the known baseline. Also, the sum of all the double difference ambiguities had to equal zero. If either of these checks failed, the ambiguity search was reset.

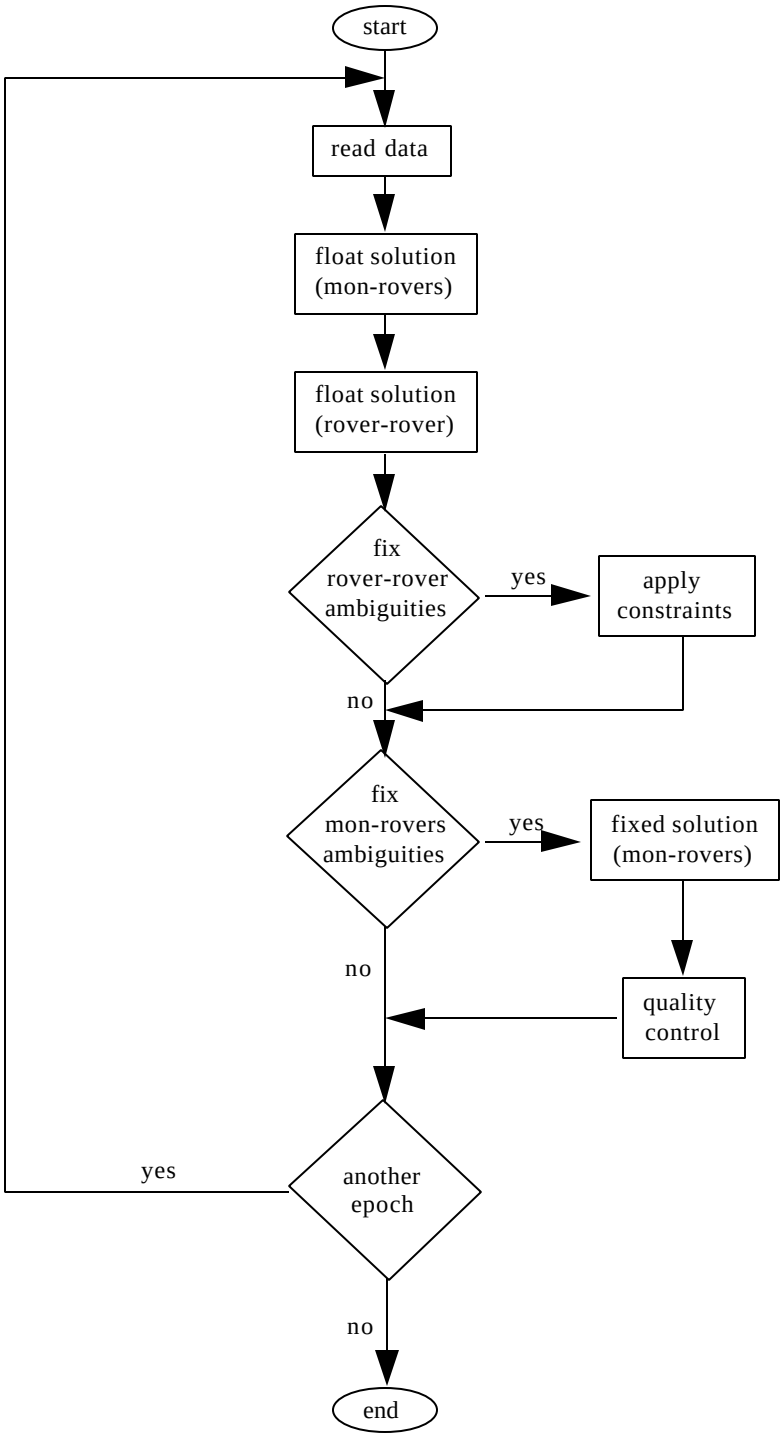

Figure 6.8 SEAFLY Flow of Control

6.3 Effect of Constraints on Possible Ambiguity Sets

The number of possible ambiguity sets is directly associated with the ambiguity covariance matrix for the float solution. In order to demonstrate the effect of the constraints on the covariance matrix, the number of possible ambiguity sets for a trial in Kelowna is shown in Figure 6.9. It should be noted that a height constraint with a standard deviation of 0.5 m was used. The value of the constraints becomes obvious in the figure. By applying all constraints, the number of possible ambiguity sets in both the L1-only and the widelane cases are significantly reduced.

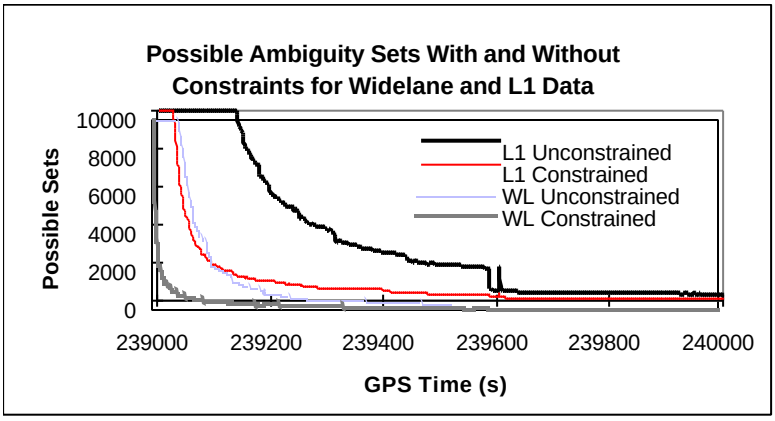

Figure 6.9 Effect of All Constraints on the Number of Possible Ambiguity Sets for Widelane and L1 Data

Thus, with the faster reduction in the number of ambiguity sets that are required to be searched, the ambiguity resolution process can be done faster.

6.4 Effect of Constraints on DOPs

Since the constraints effect the solution in such a way that the number of possible ambiguity sets is reduced, it is worth while to inspect the effect of the constraints on the Dilution of Precisions (DOPs), which give an indication of the geometric strength of the

solution. In this case, however, the DOP values shown in the Figures below are actually Relative Dilution of Precisions (RDOPs). The difference between DOPs and RDOPs is that DOPs are computed using the single point design matrix while the RDOPs are computed the double difference design matrix. The reason RDOPs are presented is because a double difference solution is used to apply several of the constraints, and in the case of the ambiguity constraint, a double difference solution is necessary.

The effect of the constraints are shown in the figures below. The ambiguity, heading, and pitch constraints are not shown because they do not significantly effect the RDOPs. Figures 6.10 and 6.11 show the effects of the constraints on the RNDOP and REDOP respectively. It can be seen that in both cases, the baseline constraint causes the RDOPs to slightly decrease and also become noisier while the height constraint has a very minor effect. The reason for the minimal effect of the height constrain is that the height constraint should mostly effect the RVDOP. The baseline constraint actually reduces the RNDOP and REDOP. This is likely because the relative position of one receiver with respect to the other is constrained to a sphere. The heading and pitch constraints have no effect because they only constrain the relative position to an infinite plain. The RVDOP is not effected at all by any of the constraints other than the height.

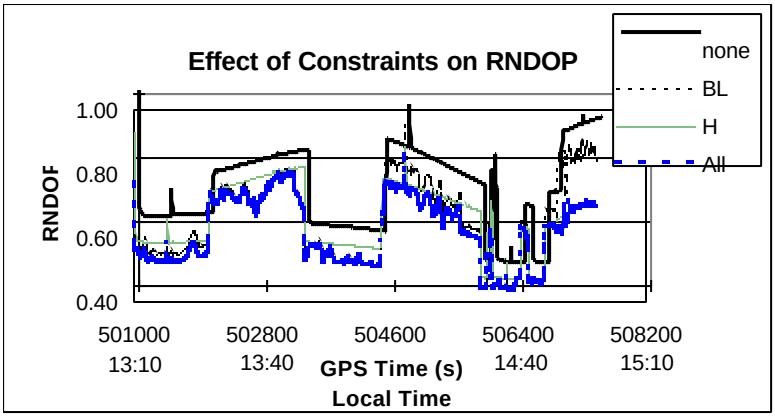

Figure 6.10 Effect of Constraints on RNDOP

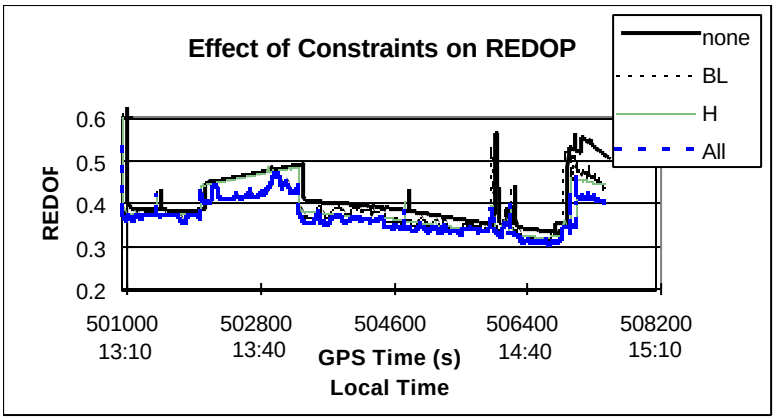

Figure 6.11 Effect of Constraints on REDOP

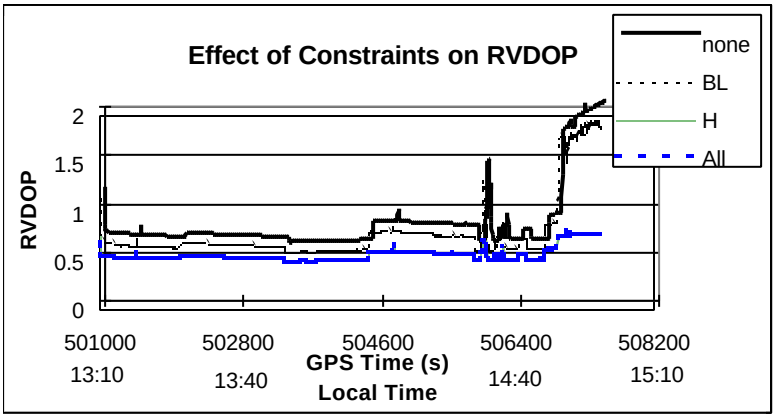

Figure 6.12 Effect of Constraints on RVDOP

In this case, the height has a more significant effect on the RVDOP compared to the other RDOPs, especially at the very end of the data set where the RVDOP of the unconstrained case becomes larger than two, while the height constrained RVDOP remains under one.

In all cases, the effect of the constraints other than the height constraint are quite minimal. For the heading, pitch, and baseline constraints, this is because these constraints only constrain the relative positions on one receiver with respect to another. The ambiguity constraint has no effect on these RDOPs because it constrains the ambiguities, not the positions, thus, no improvement in RDOPs is apparent. The height

constraint is the most effective of all constraints in reducing RDOPs because it directly assists the absolute height.

6.5 Effect of Constraints on Float Solution

The effect of the constraints on the float solution is very important because the float solution is used to steer the ambiguity search in the correct direction. If the float solution is incorrect or the estimated covariance for the float solution is overly optimistic, serious implications could arise. If either of these were to happen, the time to resolution could be slowed or the ambiguities may not be solved. In a severe case, the incorrect ambiguities may be chosen. Thus, it is important to be sure that the implementation of the constraints is done in such a way that the float solution and the estimated covariances reflect the true solution.

Figures 6.13 to 6.16 show the effect of all constraints compared to the unconstrained case on the latitude, longitude, height, and a selected ambiguity state respectively. The standard deviation of the height constraint was 0.5 m. In each of the figures, the outer envelopes represent the standard deviation (multiplied by two) output by the filter for the unconstrained case. The inner envelopes represent the standard deviation (multiplied by two) for the fully constrained case. The thickest line is the solution output by the filter for the fully constrained case while the remaining line is the solution output by the filter for the unconstrained case.

The reference trajectory was computed using a fixed ambiguity solution. The value of the constraints is clear in all cases. The constraints cause the errors in both position and ambiguity states to decrease. This is also shown in the estimated 2 sigma envelopes. Figure 6.16 shows the reason for the decrease in possible ambiguity sets discussed in the

previous section. With reduced standard deviations on each of the ambiguity states, the number of ambiguity sets which must be searched is decreased.

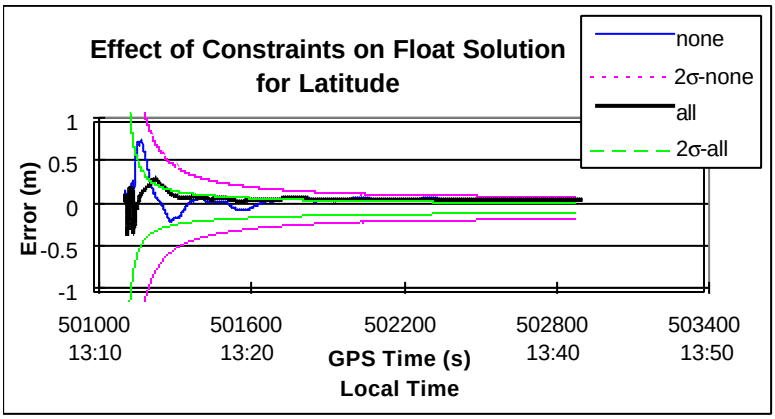

Figure 6.13 Effect of Constraints on Float Solution for Latitude

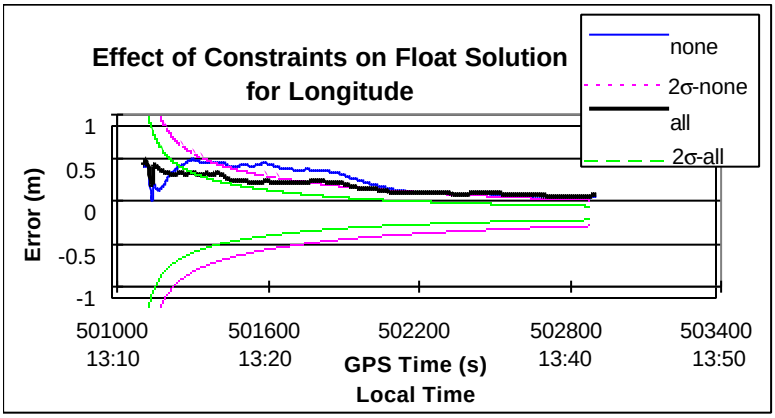

Figure 6.14 Effect of Constraints on Float Solution for Longitude

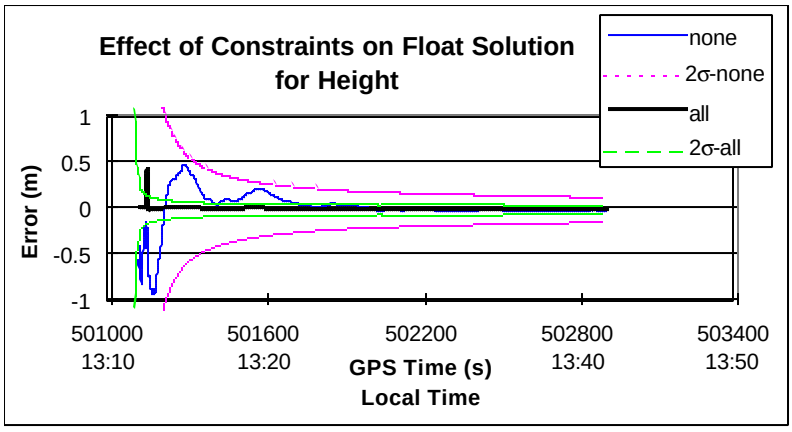

Figure 6.15 Effect of Constraints on Float Solution For Height

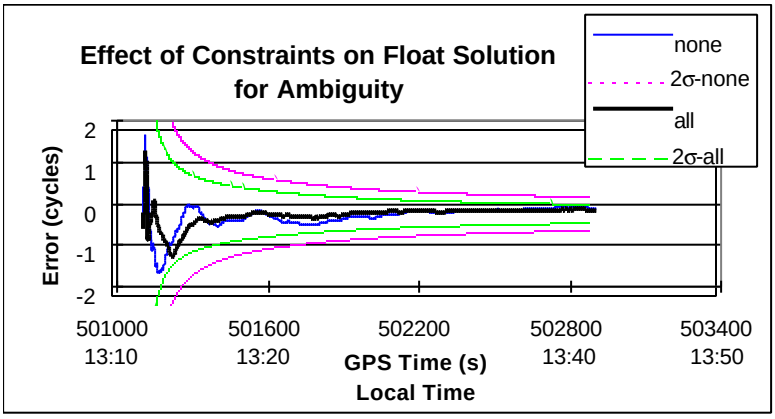

Figure 6.16 Effect of Constraints on Float Solution for Ambiguity

The effects of each individual constraint on the float solution are not shown. In the latitude, longitude, and ambiguity cases, each constraint demonstrated similar improvements in both the estimated covariances and the absolute errors. The height, however, was effected very little by any of the constraints other than the height constraint.

6.6 Results and Analysis

The results of the three tests are presented below. The statistics shown in the graphs were formed by processing each data set many times. Each time the data set was processed, the start time was incremented by 100s (Lachapelle, 1992). Once the entire data set had been processed, the RMS and mean epochs to ambiguity resolution were computed using all of the results.

6.6.1 Effects of Height Constraints on Ambiguity Resolution

Because the height constraint can have a large variation in the input standard deviation depending on the wave conditions encountered, the sensitivity of the standard deviation must be analyzed. Figures 6.17 and 6.18 show the effect of height constraints on the Calgary data set using L1-only data and widelane data respectively. Similar graphs for the Kelowna data set are shown in Figures 6.19 and 6.20. The input heights for the Calgary and Kelowna cases were 1060.27 m and 332.05 m respectively. These values were found by examining Figures 6.5 and 6.7 and taking an average value. Generally, such information will either have to be known beforehand otherwise the height constraint will only be useful if the ambiguities have been previously solved for and lost.

From Figures 6.17 to 6.20 it becomes obvious that the height constraint can be very significant when using both widelane and L1-only data. As the standard deviation of the height constraint was reduced, the amount of reduction compared to a slightly larger height constraint decreased for the L1-only data. The widelane case, however, shows little improvement after the standard deviation is decreased below the 1 m level. This is because of the large wavelength of the widelane observable (i.e. 86 cm). Once the height becomes known at this level, the ambiguities become much easier to solve, thus, a smaller standard deviation is of little consequence.

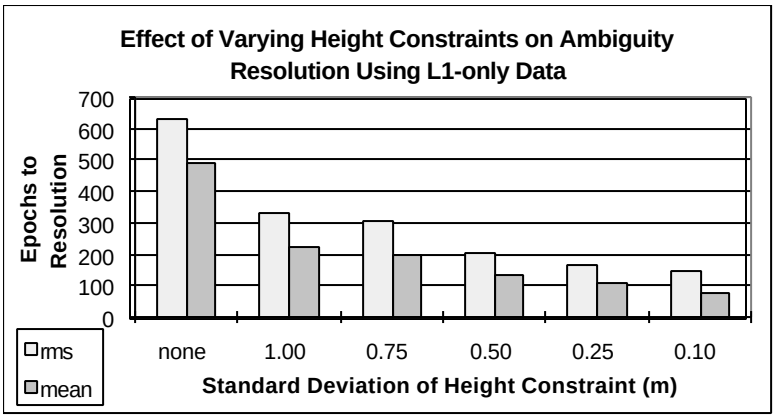

Figure 6.17 Height Constraint Sensitivity Using L1-only Data - Calgary Case

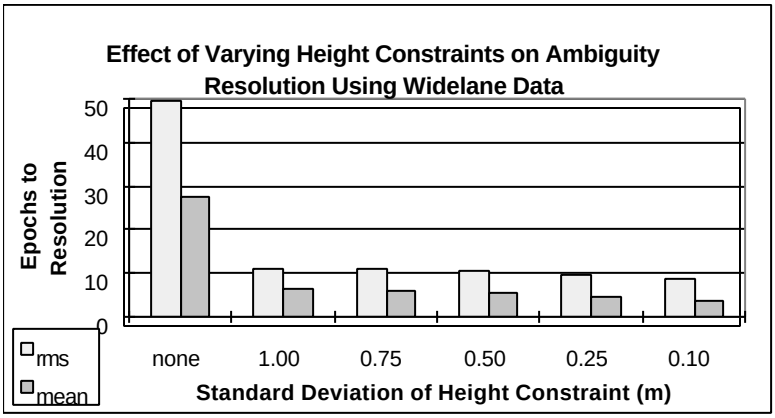

Figure 6.18 Height Constraint Sensitivity Using Widelane Data - Calgary Case

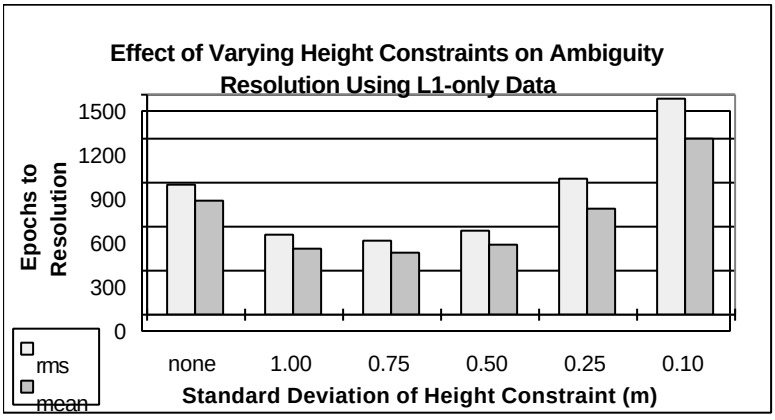

Figure 6.19 Height Constraint Sensitivity Using L1-only Data - Kelowna Case

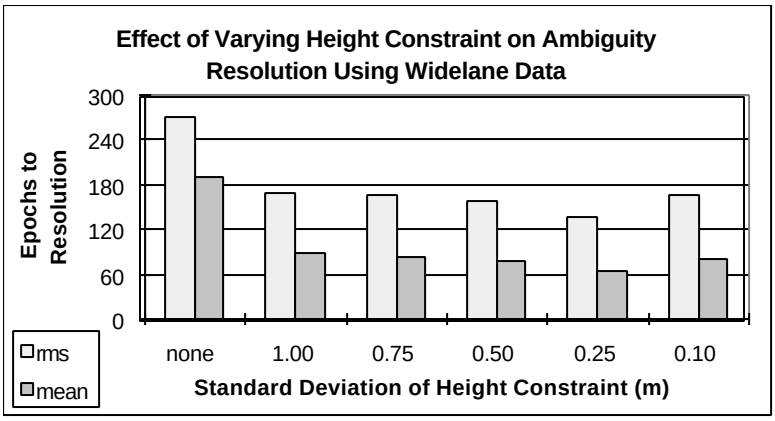

Figure 6.20 Height Constraint Sensitivity Using Widelane Data - Kelowna Case

The results from the Kelowna data show somewhat different results compared to the Calgary case. Firstly, the effect of the slightly biased input height becomes obvious in the L1-only case (Figure 6.19). Once the input standard deviation falls below 0.75 m, the time to resolution is generally longer than with a larger standard deviation. If the standard deviation is smaller than 0.25 m, the constrained solution often takes longer to converge upon the correct integer ambiguities than the unconstrained solution. Thus, if a biased height is to be used as a constraint, the standard input deviation must be large enough to hide the bias in the measurement noise. In this case, the bias is approximately 10 cm for the last half of the data set. Figure 6.19 shows that a 1 m height constraint performs quite well.

A second discrepancy between the Calgary and Kelowna data sets is the percent improvement of the widelane cases. For the Calgary case, the improvement of a 0.75 m height constraint was approximately 500%, while the Kelowna case only improved by 200%.

To investigate the effect of the monitor rover separation on the height constraints the widelane data from Peachland was processed. In this case, the monitor rover separations

varied between 20 km and 40 km as compared to the Kelowna case in which separations ranged between 2 km and 20 km. The results are shown in Figure 6.21.

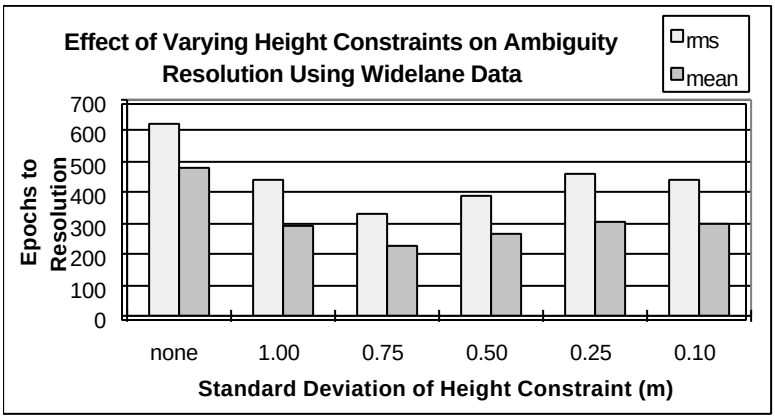

Figure 6.21 Height Constraint Sensitivity Using Widelane Data - Peachland Case

It can be seen that the effect of the height constraint is still significant over longer distances, however, the improvement is approximately 140%, which is less than both the Kelowna and Calgary cases.

Thus, as the distance between the monitor and rovers increases, the height constraint begins to lose its effectiveness. This is because at large monitor-rover separations, the height constraint cannot speed up the convergence of the float solution by as much as at shorter distances, where the ambiguities converge quicker.

It should be noted that because the number of satellites drops to 4 for a period of approximately 1000 s, the times to resolution become artificially large. To remove this effect from Figure 6.21, all trials effected by this portion of the data were excluded from the statistics. Also, the L1-only data for the Peachland case is not presented because ambiguity resolution on-the-fly with L1-only data becomes very difficult and unreliable for long monitor-rover separations.

In both the Calgary and the Okanagan cases, the wave conditions were very calm, thus small standard deviations could be easily tested. In an oceanic situation, such calm conditions would not likely be encountered and larger standard deviations would be required. With very large waves, the height constraint would quickly lose its effectiveness because of the increased standard deviations. However, in constricted waterways, where waves are generally minimal, a height constraint with a 1 m standard deviation becomes reasonable and very effective in decreasing the time to resolve the integer ambiguities.

6.6.2 Effects of Other Constraints on Ambiguity Resolution

Figures 6.22 to 6.25 show the effects of different individual constraints for both the L1-only and widelane cases for Calgary and Kelowna while Figure 6.26 shows the widelane case for Peachland. As expected, the use of all constraints made a considerable impact on the time to ambiguity resolution.

The baseline constraint appears to be the least help to the ambiguity resolution process, while the height constraint is the most useful individual constraint assuming a fairly small standard deviation.

Overall, each case follows the same general pattern regarding the usefulness of constraints for ambiguity resolution.

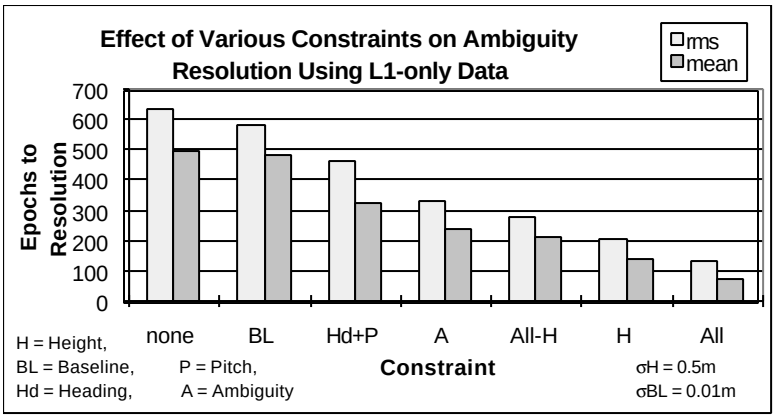

Figure 6.22 Effect of Various Constraints on Ambiguity Resolution Using L1-only Data - Calgary Case

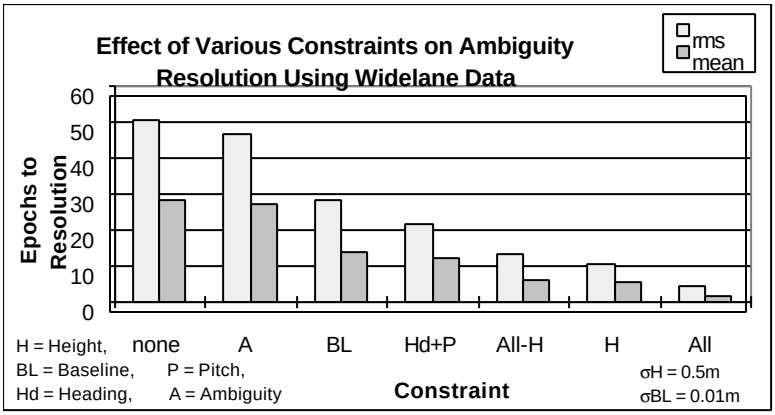

6.23 Effect of Various Constraints on Ambiguity Resolution Using Widelane Data - Calgary Case

Several discrepancies, however, do exist. Firstly, in Figure 6.23, the ambiguity constraint is of less importance than the baseline constraint. This is probably due to the fact that the monitor is always close to the rover stations, the geometry is excellent, and a widelane observable is being used.

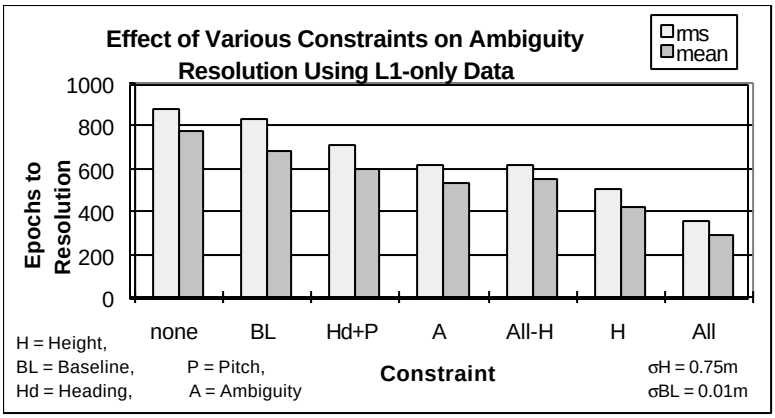

Figure 6.24 Effect of Various Constraints on Ambiguity Resolution Using L1-only Data - Kelowna Case

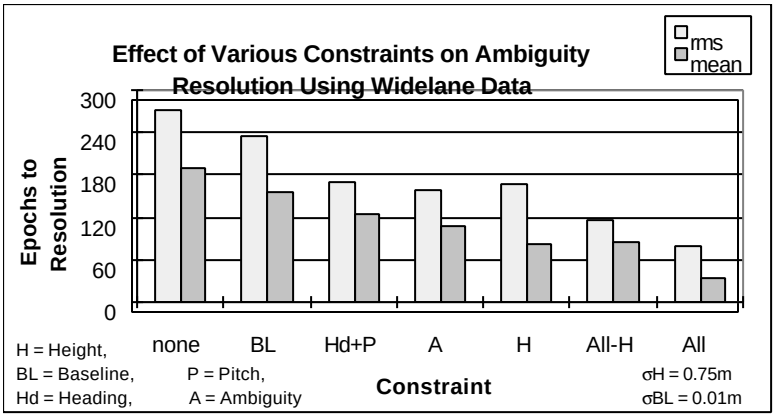

Figure 6.25 Effect of Various Constraints on Ambiguity Resolution Using Widelane Data - Kelowna Case

Because of these reasons, the ambiguities converge very quickly, thus the constraint results in a minimal gain. The second discrepancy is the height constraint in Figure 6.25. In all other cases, the RMS time to resolution using the height constraint is smaller than all other constraints combined. Note that the mean height still fits the general trend.

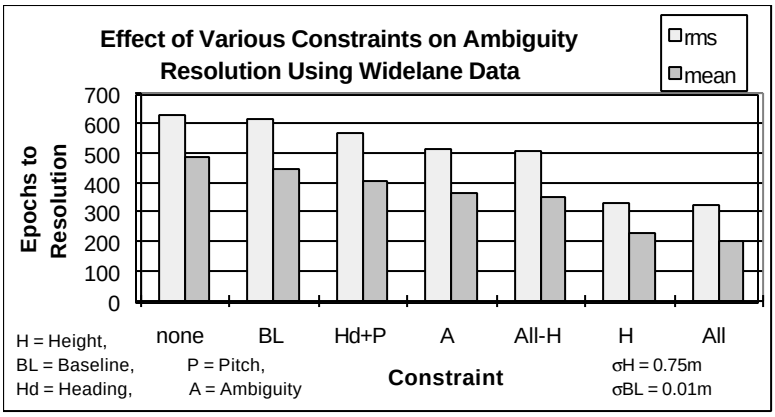

Figure 6.26 Effect of Various Constraints on Ambiguity Resolution Using Widelane Data - Peachland Case

This means that there were a few epochs in the data set which caused the RMS of this constraint to become very large. If these epochs were removed from the statistics, the constraint would fit the same general trend. Finally, in Figure 6.26 the effect of the baseline, heading and pitch, and ambiguity constraints combined have very little effect on the times to ambiguity resolution. This is because of the large distance separating the monitor and rover receivers. This shows that for long inter-receiver separations, in this test only the height constraint is of much use to decrease the time to resolution, while the other constraints can be more importantly used as quality assurance of the correct integer ambiguities.

Table 6.1 summarizes the improvement obtained by using all of the previously described constraints. Comparing the Calgary case to the Okanagan cases, it can be seen that the Calgary case shows a much greater overall improvement when the constraints are applied. This is mainly due to the non-random effect of spatially correlated errors in the case of long monitor rover separations.

Table 6.1 Summary of Results

	Percent Reduction over Unconstrained Case	
Area	L1-only	Widelane
Calgary	79%	91%
Calgary (reduced)	84%	91%
Kelowna	59%	70%
Peachland	---	52%

6.6.3 Effect of Constraints Under Reduced Geometry

To assess the value of the constraints under a poorer geometry, the Calgary data was used with three satellites rejected from the solution to form the DOPs shown in Figure 6.27. Although the DOPs are still quite good, the number of satellites drops to only five for much of the data set.

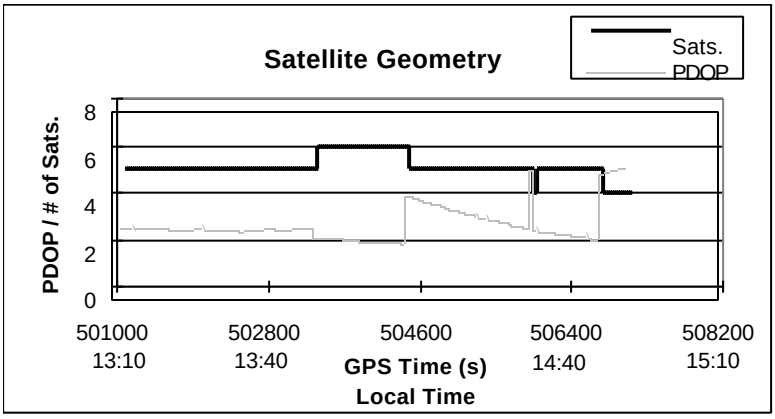

Figure 6.27 Reduced Satellite Geometry for Calgary

A summary of the results are shown in Table 6.1. It can be seen that for the L1-only case, the improvement was greater under poorer geometric conditions while the widelane observable showed a similar improvement relative to the full geometry case.

6.6.4 Increased Reliability

The reliability of the correct integer ambiguities is a very important part of integer ambiguity resolution. If the incorrect ambiguities are resolved, incorrect positions will be output, and because ambiguities are only resolved if centimetre level positioning is needed, such an incorrect position could have grave consequences.

The discrimination tests described in Chapter 3.3.4 should in theory result in the correct ambiguity set being chosen. Unfortunately, each of the tests is formulated under the assumption that all errors encountered in the GPS observations are Gaussian in nature. This assumption is not always true as multipath is always present and at long receiver separations, the differential atmosphere and orbital errors begin to add to the non-Gaussian errors.

One of the advantages of using two or more rover receivers is that the relative information between them can be used to confirm whether or not the chosen integer ambiguity set is correct. The resulting relative positions of the two rover receivers from the primary filter must agree with the relative positions output by the secondary filter. If either the baseline, the heading, or the pitch do not match within a certain tolerance, it can be assumed that the incorrect ambiguity set has been chosen and the search should be reset. Naturally, the secondary filter still suffers from multipath. The differential atmospheric errors are generally not a problem, however, because of the very short baseline between the two rovers. Thus, the reliability of the secondary filter is the main limiting factor. Of course, the secondary filter can also be checked for correct ambiguities using the fixed baseline.

In the Kelowna data set, the L1-only data processing resulted in an 80% success rate for finding the correct ambiguities without the constraints. Once the constraints were applied, this number increased to 95%, which is a 15% improvement in reliability over the unconstrained case. No incorrect ambiguities were found when processing the widelane data. The reduced geometry described previously resulted in only 1 incorrect ambiguity when processing in L1-only mode. Once the constraints were applied, no incorrect ambiguities were encountered.

When the incorrect ambiguities were encountered, they were often discovered within a short period of time because of the checks described in Chapter 6.2. Although it is still possible for an incorrect ambiguity set to pass all of the tests, after several epochs one or more of the tests are bound to fail causing the search to reset.

CHAPTER 7
MULTIPLE MONITOR STATIONS

By using double differencing techniques and remaining relatively close to the monitor station, all of the correlated errors are either eliminated or significantly reduced. This leaves the uncorrelated errors, i.e. multipath and receiver noise, as the dominant error sources that effect ambiguity resolution. In an attempt to reduce these correlated errors, and in turn decrease the amount of time required for ambiguity resolution, a method of using multiple monitor stations was implemented.

In this chapter, the method used will be described and the results shown. The results of combining both multiple monitor stations and dual rover stations are presented.

7.1 Multiple Monitor Station Adjustment

The method chosen to make use of the multiple monitor station data was first described in Raquet (1996) for networks within a small area. The method was then extended to larger areas in Raquet (1997). The approach taken is to use a least squares condition adjustment to reduce the uncorrelated errors within the network. The observations to each of the monitor station are first adjusted. Then, with these adjusted monitor observations, one can simply use data from a single corrected monitor station to resolve the ambiguities between it and the rover stations. The choice of monitor station is arbitrary as it was shown in Raquet (1997) that after the monitor station observations have been adjusted, each of the stations will give similar results.

In a condition adjustment, there are no unknowns, only observations. That is:

$$f\left(\hat{\mathbf{l}}\right) = \mathbf{0} \tag{7.1}$$

where $\hat{\mathbf{l}}$ is the adjusted observation vector. The adjusted observations are found using the equations

$$\hat{\mathbf{l}} = \mathbf{l} + \hat{\mathbf{r}} \tag{7.2}$$

where $\hat{\mathbf{r}} = -\mathbf{C_l B^T}\left(\mathbf{B C_l B^T}\right)^{-1}\mathbf{w}$ (7.3)

$$\mathbf{w} = f\left(\mathbf{l}\right) \tag{7.4}$$

and $$\mathbf{B} = \left.\frac{\partial f}{\partial l}\right|_l \tag{7.5}$$

B is called the observation design matrix while **w** is referred to as the misclosure vector.

For the case at hand, an appropriate mathematical model must first be found. Because the positions of the monitor stations are known, it seems logical to implement a model that equates the observed ranges to the known ranges. For the double difference pseudoranges, this becomes:

$$f\left(\hat{l}\right) = \nabla\Delta\hat{p}_{ij}^{xy} - \nabla\Delta\rho_{ij}^{xy} = 0 \tag{7.6}$$

where p is the measured pseudorange, ρ is the calculated range, i and j represent receivers, and x and y represent satellites. It is assumed that the atmospheric errors are zero. Thus, by expanding equation (7.6), one obtains:

$$f\left(\hat{l}\right) = \left[\left(\hat{p}_j^y - \hat{p}_i^y\right) - \left(\hat{p}_j^x - \hat{p}_i^x\right)\right] - \left[\left(\rho_j^y - \rho_i^y\right) - \left(\rho_j^x - \rho_i^x\right)\right] = 0 \tag{7.7}$$

Therefore, **B** is an mxn matrix filled with either a 0, 1, or -1 where n is the number of observations and m is the number of mathematical models. The total number of mathematical models is the number of linearly independent possible combinations of receivers and satellites. That is, if n_{sats} is the number of satellites and n_{rec} is the number of receivers, there are $\left(n_{sats} - 1\right)\left(n_{rec} - 1\right)$ linearly independent mathematical models.

The misclosure vector $\mathbf{w}$ is simply the calculated double difference ranges subtracted from the observed double differences. The misclosure is generally nonzero. This is because of the existence of multipath and receiver noise within the observations.

The double difference carrier phase observables can be adjusted in a similar manner to the code observations. The phase equivalent to equation (7.6) is

$$f\left(\hat{l}\right) = \nabla\Delta\hat{\Phi}_{ij}^{xy} + \nabla\Delta N_{ij}^{xy} - \nabla\Delta\rho_{ij}^{xy} = 0\,. \tag{7.8}$$

Unfortunately, in order to adjust the carrier phase observations, it is necessary to know the ambiguities. This is trivial for short baselines as the difference between the observed and calculated phases can simply be rounded to the nearest integer. For longer baselines, however, this is not the case as atmospheric errors can cause pseudorange errors larger than one cycle. Thus, rounding may not be possible and some other means of resolving the correct integers must be found. Naturally, if a widelane observable is to be used, this becomes much less of a problem.

One of the critical elements in this algorithm is the observation covariance matrix $\mathbf{C_l}$ which should reflect the behavior of the errors. If the network is in a very small area (i.e. several kilometres) it can be assumed that there are no correlated errors and the matrix is diagonal. Over larger distances, however, correlated errors begin to creep into the observations. For optimal results, these correlations must be accounted for by filling in the off diagonal terms in the $\mathbf{C_l}$ matrix. Deriving these off diagonal elements is dependent on several factors including the distance and direction from the rover to each of the monitor stations. Thus, it is also necessary to know the rover position within several kilometres to compute this matrix. The method for computing the off diagonal elements which is used in the results that follow is presented in Raquet (1997).

Using a condition adjustment and then processing the rover data with only one of the monitor stations has several advantages over a single batch adjustment. Firstly, any

existing software can be used to process the adjusted data as the information from all of the monitors has been used to adjust each monitor. Also, no special hardware is required, other than the multiple reference station requirement. Finally, both the phase and code multipath and noise can be reduced.

The one major drawback of this method is that by adjusting the observations and then only using one monitor station, the ambiguity conditions between each pair of monitors and each rover (similar to Chapter 5.1.5) cannot be used as either a constraint or a quality control measure. Thus, a small amount of information is lost.

It should be noted that in order for the condition adjustment to be successful, it is necessary to know the coordinates of the monitor stations with a very high accuracy. In the case of the phase adjustment, the combined effect of the phase noise and multipath is generally of the order of several centimetres. Thus, the coordinates of the monitor stations must be known better than this for the adjustment to work effectively (Varner and Cannon, 1997).

7.2 Data Description

The data used to test the effectiveness of the algorithms described above is the same data set described in Chapter 6.1. Three monitor receivers were used. The positions of the monitor stations are shown along with the reference trajectory in Figure 7.1, which is the same trajectory presented in Figure 6.6. As stated in Chapter 6.1, both the Peachland and Kelowna stations were Trimble 4000SSi receivers with groundplane antennas. The Plains station consisted of a NovAtel MiLLennium receiver with a chokering antenna. Both receivers on the vessel were NovAtel MiLLennium receivers with chokering antennas. For all following tests, it was assumed that the errors due to phase center stability (which will not cancel because of different antenna types) is negligible.

The Kelowna and Peachland receivers collected data at a rate of 1 Hz. An error occurred at the Plains receiver, however, and data was collected at a rate of 0.5 Hz. Thus, half of the adjusted observations were generated using three monitor stations, while every other set of adjusted observations was generated using only two monitors.

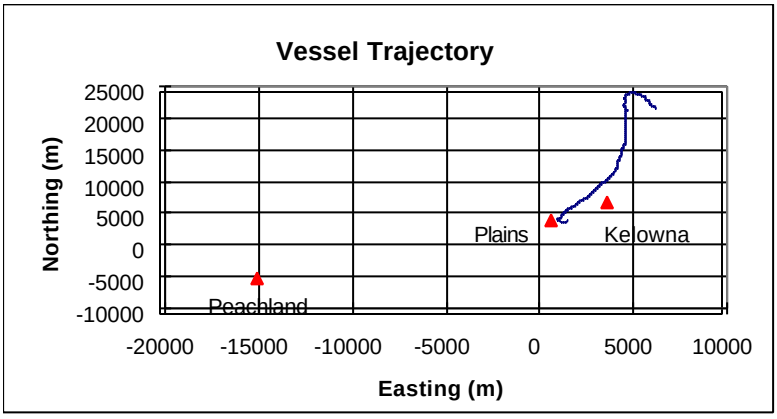

Figure 7.1 Vessel Trajectory

7.3 Results and Analysis

To test the effectiveness of the algorithms presented above, a conditional adjustment was carried out followed by processing in the same manner presented in Chapter 6. Because of the long distance between the three monitor stations (≈ 40 km), only the widelane results are presented.

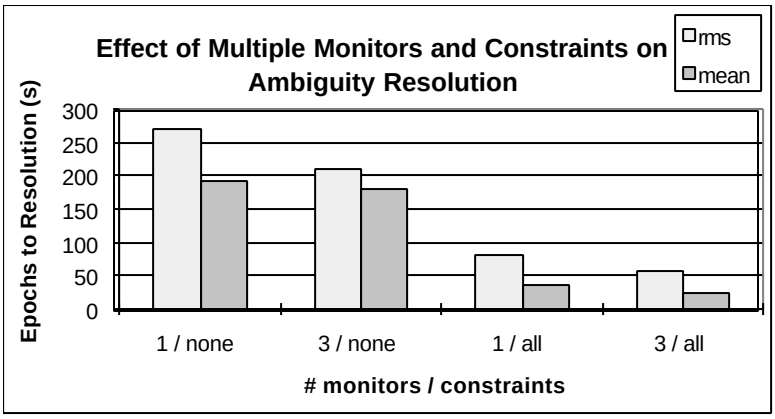

Figure 7.2 Effect of Multiple Monitors and Constraints on Ambiguity Resolution

Figure 7.2 shows the effect of multiple monitor stations on ambiguity resolution. The first column shows the results if no constraints are applied and the Kelowna station is the sole monitor. The second column shows the results of using all monitor stations. By adjusting the monitor station observations using the condition adjustment, a noticeable amount of improvement becomes obvious as the RMS number of epochs required to resolve the ambiguities decreased by approximately 60 epochs, which is a 22% reduction. The third and fourth columns show the effect of using all constraints, including a 0.75 m height constraint, on the time to ambiguity resolution. The use of three monitor stations as opposed to one resulted in a 29% decrease in the RMS mean time to resolve the ambiguities.

The results presented above show that the use of multiple monitor stations can be very valuable to ambiguity resolution. These results are a nearly worst case scenario because the variances of both the code and phase were not reduced to reflect the reduction in errors such as multipath and code noise which should have been reduced because of the conditional adjustment. Figure 7.3 shows the effect of reducing the code variance from 16.0 m to 4.0 m and the widelane phase variance from 0.0025 m to 0.0016 m. These numbers were selected by processing several sections of data with various different

combinations of code and phase variances. The improvement over the results in Figure 7.2 is again significant.

Note that in Figure 7.3, the results for the case where only one monitor with reduced code and phase variances are also presented for comparison purposes. In both the unconstrained and fully constrained cases, the RMS and mean number of epochs to integer ambiguity resolution was decreased (compared to Figure 7.2) by reducing the code and phase variances. The reliability, however, is not shown in the figure.

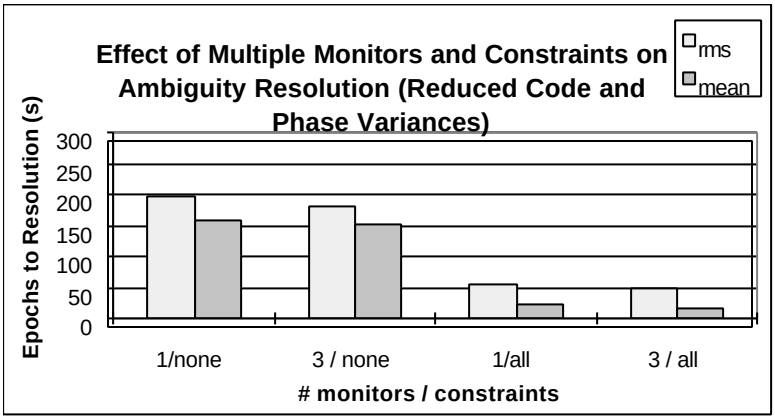

Figure 7.3 Effect of Multiple Monitors and Constraints on Ambiguity Resolution (Reduced Code and Phase Variance)

When all three monitor stations were used, no incorrect ambiguities were found. Thus, the reduction in time to ambiguity resolution is likely due to the decrease in multipath and receiver noise. The cases in which only one monitor station was used resulted in decrease in reliability to a 93% and 95% success rate of correctly choosing the integer ambiguities for the unconstrained and constrained cases respectively. Incorrect ambiguities are not acceptable, thus, reducing the variances to decrease the time to ambiguity resolution is not an option.

A summary of the results obtained are shown in tabular form in Table 7.1. By using three monitors and no constraints, the RMS epochs to resolution is reduced by approximately 22%. The percent improvement of the constrained case is nearly 29%. By making use of all available constraints and all three monitor stations, the total number of epochs required for ambiguity resolution is reduced by 79%, which is quite remarkable.

At first glance, it seems that the pair of rover receivers is more effective than the three monitor stations as most of the reduction in time to ambiguity resolution was still from the constraints. This is not the case, however, as most of the reduction from the constraints is due to the height constraint.

Table 7.1 Summary of Results Using Three Monitor Stations and Two Rovers

RMS Epochs to Resolution	1 Monitor Station		3 Monitor Stations	
	No Constraints	All Constraints	No Constraints	All Constraints
unchanged σ	270	80	211	57
reduced σ	---	---	178	48

CHAPTER 8
COMPARISON BETWEEN FASF AND LAMBDA AUGMENTED FASF

In an attempt to assess the usefulness of the LAMBDA method (see Chapter 3.3.3), the transformation algorithm was implemented into the SFLY processing software described in Chapter 4. The data chosen to be analyzed using the two techniques is the Calgary data set described in Chapter 6. The performance of the two methods are compared under both the full geometry situation and the artificially reduced geometry situation.

8.1 Full Geometry

The full geometry can be seen in Figure 6.1 while the vessel trajectory can be seen in Figure 6.4. The performance of the L1 observable and the widelane observable is shown in Figures 8.1 and 8.2 respectively.

From Figure 8.1 it can be seen that the LAMBDA method makes a difference in the RMS time to resolution by approximately 20 s which is significant under these circumstances. These results, however, are somewhat artificial and in the following paragraph, it will be shown that the improvement is due to the limit placed upon the number of ambiguities the software checks before aborting the search because of too many possible ambiguity sets. The widelane processing with the addition of LAMBDA showed very little improvement over the FASF only case.

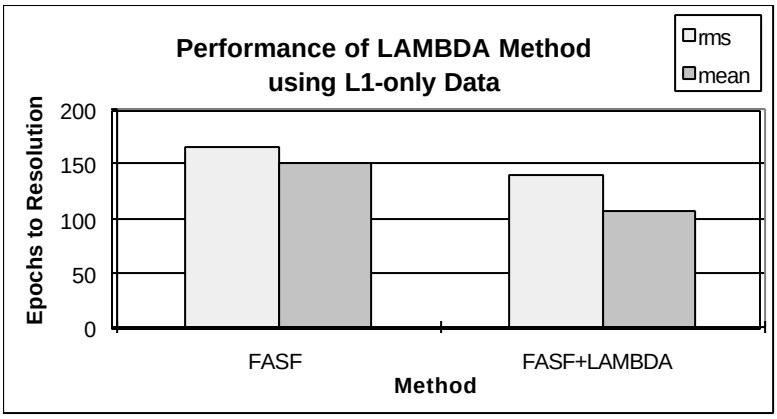

Figure 8.1 Performance of LAMBDA Method using L1-only Data

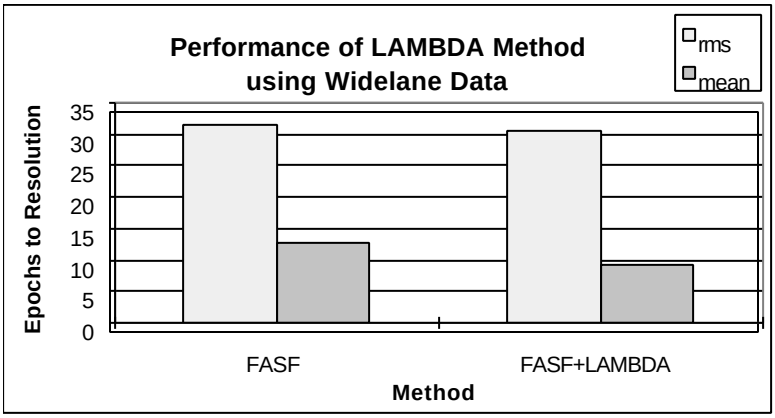

Figure 8.2 Performance of LAMBDA Method using Widelane Data

The L1-only data was reprocessed using the same software described in Chapter 4, with the exception that the maximum number of possible ambiguity sets before the search was aborted was raised to 10000. When this was done, the statistics shown in Figure 8.1 corresponding to the FASF processing approached the same level as the LAMBDA augmented statistics. This shows that the differences between the statistics is mainly due to the approach taken in the processing.

It was found that under ideal geometric conditions with six or more satellites, the ambiguities were often fixed immediately after the number of possible ambiguity sets fell

below 2000 possibilities. In the case of the LAMBDA augmented software, this occurred much sooner than the software which did not use the LAMBDA method. Thus, the LAMBDA method is very efficient in reducing the number of possible ambiguity sets.

Figure 8.3 is an example of how efficient the LAMBDA method is at reducing the number of possible ambiguity sets. It can be seen that the major advantage of using the LAMBDA method along with the FASF method is the reduction in possible ambiguity sets during the first several minutes of data processing. At approximately 13:12 local time (about 20 seconds after processing began), the number of ambiguity sets to be searched is greater than 5000 when using FASF alone. The addition of the LAMBDA method reduces this number to about 1000. Thus, if efficiency and computer processing speed are required, the LAMBDA method can be quite valuable. Also, if an upper bound is placed on the number of ambiguities to be searched (as in Chapter 4.2) the LAMBDA method can result in the number of possible ambiguity sets falling below this threshold much quicker. In situations of good geometry, this could result in shorter times to ambiguity resolution.

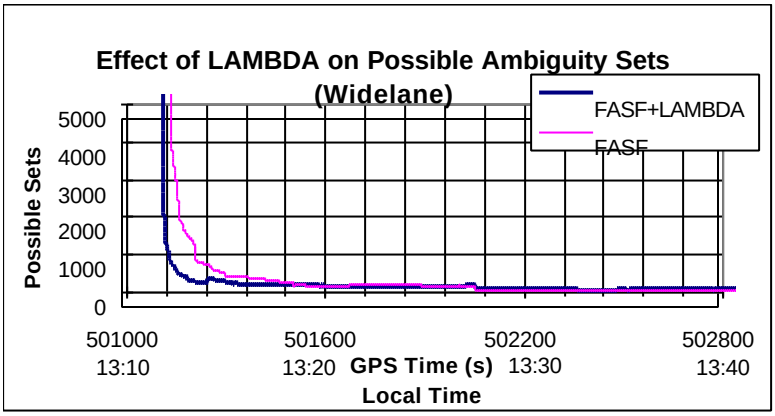

Figure 8.3 Effect of LAMBDA on Possible Ambiguity Sets

8.2 Reduced Geometry

The reduced geometry can be seen in Figure 6.19. The results of the L1-only and widelane processing are shown in Figures 8.4 and 8.5 respectively.

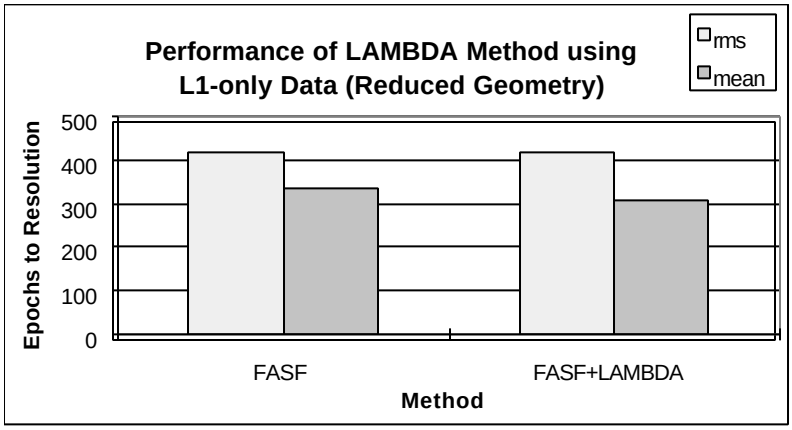

Figure 8.4 Performance of LAMBDA Method using L1-only Data - Reduced Geometry

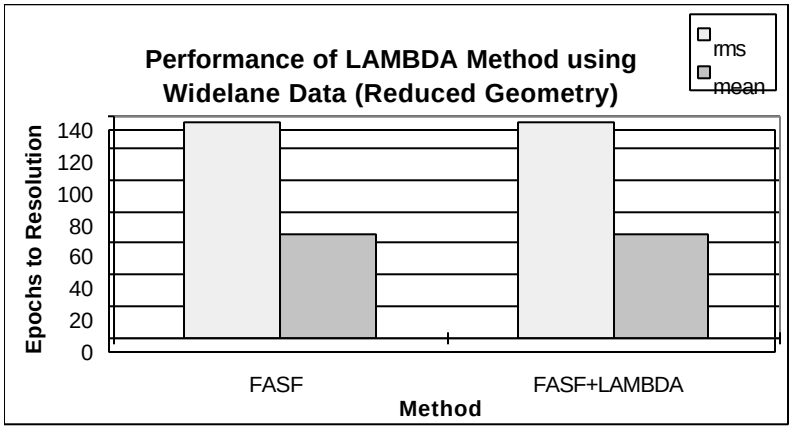

Figure 8.5 Performance of LAMBDA Method using Widelane Data - Reduced Geometry

It can be seen in the figures that the LAMBDA method had little effect on the RMS and mean times to ambiguity resolution. This is because the time to resolve the integer

ambiguities is generally longer than the time needed to reduce the number of possible ambiguity sets below 2000. This also supports the results obtained in Figures 8.1 and 8.2.

From the results presented it seems that the LAMBDA method is very efficient at reducing the number of possible ambiguity sets. This is very advantageous when real time processing is necessary as the amount of computing power is not as great for fewer possible ambiguity sets. If all ambiguity sets were searched, the method chosen, either FASF only or LAMBDA augmented FASF will generally not effect the time to resolve the ambiguities, only the processing time necessary for all possible sets to be checked.

The effect of the LAMBDA method on ambiguity resolution when all constraints are applied is very minimal. This is because the constraints cause the number of ambiguity sets to be reduced much quicker than without them (Chapter 6.2). The introduction of the LAMBDA method simply causes the number of ambiguities to be reduced even quicker. As shown above, this generally does not make ambiguity resolution quicker unless an upper bound has been placed on the number of possible ambiguity sets to be searched.

CHAPTER 9
CONCLUSIONS AND RECOMMENDATIONS

9.1 Conclusions

Carrier phase ambiguity resolution is an extremely delicate process which requires much care to ensure a quick and reliable solution. This process is dependent on many factors including the type of observable used, (widelane or L1 only), the satellite geometry, the number of satellites, and the monitor - rover separation. If an L1 observable is used, the time to ambiguity resolution is affected mostly by the separation between the monitor and rover receivers. The widelane, however, is much less sensitive to this separation for distances less than 35 km. Both the widelane and L1 only integer ambiguity resolution processes are affected by a reduced number of satellites and poorer geometry. In several cases, it was found that the ambiguities could be found quicker under the poorer geometry. This is because the number of possible ambiguity sets is significantly decreased by less satellites. On the other hand, with the reduced geometry and fewer satellites, the frequency of incorrect ambiguities was significantly increased. As a consequence, it was shown that the number of incorrect ambiguities is directly correlated with the satellite geometry.

In an attempt to increase the reliability of the ambiguity resolution process and at the same time decrease the time to resolution, several constraints were tested. By using two rover receivers on a vessel which were fixed with respect to one another, four constraints were formed. These include heading, pitch, ambiguity, and baseline constraints. Because an emphasis was placed on navigation in a marine environment, a height constraint was also used. From the marine tests used in this analysis, the following

conclusions can be made:

1) The single most useful constraint was the height constraint as it resulted in the largest decrease in time to ambiguity resolution. The effectiveness of the other constraints was mostly dependent on the separation between the monitor and rover, with the type of phase observable being a less important factor.

2) As the distance between the monitor and rover stations increased, the usefulness of the baseline, heading, pitch, and ambiguity constraints decreased until they were of little use to the ambiguity resolution process.

3) The baseline, heading, pitch, and ambiguity constraints were very valuable as reliability checks once the ambiguities were resolved. That is, if an ambiguity set was chosen, but did not result in the correct baseline, these were not the correct ambiguities.

4) When all possible constraints were applied and the separation between the monitor and rover receivers was kept under 2 km, a widelane observable was used, and a near ideal constellation was available, the RMS epochs to resolution for a given data set was reduced by 91%. When a L1 only observable was used, the time to resolution was reduced by 79%. Under poorer geometric conditions, the constraints resulted in a similar performance when using a widelane observable, while the percent reduction when using the L1 only case increased to 84%. In a more realistic case where monitor rover separations ranged from 2 km to 20 km, the performance of the constraints was slightly less as the widelane and L1 observables resulted in a 70% and 59% reduction in the RMS times to resolution.

5) By adding several monitor stations along with the dual rover stations, the time to ambiguity resolution was further decreased. A method of adjusting a network of monitor stations developed by Raquet (1996) was used to help reduce the multipath and receiver noise of the monitor station observations. The effect of the multiple monitor station combined with the constraints for a given data set was a decrease in the amount of time required to solve the integer ambiguities by approximately 79%, of which 70% was due to the constraints, and the remaining 9% can be attributed to the use of three monitor stations.

6) The LAMBDA method is a very efficient means of reducing the number of possible ambiguity sets. However, it is still the ability of the discrimination test to choose the correct integers which determines when the correct ambiguity set can be chosen. The LAMBDA method was found to be extremely efficient, and thus an excellent tool for real time applications.

9.3 Recommendations

Based on the research presented in this thesis, the following recommendations can be made:

1) Some research is needed to gain more insight into other possible statistical tests which could improve the reliability of the distinguishing test in the presence of colored noise.

2) A more sophisticated method of choosing the maximum allowable residual for quality control than Table 4.1 may be useful for detecting incorrect ambiguities quicker.

3) Further testing of the constraints in environments other than a marine environment is recommended. The effectiveness of the constraints in a more dynamic environment such as an airborne environment may give more insight into the behavior of the constraints.

4) It is recommended that similar tests to those presented in this thesis be carried out in the year 2001 so that the effect of the ionosphere on ambiguity resolution can be examined.

5) An investigation of the second order effects which affect the constraint is recommended. By implementing the method presented by Widnall, (1972), the behavior of the effects may become clearer.

6) Since heading and pitch constraints were shown to be useful, the next step would be to incorporate a gyroscope, which once initialized, could sense heading or pitch. The use of differential barometry could also be used as a means of obtaining a height constraint for situations in which the height is not constant.

7) The incorporation of one or two more rover receivers would result in the attitude of the vehicle. Thus, the roll, as well as one or two more ambiguity constraints (depending on how many receivers are added) become available. An investigation of the impact of these additional constraints on ambiguity resolution is recommended.

8) An investigation of the effects of the constraints on both the internal and external reliability is recommended.

9) A more theoretical approach to the adaptive filtering should be investigated.

10) The effect of the ionosphere on the maximum achievable baseline lengths should be analyzed in the future, preferably closer to 2001, when the solar maximum is reached. Also, the effect of the ionosphere on the constraints when ionospheric activity is maximum is recommended.

References

Abidin, H. Z. (1990), "Extrawidelaning For 'On the Fly' Ambiguity Resolution: Simulation of Multipath Effects", pp. 525-533, **Proceedings of the Third International Technical Meeting of the Satellite Division of ION GPS-90**, Colorado Springs.

Ashjaee, J. and R. Lorenz (1992), "Precision GPS Surveying After Y-Code", **Proceedings of ION GPS-92, Fifth International Technical Meeting of the Satellite Division of the Institute of Navigation**, pp. 657-659, Albuquerque, September.

Borge, T. K. (1996), **GPS Carrier Phase Ambiguity Resolution and Cycle-Slip Processing on a Moving Platform**, Report 96-49-W, Department of Engineering Cybernetics, Norwegian University of Science and Technology, N-7034 Trondheim, Norway.

Braasch, M. (1996), Multipath Effects**, Global Positioning System: Theory and Applications**, Vol. 1, Ch. 14, American Institute of Aeronautics and Astronautics, Inc., Washington.

Brown, R. G. and P. Y. C. Hwang (1992**), Introduction to Random Signals and Applied Kalman Filtering**, 2nd Ed. John Wiley & Sons, Inc., New York.

Burgess, J. and S. Frodge (1992), "Performance Testing of On-the-Fly GPS Technology", **Proceedings of ION GPS-92**, pp. 1071-1077, Salt Lake City, September.

Cannon, M. E. (1991), **Airborne GPS/INS with an Application to Aerotriangulation**, UCSE Reports No. 20040, Department of Surveying Engineering, University of Calgary.

Cannon, M.E., E. Berry, and N. King (1993), "Testing a Lightweight GPS/GIS Terminal for Sub-Meter DGPS Positioning", **Proceedings of ION GPS-93**, pp. 1011-1020, Salt Lake City, September

Chen, D. and G. Lachapelle (1994), "A Comparison of the FASF and Least-Squares Search Algorithms for Ambiguity Resolution On The Fly", **Proceedings of International Symposium on Kinematic Systems - KIS 94**, pp. 241-253, Banff, Canada, August 30 - September 2.

Counselman, C. C. and S. A. Gourevitch (1981), "Miniature Interferometer Terminals for Earth Surveying: Ambiguity and Multipath with Global Positioning System"**, IEEE Transactions on Geoscience and Remote Sensing**, Vol. GE-19, No. 4, pp. 244-252.

Erickson, C. (1992), "An Analysis of Ambiguity Resolution Techniques for Rapid Static GPS Surveys Using Single Frequency Data", **Proceedings of ION GPS-92**, pp. 453-462, Albuquerque, September.

Ford, T. and J. Neumann (1994), 'NovAtel's RT20 - A Real Time Floating Ambiguity Positioning System", **Proceedings of ION GPS-94**, pp. 1067-1076, Salt Lake City, September.

Frei, E. and G. Beutler (1990), "Rapid Static Positioning Based on the Fast Ambiguity Resolution Approach 'FARA': Theory and First Results", **Manuscript Geodetica**, Vol. 15, pp. 325-356.

Frodge, S., V. Labrecque, and R. Barker (1995), "Performance of the Real-Time On-The-Fly GPS Positioning System on Board a Dredge", **Proceedings of the National Technical Meeting**, pp. 505-513, Institute of Navigation, Anaheim, California, January.

Goad, C. C. and L. Goodman (1974), "A Modified Hopfield Tropospheric Refraction Correction Model", Presented at the Fall Annual Meeting American Geophysical Union, San Francisco, December.

Hamada, K., T. Hayashi, N. Shimizu (1996), "Applicability of GPS to Tide Level Observations in "KANMON" Strait Area", **Proceedings of ION GPS-96**, pp. 393-402, Kansas, September.

Han, S. (1996), "Quality Control Issues Relating to Instantaneous Ambiguity Resolution for Real-Time GPS Kinematic Positioning", **Proceedings of ION GPS-96**, pp. 1419-1430, Kansas, September.

Han, S. and C. Rizos (1996), "Integrated Method for Instantaneous Ambiguity - Resolution Using New Generation GPS Receivers", **IEEE PLANS'96**, pp. 254-261, Atlanta.

Hatch, R. (1982), "The Synergism of GPS Code and Carrier Measurements", **Proceedings of Third International Geodetic Symposium on Satellite Doppler Positioning**, pp. 1213-1232, Washington.

Hatch, R. (1990), "Instantaneous Ambiguity Resolution, Kinematic Systems in Geodesy", **Surveying, and Remote Sensing**, pp. 299-308, Springer-Verlag, IAG Symposia 107.

Hatch, R. (1991), "Ambiguity Resolution While Moving - Experimental Results", **Proceedings of ION GPS-91**, pp. 707-713, Albuquerque, September 11-13.

Haykin, S. (1996), **Adaptive Filter Theory, Third Edition**, Prentice Hall Information and System Series, New Jersey.

Hein, G. and W. Werner (1995), "Comparison of Different On-The-Fly Ambiguity Resolution Techniques", **Proceedings of ION GPS-95**, pp. 1137-1153, Palm Springs, September.

Hoffman-Wellenhof, B., H. Lichtenegger, J. Collins (1993), **GPS Theory and Practice**, 2nd Edition, Springer-Verlag, New York.

Hopfield, H. (1969), "Two-quartic Tropospheric Refractivity Profile for Correction Satellite Data", **Journal of Geophysical Research**, 74(18), pp. 4487-4499.

Jonge de, P. J. and C. Tiberius (1996**), The LAMBDA Method for Integer Ambiguity Estimation: Implementation Aspects**, Delft Geodetic Computing Centre LGR Series, No. 12, Delft University of Technology, Netherlands.

Kielland, P. and J. Hagglund (1995), "Using DGPS to Measure the Heave Motion of Hydrographic Survey Vessels", **Proceedings of ION National Technical Meeting**, pp. 495-504, Institute of Navigation, Anaheim, California, January.

Krakiwsky, E. J. (1990), **The Method of Least Squares: A Synthesis of Advances**, UCGE #10003, Department of Geomatics Engineering, The University of Calgary, August.

Krakiwsky, E.J. and M. Abousalem (1993), **Viewgraphs for Adjustment of Observations Engo 411**, Department of Geomatics Engineering, The University of Calgary, Fall.

Kumar, R. and K. Lau (1996), "Deconvolution Approach to Carrier and Code Multipath Error Elimination in High Precision GPS", **Proceedings of the National Technical Meeting**, Institute of Navigation, pp. 729-736, Santa Monica, January.

Lachapelle, G., W. Falkenberg, D. Neufeldt, P. Keilland (1989), "Marine DGPS Using Code and Carrier in a Multipath Environment", **Proceedings of ION GPS-89**, pp. 343-347, Colorado Springs.

Lachapelle, G., M.E. Cannon, G. Lu (1992), "Ambiguity Resolution on the Fly - A Comparison of P Code and High Performance C/A Code Receiver Technologies", **Proceedings of ION GPS-92**, pp. 1025-1032, Albuquerque, September.

Lachapelle, G. M.E. Cannon, G. Lu (1992), "High Precision GPS Navigation with Emphasis on Carrier Phase Ambiguity Resolution", **Marine Geodesy**, Vol. 15, pp. 253-269.

Lachapelle, G., C. Liu, G. Lu (1993), "Quadruple Single Frequency Receiver System for Ambiguity Resolution On The Fly", **Proceedings of ION GPS-93**, pp. 1167-1172, Salt Lake City, September.

Lachapelle, G., C. Liu, G. Lu, Q. Weigen, and R. Hare (1994), "Water-Borne Leveling with GPS", **Maritime Geodesy**, Volume 17, pp. 271-278.

Lachapelle, G., H. Sun, M. E. Cannon, G. Lu (1994), "Precise Aircraft-to-Aircraft Positioning Using a Multiple Receiver Configuration"**, Canadian Aeronautics and Space Journal**, Vol. 40, No. 2, pp. 793-799, June.

Lachapelle, G. (1995), **Engo 625 GPS Theory and Applications**, University of Calgary, Fall.

Lachapelle, G., A. Bruton, J. Henriksen, M. E. Cannon, C. McMillan (1996), "Evaluation of High Performance Multipath Reduction Technologies for Precise DGPS Shipborne Positioning", **Proceedings of the National Technical Meeting**, Institute of Navigation, pp. 399-406, Santa Monica, January.

Lan. H. and M. E. Cannon (1996), "Development of a Real-Time Kinematic GPS System: Design, Performance and Results", **Proceedings of ION National Technical Meeting**, pp. 605-613, Santa Monica, January.

Landau, H. and H. Euler (1992), "On the Fly Ambiguity Resolution for Precise Differential Positioning", **Proceedings of the Fifth International Technical Meeting of the Institute of Navigation**, pp. 607-613, Albuquerque, September.

Leick, A. (1995), **GPS Satellite Surveying**, 2nd Ed., John Wiley & Sons, Inc., New York.

Lu, G. (1995), **Development of a GPS Multi-Antenna System for Attitude Determination**, UCGE Reports No. 20073, Department of Geomatics Engineering, University of Calgary.

Mader, G. L. (1990), "Ambiguity Function Techniques for GPS Phase Initialization and Kinematic Solutions"**, Proceedings of the Second International Symposium on Precise Positioning System**, pp. 1233-1247, Ottawa, September, The Canadian Institute of Surveying and Mapping.

Maybeck, P. S. (1994), **Stochastic Models, Estimation, and Control Volume 1**, Navtech Book and Software Store, Arlington, VA.

Mohamed, A. H. (1996), "Robust and Reliable Kalman Filtering of GPS Data"**, Proceedings of ION GPS-96**, pp. 1441-1456, Kansas City, September.

Neumann, J.B., A. Manz, T.J. Ford, and O. Mulyk (1996), "Test Results from a New 2 cm Real Time Kinematic GPS Positioning System", **Proceedings of ION GPS-96**, pp. 873-882, Kansas City, September.

Parkinson, B.W., T. Stansell, R. Beard, and K. Gromov (1995), "A History of Satellite Navigation", **Navigation Journal of the Institute of Navigation**, Vol. 42, No. 1, pp. 109-164, Spring.

Parkinson, B.W. (1996), Introduction and Heritage of NAVSTAR, the Global Positioning System**, Global Positioning System: Theory and Applications**, Vol. 1, Ch. 1, American Institute of Aeronautics and Astronautics, Inc., Washington.

Qui, W. (1993), **An Analysis of Some Critical Error Sources in Static GPS Surveying**, UCGE Reports No. 20054, Department of Geomatics Engineering, University of Calgary.

Raquet, J. (1996), "Multiple Reference GPS Receiver Multipath Mitigation Technique", **Proceedings of ION Annual Meeting**, pp. 681-690, Boston, June.

Raquet, J. (1997), "A New Approach to GPS Carrier-Phase Ambiguity Resolution Using a Reference Receiver Network", **Proceedings of ION National Technical Meeting**, pp. 357-366, Santa Monica, January.

Remondi, B. W. (1984), **Using the Global Positioning System (GPS) Phase Observable for Relative Geodesy: Modeling, Processing, and Results**, Ph.D. Dissertation, Center for Space Research, The University of Texas, Austin.

Remondi, B. W. (1991), "Kinematic GPS Results Without Static Initialization", **NOAA Technical Memorandum NOS NGS-55**, Rockville, MD.

Remondi, B. W. (1992), "Real-Time Centimeter-Accuracy GPS: Initialization While in Motion (Warm Start Versus Cold Start)", **Proceedings of ION GPS-92**, pp. 1053-1061, Albuquerque, September.

Saastamoinen II (1973), Contribution to the Theory of Atmospheric Refraction, **Bulletin Geodesique**, 107, pp. 13-34.

Schwarz, K.P. and J. Krynski (1992), **Fundamentals of Geodesy**, UCGE Reports No. 10014, Department of Geomatics Engineering, University of Calgary.

Shi, J. (1994), **High Accuracy Airborne Differential GPS Positioning Using a Multi-Receiver Configuration**, UCGE Reports No. 20061, Department of Geomatics Engineering, University of Calgary.

Shi, J. and M.E. Cannon (1995), "Critical Error Effects and Analysis in Carrier Phase-Based Airborne GPS Positioning Over Larger Areas", **Bulletin Geodesique**, 69, pp. 261-273.

Spilker, J.J. (1996), GPS Signal Structure and Theoretical Performance, **Global Positioning System: Theory and Applications**, Vol. 1, Ch. 3, American Institute of Aeronautics and Astronautics, Inc., Washington.

Teunissen, P.J.G. (1993), "Least Squares Estimation of the Integer GPS Ambiguities, Invited Lecture", Section IV Theory and Methodology, IAG General Meeting, Beijing China, August.

Teunissen, P.J.G. (1994), "A New Method for Fast Carrier Phase Ambiguity Estimation", **Proceedings of the IEEE PLANS'94**, pp. 562-573, Las Vegas, April.

Tiemeyer, B., M.E. Cannon, G. Lachapelle, G. Schanzer (1994), "Satellite Navigation for High Precision Aircraft Navigation with Emphasis on Atmospheric Effects", **Proceedings of the IEEE PLANS'94**, pp. 394-401, Las Vegas, April.

Townsend, B. and P. Fenton (1994), "A Practical Approach to the Reduction of Pseudorange Multipath Errors in a L1 GPS Receiver", **Proceedings of ION-GPS94**, pp. 143-148 Salt Lake City, September.

Townsend, B., P. Fenton, K. Van Dierendonnk (1995), "Performance Evaluation of the Multipath Eliminating Delay Lock Loop", **Navigation**, Journal of the Institute of Navigation, Vol. 42, No. 3, pp. 503-514.

Van Dierendonck, A. J., P. Fenton, T. Ford (1992), "Theory and Performance of Narrow Correlator Spacing in a GPS Receiver", **Navigation**, Journal of The Institute of Navigation, Vol. 39, No. 3, pp. 265-283.

Van Dierendonck, A. J. (1994), "Understanding GPS Receiver Technology: A Tutorial on What Those Words Mean", **Proceedings of International Symposium on Kinematic Systems - KIS 94**, pp. 15-24, Banff, Canada.

van Nee, R., J. Siereveld, P. Fenton, B. Townsend (1994), "The Multipath Estimating Delay Lock Loop: Approaching Theoretical Accuracy Limits", **Proceedings of the IEEE PLANS**, pp. 246-251, Las Vegas, April.

Varner, C.C. and M.E. Cannon (1997), "The Application of Multiple Reference Stations to the Determination of Multipath and Spacially Decorrelating Errors", **Proceedings of the National Technical Meeting**, Institute of Navigation, pp. 323-333, Santa Monica, January.

Wei, M. and K. P. Schwarz (1995), "Fast Ambiguity Resolution Using An Integer Nonlinear Programming Method", **Proceedings of ION GPS-95**, pp. 1101-1110, Palm Springs, September.

Wells, D.E., N. Beck, D. Delikaraoglou, A. Kleusberg, E. J. Krakiwsky, G. Lachapelle, R.B. Langley, M. Nakiboglu, K. P. Schwarz, J. M. Tranquilla, and P. Vanicek (1987), **Guide to GPS Positioning**, 2nd printing with corrections, Canadian GPS Associates, Fredericton N.B.

Weisenburger, S. (1995), "Evaluation of Motorola VP Oncore, ENGO 625 Seminar #1", The University of Calgary.

Widnall, W. S. (1972), "Enlarging the Region of Covariance of Kalman Filters that Encounter Nonlinear Elongation of Measured Range", **Proc. of AIAA Guidance and Control Conf.**, pp. 1-7, Stanford, California, August.

Wubbena, G. (1989), "The GPS Adjustment Software Package GEONAP, Concepts and Models", **Proceedings of the 5th International Geodetic Symposium on Satellite Positioning**, New Mexico, March 13-17, Vol. 2, pp. 452-461.

Appendix

Derivation of Design Matrix for GPS Observables

The double difference design matrix for GPS observables is defined as:

$$\mathbf{A} = \begin{bmatrix} \frac{\partial f}{\partial \phi} & \frac{\partial f}{\partial \lambda} & \frac{\partial f}{\partial h} & \frac{\partial f}{\partial \dot{\phi}} & \frac{\partial f}{\partial \dot{\lambda}} & \frac{\partial f}{\partial \dot{h}} & \frac{\partial f}{\partial \Delta\nabla N_1} & \cdots & \frac{\partial f}{\partial \Delta\nabla N_n} \\ \vdots & \vdots & \vdots & \vdots & \vdots & \vdots & \vdots & \vdots & \vdots \end{bmatrix} \quad \text{(A1)}$$

where f is either the double difference pseudorange equation:

$$f_p = \Delta\nabla\rho = \left(\rho^i_{rem} - \rho^i_{mon}\right) - \left(\rho^{base}_{rem} - \rho^{base}_{mon}\right) \quad \text{(A2)}$$

or the double difference carrier phase equation:

$$f_\Phi = \Delta\nabla\Phi = \Delta\nabla\rho + \lambda\Delta\nabla N = \left(\rho^i_{rem} - \rho^i_{mon}\right) - \left(\rho^{base}_{rem} - \rho^{base}_{mon}\right) + \lambda\Delta\nabla N \quad \text{(A3)}$$

i is the i^{th} satellite, base is the base satellite, mon is the monitor receiver, and rem is the remote receiver. Note that it is assumet that all errors have been eliminated by the differencing process or have been appropriately modeled. Both double difference carrier phase and double difference pseudorange equations are the same with the exception of the ambiguity state.

$$\frac{\partial f}{\partial \phi} = \frac{\partial f}{\partial x}\frac{\partial x}{\partial \phi} + \frac{\partial f}{\partial y}\frac{\partial y}{\partial \phi} + \frac{\partial f}{\partial z}\frac{\partial z}{\partial \phi} \quad \text{(A4)}$$

$$\frac{\partial f}{\partial \lambda} = \frac{\partial f}{\partial x}\frac{\partial x}{\partial \lambda} + \frac{\partial f}{\partial y}\frac{\partial y}{\partial \lambda} + \frac{\partial f}{\partial z}\frac{\partial z}{\partial \lambda} \quad \text{(A5)}$$

$$\frac{\partial f}{\partial h} = \frac{\partial f}{\partial x}\frac{\partial x}{\partial h} + \frac{\partial f}{\partial y}\frac{\partial y}{\partial h} + \frac{\partial f}{\partial z}\frac{\partial z}{\partial h} \quad \text{(A6)}$$

given that (Schwarz and Krynski, 1992)

$$x = (N + h)\cos\phi\cos\lambda \quad \text{(A7)}$$

$$y = (N + h)\cos\phi\sin\lambda \quad \text{(A8)}$$

and $$z = \left[\left(1 - e^2\right)N + h\right]\sin\phi \quad \text{(A9)}$$

where $$N = \frac{a}{\sqrt{1 - e^2\sin^2\phi}} \quad \text{(A10)}$$

a is the semi-major axis

e is the first eccentricity

the following partial derivatives can be formed (Cannon, 1991)

$$\frac{\partial x}{\partial \phi} \approx -(N+h)\sin\phi\cos\lambda \tag{A11}$$

$$\frac{\partial x}{\partial \lambda} = -(N+h)\cos\phi\sin\lambda \tag{A12}$$

$$\frac{\partial x}{\partial h} = \cos\phi\cos\lambda \tag{A13}$$

$$\frac{\partial y}{\partial \phi} \approx -(N+h)\sin\phi\sin\lambda \tag{A14}$$

$$\frac{\partial y}{\partial \lambda} = (N+h)\cos\phi\cos\lambda \tag{A15}$$

$$\frac{\partial y}{\partial h} = \cos\phi\sin\lambda \tag{A16}$$

$$\frac{\partial z}{\partial \phi} \approx \left(N\left(1-e^2\right)+h\right)\cos\phi \tag{A17}$$

$$\frac{\partial z}{\partial \lambda} = 0 \tag{A18}$$

$$\frac{\partial z}{\partial h} = \sin\phi \tag{A19}$$

$$\frac{\partial f}{\partial x} = \frac{-\left(x^i - x_{rem}\right)}{\rho^i_{rem}} + \frac{-\left(x^j - x_{rem}\right)}{\rho^j_{rem}} \tag{A20}$$

$$\frac{\partial f}{\partial y} = \frac{-\left(y^i - y_{rem}\right)}{\rho^i_{rem}} + \frac{-\left(y^j - y_{rem}\right)}{\rho^j_{rem}} \tag{A21}$$

$$\frac{\partial f}{\partial z} = \frac{-\left(z^i - z_{rem}\right)}{\rho^i_{rem}} + \frac{-\left(z^j - z_{rem}\right)}{\rho^j_{rem}} \tag{A22}$$

where

$$\rho_{rem}^{i} = \sqrt{\left(x^{i} - x_{rem}\right)^{2} + \left(y^{i} - y_{rem}\right)^{2} + \left(z^{i} - z_{rem}\right)^{2}} \qquad \text{(A23)}$$